POLITECNICO DI TORINO

Facoltà di ingegneria

Corso di laurea magistrale in ingegneria Energetica e Nucleare

Tesi di Laurea Magistrale

REALIZATION OF CHEMICAL LOOPING PROCESS AND PRODUCTION OF SYNGAS THROUGH CONCENTRATED SOLAR POWER.

Relatori:

Ing. Davide Papurello

Ing. Domenico Ferrero

Prof. Massimo Santarelli

Candidato:

Daniele Ciparelli

Summary.

Abstract.

The energetic transition from fossil fuel technologies to renewable energy sources is a process that cannot be avoided. Global warming with the related damage to our ecosystem and the decreasing amount of fossil fuel resources have led to the development of an alternative solution to produce energy. Particularly the worldwide attention is focused on possible solutions to reduce the CO_2 emissions.[1]

Carbon dioxide is the main cause of the greenhouse effect; however its emissions are not easy to contain as they are produced by most of the technologies currently used by the energetic sector. Those can only be reduced in three different ways: implementing reliable carbon capture and sequestration technologies; consuming less energy than in the past and use low-carbon technologies and energy sources.

The solar energy is one of the most interesting renewable sources, the Sun will continue to shine for billions of years, for this reason, it is abundant, inexhaustible and well distributed. However, due to the earth revolution and the elliptical path of the earth around the Sun, the solar energy will vary based on the period of the years and the different time of the day.

Hydrogen is an alternative energy sources and a solar fuel meaning that it is an energy carrier that can be transported, storage and especially produced through solar-powered processes. Thanks to its elevated energy content and the good reactivity it is considered a highly performing fuel. Nevertheless hydrogen is not a primary resource so it cannot be found in its pure state in nature but it must be produced through electro chemical processes that require an energy's input. In detail we are interested in hydrogen production through the split of H_2O molecules. This process could be used also to split the CO_2 molecules and produce carbon in form of CO.

The energy sources used to produce hydrogen or syngas, that is a mixture composed by hydrogen, oxygen and carbon monoxide, will determine whether or not the final energy is clean. The usage of fossil fuels to produce syngas is useless because will create the same CO_2 emissions and will have the same ecological impact. Syngas/ hydrogen can be used in gas turbines, diesel cycle engines or directly used in Direct-Methanol Fuel Cells (DMFC).

In view to low carbon economy, solar-powered CO_2 and H_2O dissociation processes have been developed and perfected to produce syngas/hydrogen. The thermochemical cycles used for the splitting of the molecules involves redox couples, usually metal oxides, that through a two phases cycle can generate sustainable fuels.

The following thesis aims to study and analyze a parabolic dish solar concentrator coupled to a ceramic receiver for the production of syngas. The study focuses on the possibility of performing thermochemical processes through the thermal energy supplied by the solar dish by analyzing, in particular, the efficiency of the process and its feasibility.

At the beginning theoretical concepts are introduced to describe the hydrogen properties and the way to storage and product it. The operating of the thermochemical cycle is discussed to understand which are the phases that compose the cycle, how are classified and the possible optimization processes.

The next chapter is focused on the sun's structure and the phenomena that influence the solar radiation incident on the Earth. Concentrated solar technologies (CSP) are introduced, describing their different types and the potential final uses. This part also included a description of the solar receivers and the solar reactors in which the reaction take place paying particular attention on the Aerosol reactors which are considered the current state of the art for the ceria's thermochemical cycle.

The theoretical part ends with the description of the main redox couples used in the volatile and non-volatile thermochemical cycles with a particular focus on the temperature that is required to activate the reaction and their kinetic. The Ceria oxide non-stoichiometric reduction has established as the reference redox material for the realization of two-phase thermochemical cycles and the consequent generation of sustainable fuels.

In the second part of the work the software "COMSOL MULTIPHYSICS" is used to create a useful forecast model to estimate the manufacturability of the system for the different periods of the year.

A first model is obtained through a special function of the software called "Ray optics model" which allows to simulate the ray trajectories on the concentrator through the Montecarlo methods and evaluate the average temperature and heat flux distribution on the receiver's focal plane. The results obtained are processed in Matlab and imported in a second model that represents the bi-dimensional configuration of the receiver and that taking into account the heat losses due to the exposition of the system at the external atmosphere. The simulations are applied at four different periods of the years to evaluate in which seasons are reached temperatures high enough to activate the ceria's thermal reduction.

Due to non-university causes it was not possible to perform real tests on the concentrator during the summer period. However the CO_2 splitting through the ceria's thermochemical cycle is simulated through a thermogravimeter at the energy department of Politecnico di Torino. The main results

obtained by the thermogravimetric analysis are reported and the solar to chemical efficiency obtained by the different cycles is analyzed. Furthermore through a Spectrometer it was possible to study the CO and O_2 production.

In conclusion is reported an experimental demonstration of a group of Zurich's researcher who carried out the thermal reduction of the ceria for the split of CO_2 and H_2O molecules in an aerosol reactor. These simulation's results are compared with our experiment to analyze the feasibility of the process.

1-Hydrogen.

H_2 represents a fundamental brick to produce synthetic chemicals that can be used as a renewable fuel for different application.

Figure 1.1-Microscopic view of liquid hydrogen molecules.

1.1- Hydrogen properties.

H_2 is considered an extremely performing fuel.

It is characterized by a high reactivity and good diffusivity that allow to use it into an electro-chemical system. The very low emissivity of the hydrogen-powered systems makes the hydrogen an ecological fuel.

H_2 molecules exist in nature in two different configurations:

- Orto configuration in which the two protons in the molecules have parallel spin.
- Para configuration in which the two protons of H_2 have an anti-parallel spin.

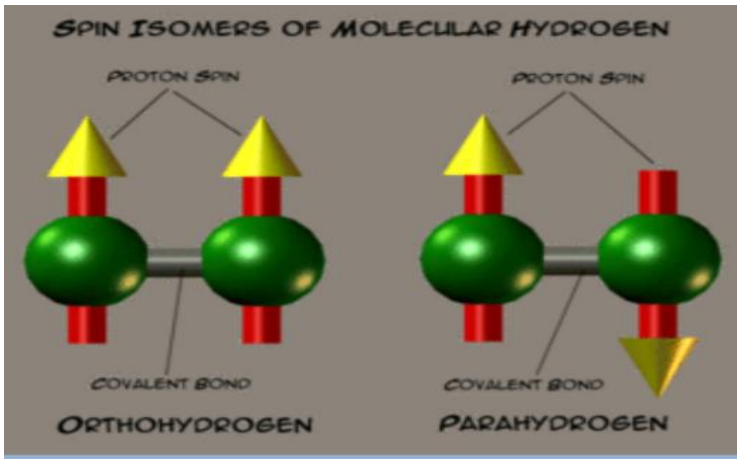

Figure 1.2 -Orto/Para Hydrogen configuration.

The transition from one configuration to another one is an exothermic process with the enthalpy that increasing as the temperature T drops as long as heat flux is emitted.

1.2-Hydrogen Production.

There are at least four methods to produce Hydrogen:

Steam reforming of natural gas.

It is a process in which the natural gas is converted into hydrogen through the steam methane reaction and the water gas shift reaction.[2]

Steam methane reforming (SMR):

$CH_4 + H_2O \rightarrow 3H_2 + CO$ endothermic reaction Δh= 206 Kj/mol (1)

Water Gas Shift (WGS):

$CO + H_2O \rightarrow H_2 + CO_2$ exothermic reaction Δh= - 41 Kj/mol] (2)

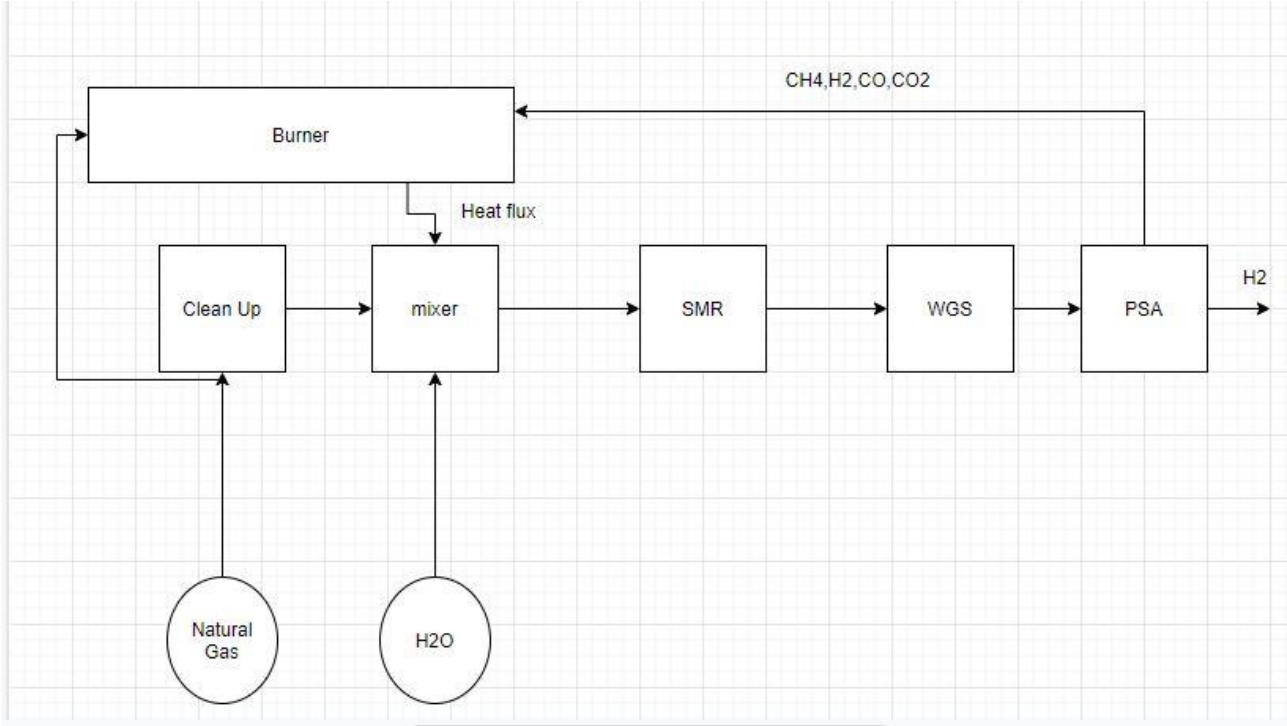

Figure 1.3- Hydrogen production through steam methane reforming.

The heat that is required for the endothermic reaction (SMR) is supplied by a burner.

Hydrogen production from liquid/solid.

In this process a solid feedstock or liquid char is converted into syngas through a gasification process. In a second step the gas is treated with a series of filters in order to obtain purest H_2 possible.

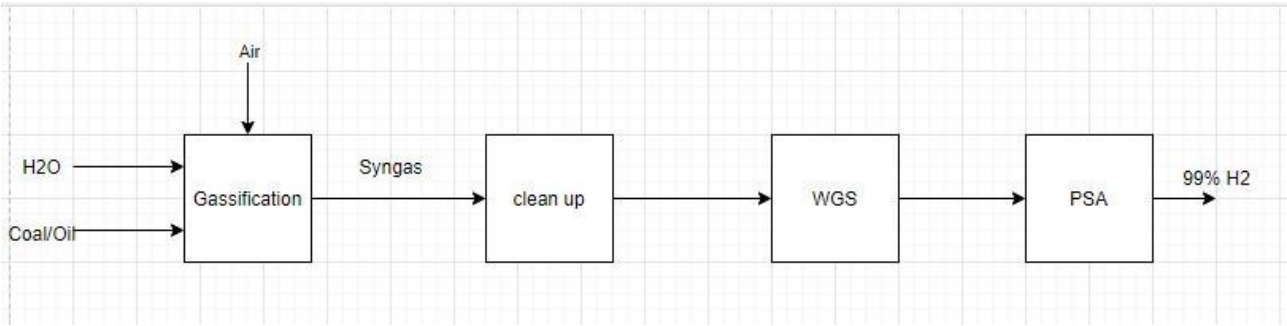

Figure 1.4-Liquids/Solids hydrogen production.

Catalytic-process.

In this process a photo-catalytic cell captures the solar radiation and use its energy to split the water into hydrogen and oxygen.

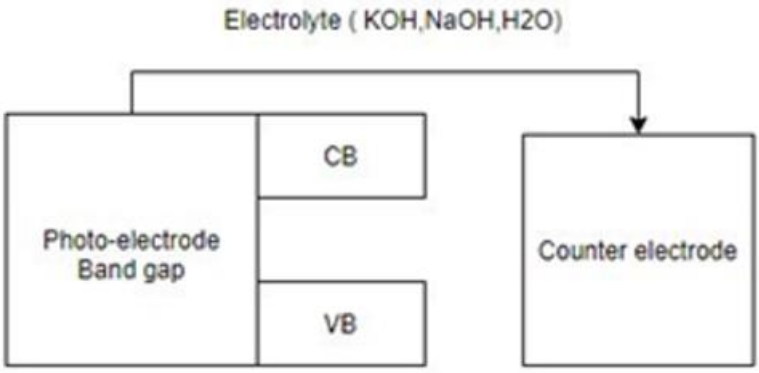

Figure 1.5-Catalytic process for the hydrogen production.

The solar radiation hit the photo electrode and if the protons contained by the wave have the proper level of energy the electrons that are present in the band gap can be removed and generate electron holes.

The H_2O molecules in contact with photo-electrode undergo in an oxidation state which delivers electrons to the electron holes in the valence band:

$$H_2O \rightarrow 2H^+ + 2e^- + \frac{1}{2}O_2 \quad (3)$$

This reaction creates a difference of potential between the valance band and the conductance band that we have assumed to be equipotential with the counter electrode.

At this point the e^- follows the voltage gradient that drives the electrolytic reaction:

$$2H^+ + 2e \rightarrow H_2 \quad (4)$$

Thermochemical Cycle.

A thermochemical cycle is a series of redox reaction, activated through the use of thermal energy, in which the final products are equal to the initial reagents and during one or more intermediate reactions there is a benefit.

In our case we use several redox reactions to split the water/ carbon dioxide into hydrogen/carbon monoxide and oxygen.

1.3-H_2 Storage Methods.

Hydrogen can be used also as an energy vector to store renewable energy. Different techniques are developed to store H_2:

Compressed gas storage.

In these types of storage, the hydrogen is compressed through a membrane wall compressor to avoid the contact between the H_2 and the lubricant oil of the tool.

The compressed hydrogen is stored in a cylindrical three layers vessel composed by an external layer made of low-quality metal, a wrapping layer of Aluminum or graphite and an internal layer composed by a high-density polymer.

This kind of storage technic is not recommended because the hydrogen's compression require a high amount of electrical work so the costs will be elevated.

$$L = \frac{Cp * T * \left(\beta^{\frac{1-\gamma}{\gamma}} - 1\right)}{\eta is} \quad (5)$$

(The Hydrogen specific heat is elevated so L will be high. The compressor can reach up a power of 11.2 MW)

Another issue connected with this type of storage is the embrittlement process that is a mechanical degradation caused by the compressed H_2 molecules that breaks the big grains of metal and lead to a degradation of the tank.

Liquified gas storage.

The production of liquefied H_2 occurs through a particular cryogenic cycle called Claude cycle which taking into account the conversion from Orto to Para configuration and the relative heat flux that is emitted when Hydrogen is cooled at a temperature lower than 21 K.

Liquefied H_2 is stored into a two concentric shells tank between whom vacuum is generated to avoid thermal conduction and convective losses.

Hastelloy, a steel alloy, is used to sustain the embrittlement process furthermore the two concentric shells are coated with low emissivity layer to reduce heat transfer inside the concentric shell.

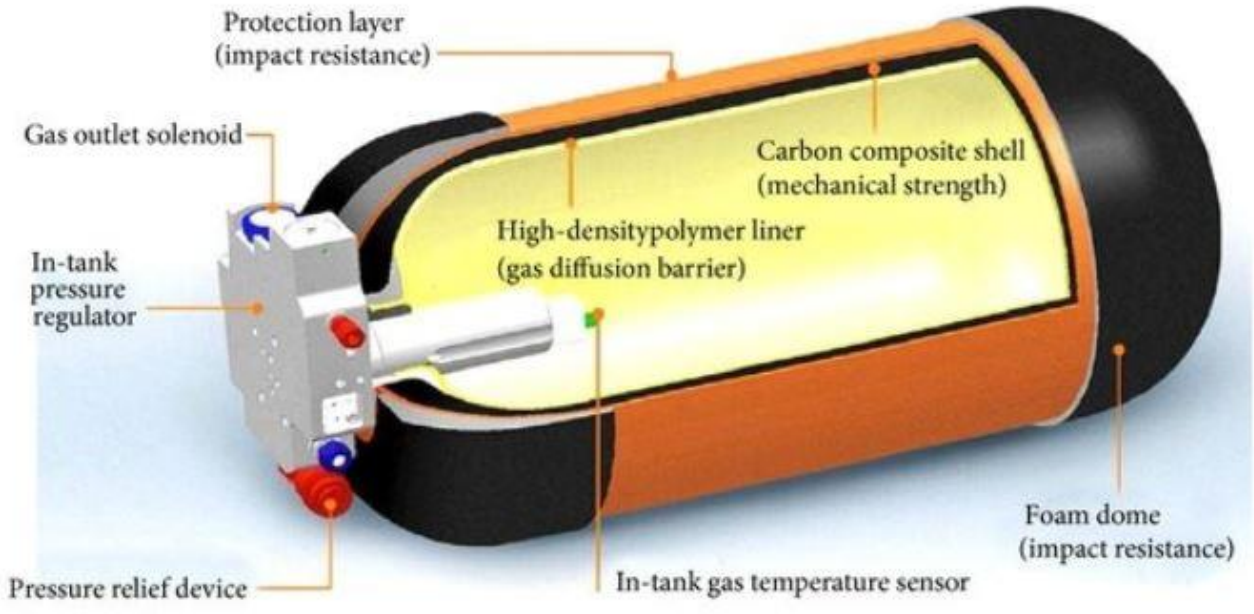

Figure 1.6-Liquified gas storage

Adsorption/Absorption.

- Adsorption of H_2 in a solid matrix.

Hydrogen is stored without chemical bonds between itself and the solid structure. Only adsorption phenomena occur at the surface of activated carbon surface, zeolites and metal organic framework.

- Absorption of H_2 in a solid structure.

Hydrogen is stored with chemical bonds between hydrogen itself and the solid structure. The most common materials used to perform hydrogen storage through the absorption process are metal hydrides because they have a good density (ρ_{H2}= 150 kg/Nm^3) and very low enthalpy of desorption. This means that from an energetic point of view it's very cheap to remove hydrogen from the solid structure and collect it back. In particular the most used metal hydride is Magnesium hydride MgH_2 that has an higher density (1.45 $\frac{g}{cm^3}$).

The thermodynamics of metal hydrides is described by the following graph:

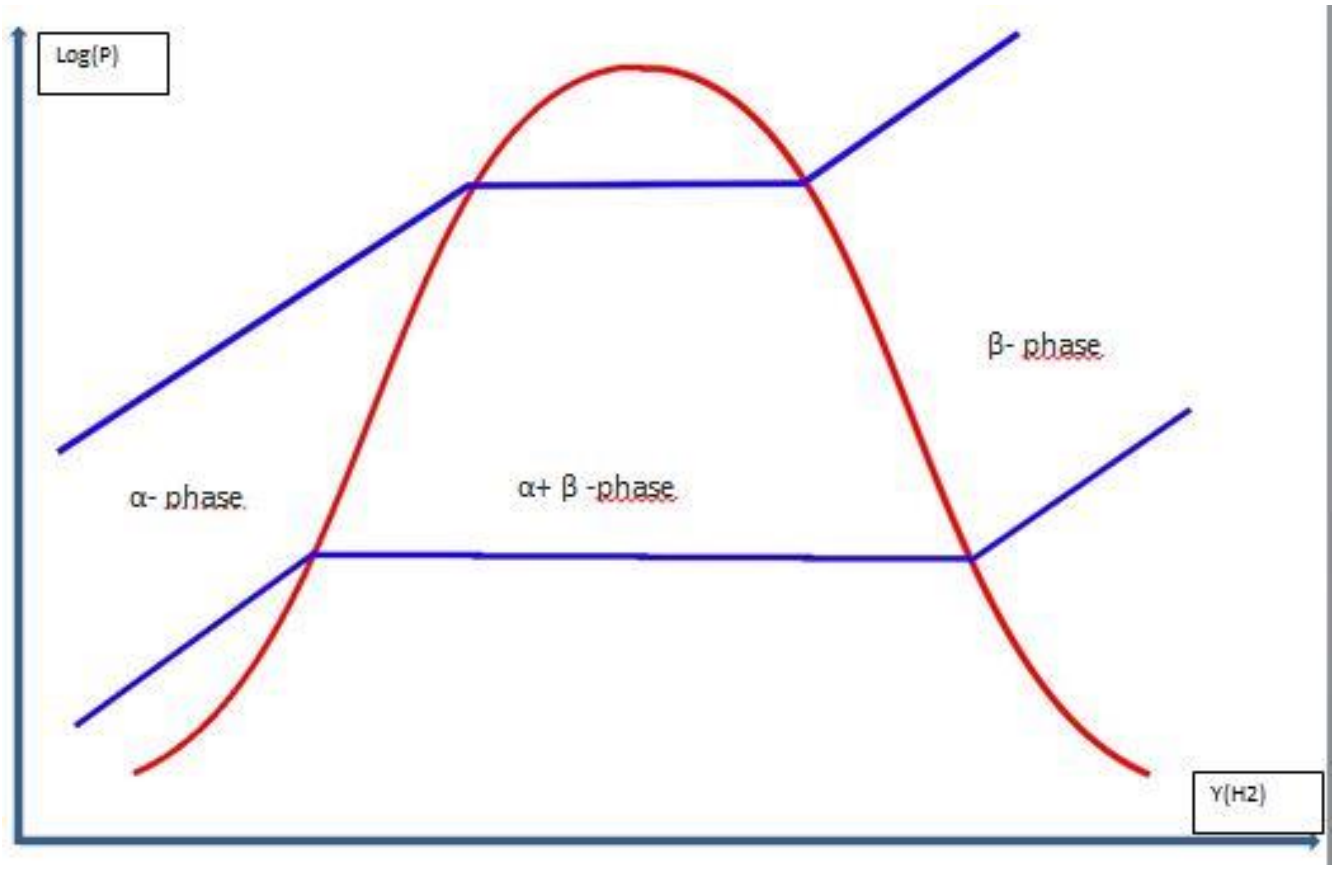

Figure 1.7-Thermodynamics of metal hydride.

In the α-phase there's only solid metallic present and H_2 is dissolved in the solid structure.

The β-phase or hydride phase is composed by the solid solution and determines the amount of H_2 that can be stored in a certain temperature.

The adsorption process is carried out on an isothermal at low temperature while desorption is carried out at high temperature.

In conclusion, H_2 storage in metal hydrides is only a matter of heat fluxes management: absorption is performed through the removal of heat while desorption is performed through a supply of heat for this reasons these systems are also called thermal pumps because they allow to store H_2 at low pressure and collect it at high pressure and the transition from low to high P is driven only by heat fluxes (no mechanical work is required).

2-Thermochemical Cycles.

Research on thermos-chemical cycles began in 1960 but obtained important results between the 1970 and 1980. The main financiers were industries and research institutions engaged in the nuclear sector diversify the final use of the thermal energy supplied by the reactors. The Joint Research Centre in Italy, Westinghouse in the U.S.A and Japanese nuclear research institute reached the main results.

Thermo-chemical cycles involve a series of chemical reactions where H_2/CO is produced with the net input of water/Carbon dioxide while other products are recycled. The process is a chemical loop so it starts and ends with the same compounds.

The global reaction is called thermochemical cycle because in one or more steps is required heat to activate the reactions. In our experience the heat is provided by concentrated solar power technology.

ADVANTAGES	DISADVANTAGES.
• $H_2$is produced from H_2O and solar energy without fossil fuel(green energy).	• A middle and high heat-input temperature is usually needed for the endothermic step and it must be optimized to be compatible with CSP technologies.
• H_2 and $O_2$are produced separately and the produced $H_2$is pure without CO or CO_2.	• Higher H_2yields prefer smaller reduced metal oxides particles. However, it is difficult to prevent nanoparticle deposition on the reactor surfaces.
• The chemicals that are employed are not corrosive.	
• The reactants are not consumed but recycled in a closed-loop.	

Figure 2.1- Advantages and disadvantages of the thermochemical cycle.

2.1 Redox reactions.

Thermochemical loops are characterized by redox reactions.

A redox reaction is a reaction in which one or more chemical species change the number of oxidation so there is an exchange of electrons. It is composed by two semi-reactions:

- Reaction of oxidation in which there is an increase of the chemical species' oxidation number due to an assignment of electrons.

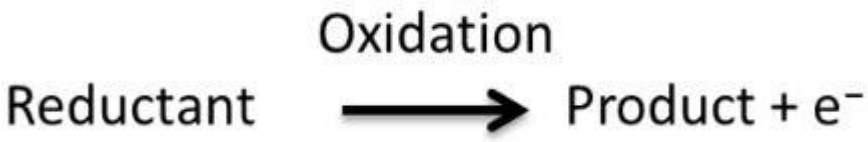

(6)

- Reaction of reduction in which there is a decrease of the chemical species' oxidation number due to an acquisition of electrons.

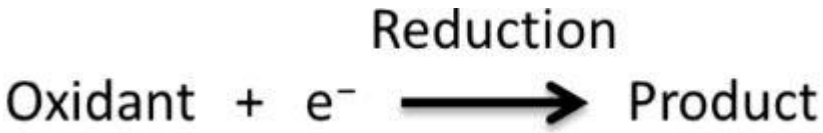

(7)

The chemical species that gains electrons are called oxidant.

The chemical species that lost electrons are called reductant.

2.2 Redox cycles of metal oxides.

In our project, we treat the redox cycles of metal oxides that are a particular thermochemical cycle in which the reactants are metal oxides.

This particular kind of cycle is exploited to split H_2O and CO_2 into H_2 and CO or both of them at the same time in this way it's possible to produce syngas that can be used in a catalytic reaction.

The cycle is composed by two semi-reactions:

- thermal reduction that is an endothermic reaction in which the metal oxide is reduced at high temperature to produce metal and oxygen.[3]

$$M_xO_y \rightarrow xM + y\frac{1}{2}O_2 \quad (8)$$

- Oxidation step (hydrolysis) that is an exothermic reaction that happens at lower temperature than thermal reduction.

In this semi-reaction we split the H_2O or CO_2 molecules to obtain CO or H_2 and the metal oxides.

$$xM + yH_2O \rightarrow M_xO_y + yH_2 \quad (9)$$

2.3 Classification of cycles.

Redox cycles of metal-oxides can be classified in two big categories:

- Volatile cycles in which the metal produced during the thermal reduction is in vapor state.

In this case Me-O is reduced so it is ready to accept a high amount of O_2.

- Non-volatile cycles that employ redox pair oxides which remains condensed during the whole process, in this way that kind of technologies bypasses the recombination issue found for the volatile cycles.

Me-O remains solid thanks to a non-stoichiometric reduction driven at a lower temperature.

$$MeOx \rightarrow MeO(x-\delta) + \frac{1}{2}O_2 \quad (10)$$

δ is the amount of oxygen removed and it depends by the temperature and pressure at which the reactions happen.

2.4 Multi-Step Thermochemical Cycles.

Multi steps thermo-cycle are composed by a series of three or more reactions.

From a plant complexity point of view this solution is less attractive than a simple thermochemical cycle because it requires at least three steps so it requires a more complex technology.

From a technological point of view this solution is much more interesting since the highest temperature required is 800 °C. The low temperature of reaction made this technology attractive for hydrogen production through nuclear reactors.

An example of a multi-step cycle is the Sulphur-Iodine cycle:

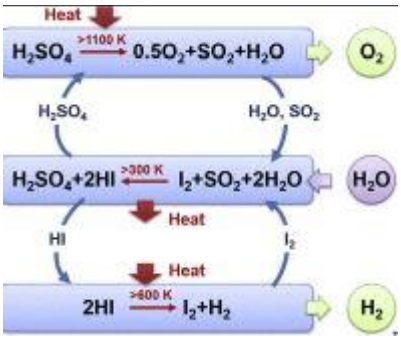

Figure 2.2-Multisteps cycle

2.5 Carbo-Thermal reduction.

It is a particular process in which the thermal-reduction of the metal is substituted with a chemically-aided reduction via carbon-containing species to reduce the thermal reduction temperature.

H_2 production by solar upgrading of carbon feed is suitable only for a transition period from hydrocarbon to H_2 economy.[4]

The reaction of an oxide with carbon or natural gas to produce the elementary metal can replace the first step of Thermal reduction:[5]

$$MexOy + yC \rightarrow xMe + y0 \quad (11)$$

An alternative solution to lower the reduction temperature is the metal's reduction under vacuum total pressures. This particular technique allows to eliminate the needs of purge gas so simplifying the process and avoid energy penalties associated with the inert gas recycling.

3-Solar Radiation.

3.1-Sun's structure.

The Sun is the star at the center of the solar system and it is the energy source that feeds CSP technologies. It has a diameter of 1.392.000 Km and a mass of 2×10^{30} Kg.

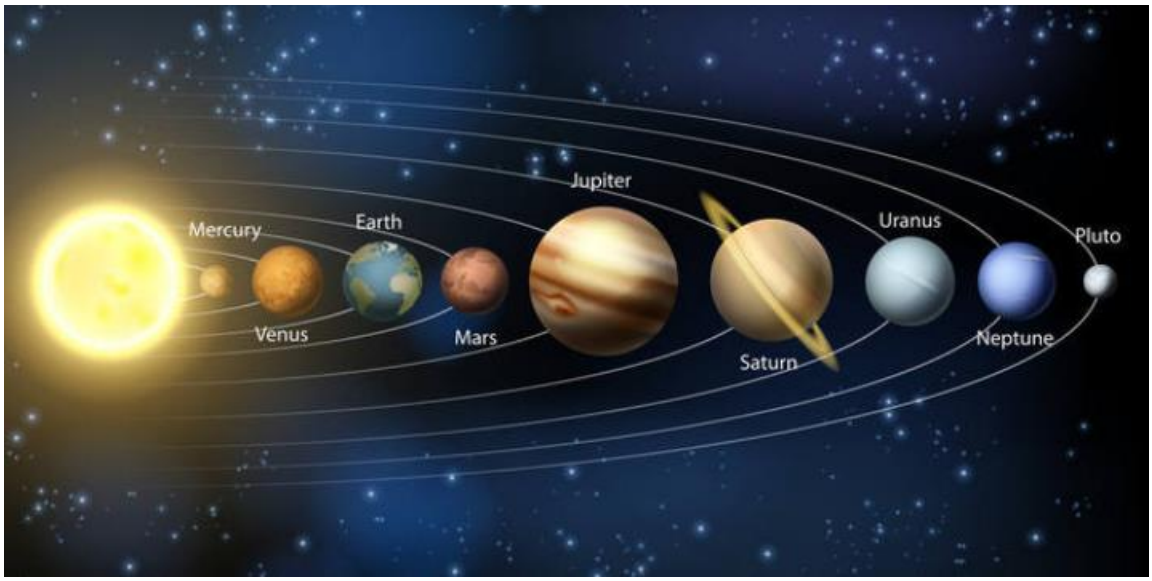

Figure 3.1-Solar system.

The celestial body is composed by Helium and Hydrogen and its structure is divided in concentric shell that creates different layers:

Core.

The internal concentric shell is the core which has an extension of 0.23R (R is the radius of the sun) and is characterized by high density and pressure.

In this layer the heat is produced by fusion process in which the Hydrogen H_2 is converted into Helium through the nuclear fusion reaction:

$$4p_+ \rightarrow 4He^{2+} + 2e^- + 2v + \Delta mc^2 \quad (12)$$

The protons of Hydrogen combine to form helium and realize positrons and neutrino. During the reaction there is a difference between the mass of the reactants and the mass of the products that is converted into energy:

$$E = \Delta m \times C^2 = 26{,}7 \text{ MeV} \quad (13)$$

Radiative zone.

The radiative zone is the layer adjacent to the core in which the energy that is generated in the centre of the sun is carried out through radiative process.

The radiative radius is included between 0.23R and 0.7R and the temperature is around 7 billion degrees Celsius while pressure and density decrease compare to the one that are reached in the core.

Convective zone.

The convective zone is the layer whose radius is included between 0.7R and R.

This part of the sun is characterized by the presence of the Solar Plasma that is an unstable fluid mixture electronically charged with a high energy density. In this layer the heat is exchanged through convective phenomena.

Photosphere.

The photosphere is the visible part of the sun and it is the site where the radiations are emitted in the space. This layer is characterized by the sunspots that are areas in which the magnetic field is elevated and the temperature is lower compare to the other part of the sun surface. These irregularities are studied because affects the temperature of our planet and can be causes of pollution.

Cromosphere.

The cromosphere is a thin layer of the sun characterized by a red colour that becomes visible during the sun's total eclipse.

This region of the sun is mainly composed by hydrogen and it is the site in which happens the solar prominences which are huge gas eruptions that reach also 150000 Km.

Corona.

The corona is the most external part of the sun and it's composed by a mixture of hydrogen and residual gasses that arrives from the underlying layers.

This region is characterized by an elevated temperature and the presence of iron ions which create spectral lines during the Sun's total eclipse.

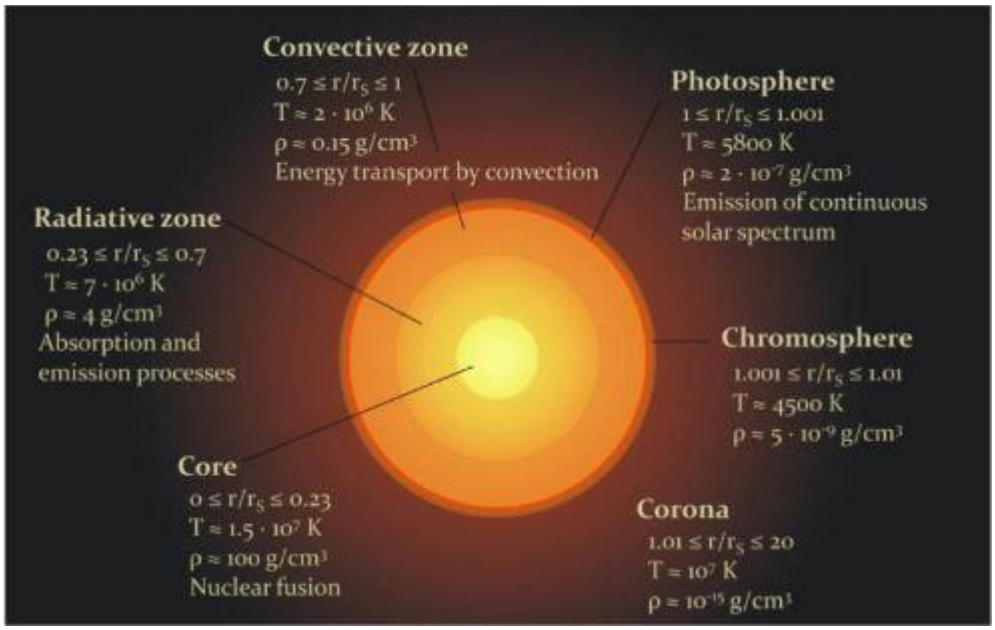

Figure 3.2-Sun's structure.

3.2-Sun's energy.

The quantum physics approximated the sun as a black body at the temperature of 5778 K. The power emitted by the celestial body can be calculated through the Stephan-Boltzman equation:

$E = \sigma T^4$ W/m^2 σ=5.67*10^8 W/m^{2}K (14)

The thermal radiation is the radiation emitted by the sun for its temperature and its behavior is described by the Plank's law:

$$E_\lambda = \frac{e_{1\times\lambda^5}}{e^{\lambda_{max}}} \quad (15)$$

The wavelength at which is reached the maximum temperature is $\lambda_{max} = \frac{2898}{T_{max}}$

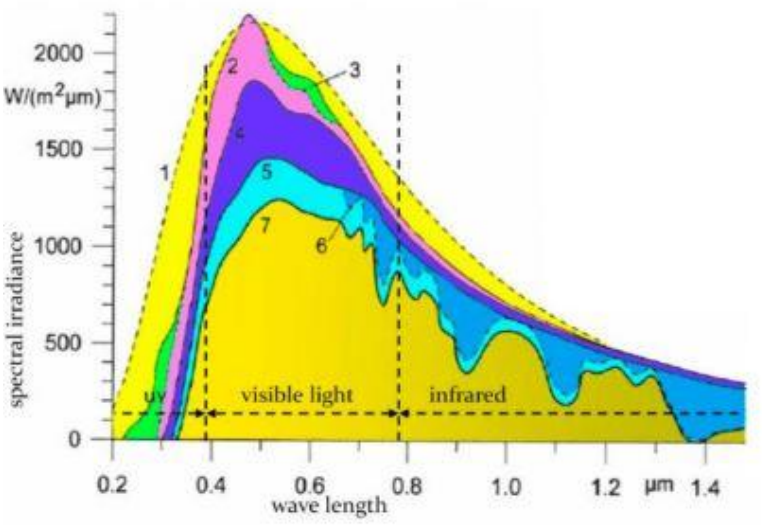

Figure 3.3-Solar spectrum.

The major part of the solar spectrum is composed by visible light which is preceded by ultraviolet radiation and it's followed by infrared rays.

3.3-Photons.

The light that is emitted by the Sun is an electromagnetic radiation with a proper frequency and wavelength. Although the radiation can be described as a wave phenomenom it can be considered also a photon flux in which the particles are absorbed or emitted by the atoms in fair quantities.

According to the quantum theory the wave behavior of the light it's evident when diffraction or interference phenomena occurs during its displacement in the space. On the other hands the corpuscular nature of the radiation occurs when it interacts with the fundamental particles.

In conclusion the matter can emits or absorbs energy through photons that are "energy pockets". The photon's power is proportional to the frequency of the electromagnetic radiation and its described by the Plank's law:

$$E = h \times v \ \text{J} \tag{16}$$

h= plank's constant.

v=wave frequency.

3.4-Interception of solar radiation.

The capturing surface of CSP technology should be oriented so that the sun's rays are orthogonal to the active surface so a reference system is needed to describe the position of the star during the different hours.

- Equatorial reference system.

In this type of system the fundamental plane is the equatorial while the coordinates that are used are the solar declination (δ) and the clockwise corner (w).

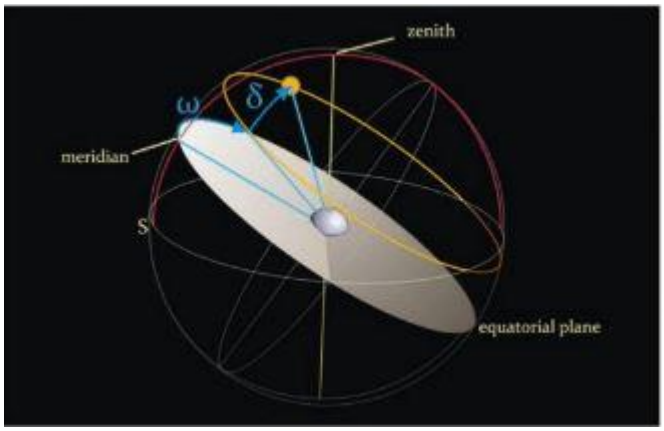

Figure 3.4-equatorial reference system.

The equator is the plane passing through the observer and the sun.

The declination is the angle between the equatorial plane and the Earth-Sun line.

The clockwise corner is the angular displacement of the Sun from East to West in the local meridian due to the rotation of the Earth around its axis.

- Horizontal reference system.

This system uses the local plane of the observer as fundamental plane. The coordinates that are used are the altitude angle (αs) that is the angle between the horizon and the Earh-Sun line, and the solar Azimuth (γ_s) that indicates the angular displacement between the south and the projection of the solar beam on the horizon plane. Instead of the solar altitude it's possible to use the Zenith angle (θz=90- αs) that is the angle between the vertical line and the Earth-Sun line.

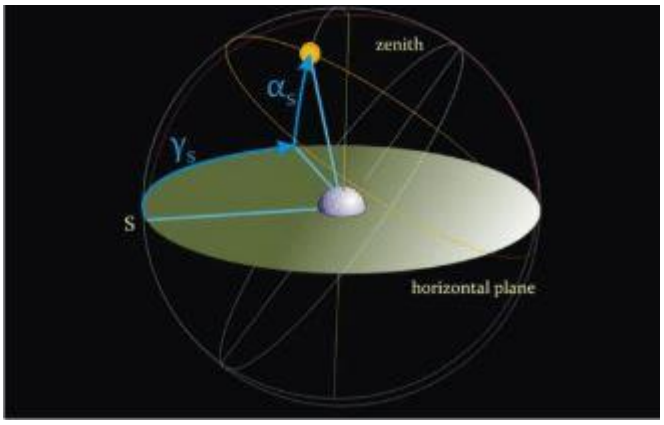

Figure 3.5-Horizontal reference system.

The calculation of the equatorial coordinates is the first step to define the sun's position:

- The solar declination is calculated through a trigonometric function that oscillates between -23.45 that coincides with the winter solstice and +23.45 that coincides with the summer solstice.

$$\delta = 23.45 \times sin\left(\frac{360\times(284+n)}{365}\right) \quad (17)$$

n=Ordinal day of the year.

- The clockwise corner is calculated keeping in mind that the earth rotates about 15 degrees per hour on its axis:

$$\frac{360}{24h} = 15\left[\frac{^\circ}{h}\right] \rightarrow \quad w = (localtime - 12) \times 15^\circ \quad (18)$$

Once that the equatorial references system is defined is possible to calculate the horizontal coordinates:

- The solar altitude is calculated through a trigonometric function: and it's positive during the sunrise while it's negative after the sunset:

  $$sin(\alpha s) = sin(\Phi) \times sin(\delta) + cos(\Phi) \times cos(\delta) \times cos(w) \quad (19)$$

  To calculate the solar altitude is necessary to define the geographical coordinates of the place:
  Latitude(Φ) that is the angle between observer-earth centre line and equator plane.
  Longitude(L) that is the angle between the local meridian plane and Greenwich meridian.

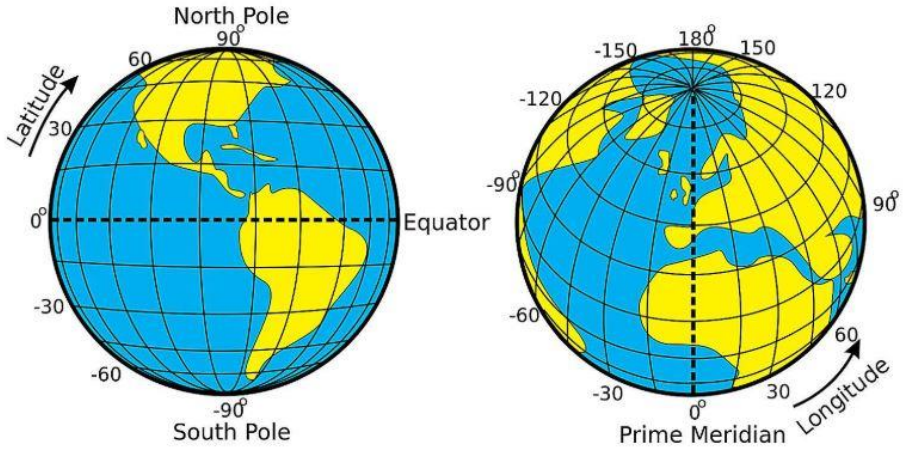

Figure 3.6-Latitude and longitude.

Finally is possible to calculate the Solar Azimuth (γs) as:

$$cos(\gamma s) = \frac{sin(\alpha s) \times sin(\Phi) - sin(\delta)}{cos(\alpha s) \times cos(\Phi)} \quad (20)$$

3.5-Time.

The time references system is fundamental to describe the sun's position.

There are two different times:

- Standard time that is the time given by the local clock.
- Solar time that is the time based on the apparent angular rotation of the sun across the sky. Conventionally the solar time is equal to 12 am at noon.

3.6-Extiction phenomena.

When the radiation crosses the atmosphere two different extinction process that reduce the energy of the solar radiation can occur:

Absorption.

Process that involves the absorption of part of the energy transported by solar radiation.

In detail the Stratospheric Ozone (O_3) absorbs the ultraviolet solar radiation with a wavelength lower than 290 nm while H_2O and CO_2 absorb the infrared part of the solar spectrum.

The final composition of the incident solar radiation on the Earth surface will be composed by 10% of ultraviolet rays, 45% visible light and 45% infrared light.

Scattering.

The scattering happens when the direct propagation of the solar radiation is deviated because of atmospheric Aerosol and so part of the radiation reaches the earth surface as diffuse radiation.

There are two different types of scattering:

Rayleigh scattering that happens when the electromagnetic radiation is deviated by particles whose diameter is much smaller than the wavelength of the solar radiation.

Mie-scattering that happens when the electromagnetic radiation is deviated by particles whose diameter is of about the same dimensions as wavelength or larger.

Rayleigh Scattering as a strong dependence on wavelength whereas Mie-scattering depends by the local conditions as the air pollution.

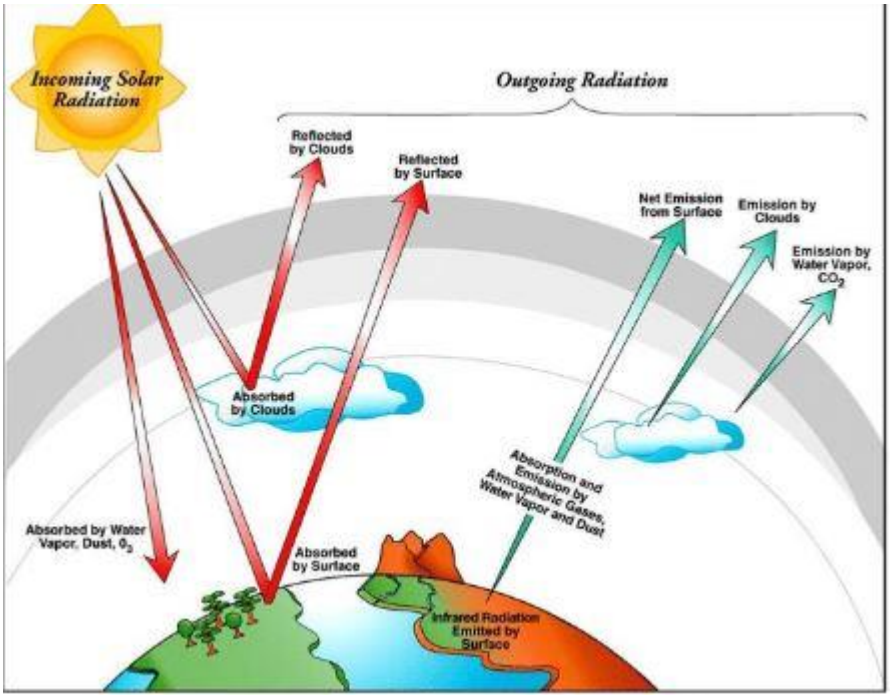

Figure 3.7-Extiction phenomena.

3.7-Irradiance.

The energy source of a CSP systems is the direct solar radiation that hit the surface of the receiver.

The first step is to calculate the solar constant G_{sc} that is the irradiance received on a Unit Area of surface perpendicular to the sun beam at mean Earth-Sun distance outside the atmosphere and can be calculated as:

$Ps = 4\pi {r_s}^2 \sigma T^4$=3.85*$10^{26}$ W (21)

$Gsc = \frac{Ps}{4\pi {r_s}^2}$=1367 W/$m^2$ (22)

At this point the radiation crosses the atmosphere and due to the scattering phenomena is splitted into:

$Gtot = Gb + Gd + Gr$ (23)

- Gb:direct solar radiation .
- Gd: Diffuse radiation that is the solar radiation received by a unit surface from the sun after that its direction has been changed by atmospheric scattering.
- Gr: reflected radiation that is the solar radiation absorbed by the ground and reissued for the reflection phenomena.

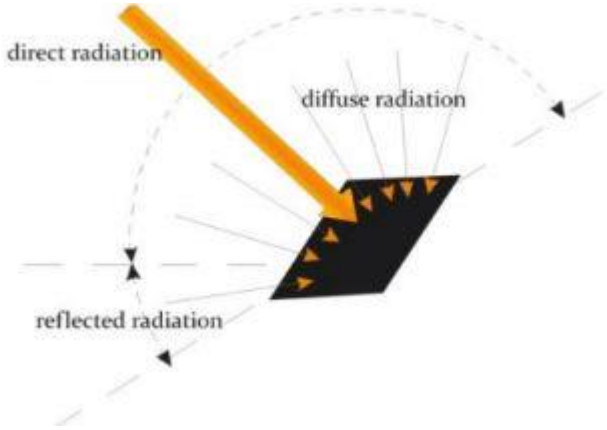

Figure 3.9-Components of the solar irrandiance..

The sum of the three components is called Total irradiance or Global solar radiation.

The global irradiance on a tilted surface that in our experiment represents the active surface of the CSP receiver can be calculated as:

$Gtot = Gb + Gd + Gr = Gbn \times cos(\Theta) + Gdn \times Fsc + Gbt \times \rho \times (1 - Fcg)$ (24)

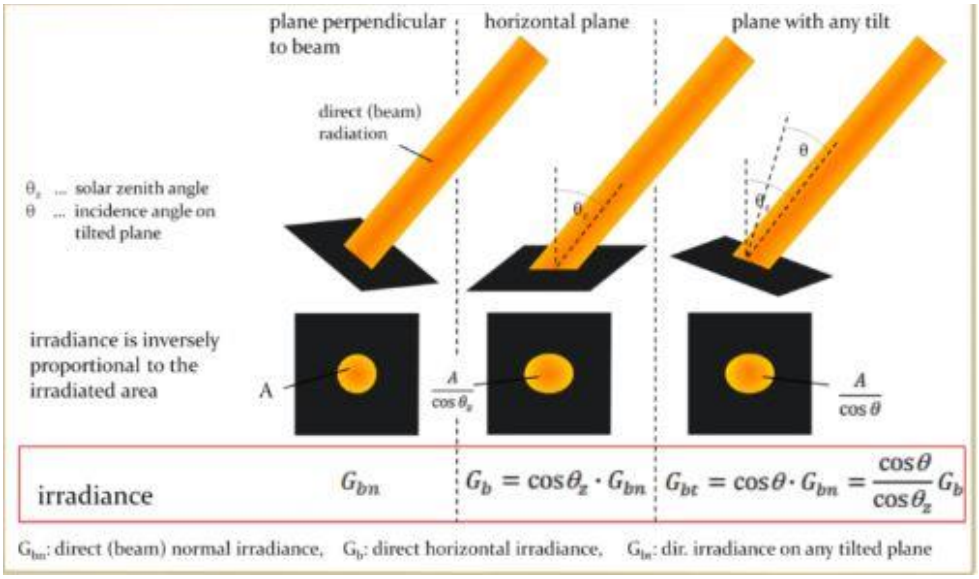

Figure 3.10-Solar Irradiance on a tilted surface.

- Gbn is the direct irradiance that perpendicular to a horizontal plane.
- Gdn is the diffuse irradiance that is perpendicular to a horizontal plane.
- G_{bt} is the irradiance of the direct solar radiation on tilted surface whose tilt angle is equal to β.
- ρ is the Albedo it's the reflection coefficient of natural surfaces.
- F_{sc} is the view factor between the collector and the sky that represent the ratio between the total energy that is emitted by the sun that is incident on the surface of the collector and the total energy of the sun.

$$F_{sc}=\frac{1+cos(\beta)}{2} \quad (25)$$

- F_{cg} is the view factor between the collector and ground and represents the losses due to the irradiation between them.

$$F_{cg}=1-F_{sc}=\frac{1-cos(\beta)}{2} \quad (26)$$

- Θ is the incidence angle that is the angle between the direction of the solar radiation and the normal on the radiated surface.

  For a plane that is perpendicular to the direction of the solar radiation the incidence angle is equal to 0 while for a horizontal surface the incidence angle is the zenith angle
- β is the tilt angle of the receiver surface. It should be optimized in order that the solar radiation will be incident on the active surface for the greatest possible amount of time during the day.

The optimal tilt angle depends by the sun's position and by the geographic coordinates of the place in which the surface is located; the general guideline is that it should be elevated during the winter because of the elevated solar altitude while it should low during the summer.

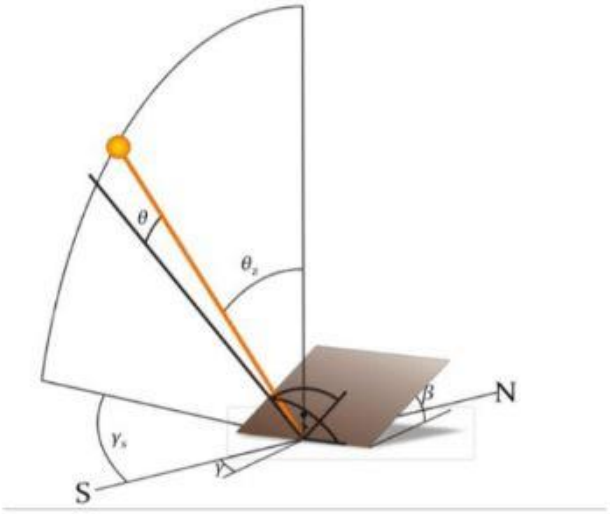

Figure 3.11-Tilt angle.

4-Concentrated Solar Power (CSP).

Concentrated solar power technology uses the concentration of direct solar beam and conventional thermal process to generate electricity and so to provides base load electricity[7]

In our experience we will use CSP in order to produce heat and obtain the temperature that is required for the thermal reduction in the chemical looping.

4.1-Components.

A CSP system is composed by different components:

- Bearing structure that has the function to maintain the parabolic through in the right position and protect it from possible hurt. In this component stiffness is required because also a little deviation increase optical losses and reduces the efficiency.
- Tracking system that should maintain the mirrors in line with the incident solar radiation. Tracking accuracy is required because a little deviation in the orientation of the mirror surface increase the optical losses. While it has possible to adjust parabolic through based on sensors, this is not easily done with heliostats or Fresnel reflectors where multiple surfaces contribute radiation to a focal point or a focal line.
- Receiver that converts the solar radiation that is projected on it into thermal energy. It should have an elevated absorption for the solar spectral range and its emissivity must be lower than infrared in this way there is a high absorption and low heat losses.
- Heat transfer fluid (HTF) that is the medium used as an energy vector for the thermal energy. There are two different configurations based on the types of HTF that is used:

Direct steam generator (DSG) in which water/steam is used as a heat transport medium. In this configuration high pressure steam is generated by concentrating solar radiation in a one-step process.

indirect steam generator that is a configuration in which an aromatic hydrocarbon as thermal or synthetic oil is used as an energy vector. One of the most important advantages of these configuration is the low vapor pressure related to the oil.[8]

- Secondary concentrator which is used to distribute the radiation flux equally on the tube of a linear collector receiver or to further concentrate the radiation flux entering an absorber.
- Absorber plate that absorbs the solar radiation and converts it into thermal energy.
  The ideal absorber plate has a high absorptivity in the solar part of the black spectrum and high reflectivity and so very low absorptivity and so emissivity from 5 to 55 um.

- Controls system which sends signals to the tracking system in order to guarantee the right tracking of the sun path. It is composed by solar sensors connected to the mirrors that absorb the radiation and it is essential in order to achieve the elevated temperatures.

4.2-Application.

Many different powers conversion cycle has been considered for use with concentrated solar power technology with different working fluid.

Stirling engines.

The Stirling cycle is generally well matched to the characteristic of a parabolic dish concentrator. Concentrated solar flux from dishes can provide isothermal, high temperature heat with good efficiency. Stirling engines can be coupled directly to the dishes or indirectly via sodium heat pipes.

Steam engines/ generation.

Concentrated solar power technologies connected with a steam engine allows to obtain an engine efficiency of 21.9%

Organic Rankine cycles.

For this system we have to use an indirect cycle in which the heat transfer fluid is the Toluene whose vapor reach a temperature of 400 C.

This cycle allows to obtain an engine efficiency of 22.9%.

Concentrator photovoltaic (CPV).

CPV is dominated by refractive optics concentrators (lens). In these systems is critically important to achieve an uniform flux profile for a good performance that can achieve also the 30% solar to electricity efficiency.

Thermochemical cycle.

Solar thermochemical processes for producing fuels and for chemical energy storage.

In our experience we will use a thermochemical cycle in order to produce H_2/CO and syngas.

4.3 – Parameters.

The main parameters that we have to consider to evaluate the performance of a Concentrated Solar Power plants are:

Efficiency.

The efficiency represents the ratio between the Thermal energy that is transfer to the fluid to the incident solar energy that heat the mirror of the CSP technologies.

In our computation we have to taking into account the optical losses due to blocking or shadowing effects that depends from the types of CSP technology that is used.

Concentration ratio.

The concentration ratio is defined as the ratio of the radiant flux after the concentration to the ratio before the concentration and can be approximate as:

$$C = \frac{ApertureArea}{AbsorberArea} \tag{27}$$

The temperature of the absorber is proportional to the concentration ratio.

4.4 – Line concentrator.

Line concentrator focus all the radiation on a line and this allows to reach lower temperature and obtain lower thermal losses.

The focal line is obtained by considering a parabolic mirror in which the radiation that arrives parallel to the optical axes are reflected in a way that it passed through the focal point whose coordinates are calculated through:[9]

$$\frac{1}{4f}x^2 = y \tag{28}$$

Where f is the focal length.

The focal-line is obtained extending the focal point along an axis.

Parabolic through.

The parabolic through collectors are the most used CSP technologies and the parameters that are used to characterize its form are:

- aperture width (a)= the distance between one rim and the other.
- Focal length (f)= distance between the vertex of the parabola and the focal point.
- Through length (l)
- Rim angle(fi)=angle between the optical axis and the line between the focal point and the mirror rim.

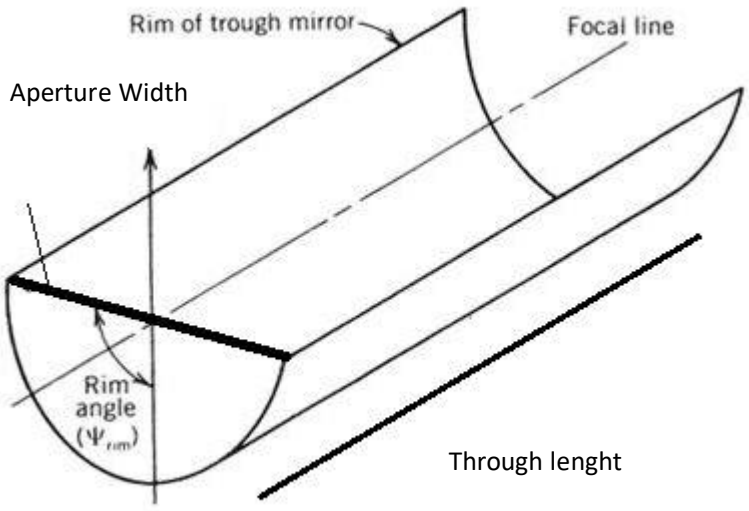

Figure 4.1-Parabolic through.

The reflectivity of the mirrors should be elevated and it is required a specular reflection so the light that come from a single incoming direction is reflected into a single outgoing direction. In order to obtain these properties, the mirrors are coated with silver glass that has a long life expectancy. An alternative can be low-iron glasses mirrors that are used to increase the transmission of the light.

The receiver is composed by an absorber tube that has the function to absorbs the solar radiation. It's composed by a ceramic layer, a cermet layer and a metallic layer. It is placed in the focal length of a parabolic stands.

A glass tube is used to protect the absorber tube and reduce the convective heat losses . Between the glass tube and the absorber tube there is the vacuum in order to decrease the radiative losses.

At last at the end of the receiver there is a bellows that is used to absorbs the different thermal expansion of the metallic components and the glass tube.

A line-focusing system require only one-axis technologies and for parabolic through technologies there is only two possible alignments:

East-West Alignment that tracks the sun from the north and south and at noon the full aperture faces the sun. In this configuration there's a high incidence angle and so the performance is reduced during the early and later hour.

North-South Alignment that tracks the sun from the east-west line. In this system there is a more equilibrate daily performance and the losses are higher in the early and later hour than at noon. On the other hands it is more sensible to the difference between summer and winter.

Linear Fresnel collector.

Fresnel principle is based on the chopping of a lens into a lot of surface with discontinuity between them. This allow a reduction of thickness and volume. This principle it is applicable also to the mirrors. So an optical element is divided into a lot of sub-elements that have the same optical effects.

Figure 4.2-Linear Fresnel collector.

Linear Fresnel Mirror can be constructed substituting - a parabolic through by linear segments that focus the radiation to the focal line. The Linear Fresnel has the same characteristics of the parabolic through that is copied.

The mirror in the Linear Fresnel collector is made of flat mirrors stripes with a small curvature. The reflected material in this set up is silver.

The main parameters that characterize this kind of collectors are:

- Width of the individual mirror stripes. It shouldn't be too narrow because we will need more flat mirror in order to obtain the same aperture Area. On the other hands it had not be too large because in this way will not be possible to reflect constantly the direct solar radiation onto fixed absorber.

- Collector width if the collector is too narrow less radiant flux will be reflective on the receiver however if it's too broad the collector will be more sensible to geometrical and tracking error.

- Distance of the absorber tube from the mirror plane. At short distance the blocking and shadowing effect will be higher and the angle of incidence will be very high. At long distance the mirror radiant flux will be lower and the system will be more sensible to geometrical and tracking error.

- Gap between the mirror stripes. Small Gap causes higher blocking and shadowing between the mirror stripes, a large gap causes a broad width collector.

- Curvature of the mirror stripes that should not be too much broad or narrow because in both cases part of the radiation will miss the receiver.

The collectors tracking system is calibrated and tracked according to the solar position algorithms. Usually the Fresnel collectors are in a north-south alignment.

The receiver is composed by an absorber tube with a selective coating and a secondary concentrator located near the absorber tube to improve the intercepts factor without increasing the diameter and so the thermal losses so create a thermal insulation.

From an economical point of view Fresnel collectors have lower investment costs, lower operation and maintenance costs and lower levelized energy costs of the electricity than the parabolic through power plants.

On the other hand Fresnel collectors have higher optical losses because mirror stripes don't follow the sun. They also present higher shading and blocking effects because of the fact that is impossible to find the right curvature due to the changing of incident angle change during the day.

4.5-Point concentrator.

Point-concentrator solar power technologies focus the solar energy in a point. This configuration allows to reach higher temperature and higher efficiency than the linear concentrator; On the other hands it is a more expensive technologies and has higher thermal losses.

Central Receiver Systems (CRS).

CRS is a point-focusing system that uses individually tracked heliostat mirrors to concentrate direct solar radiation onto a stationary receiver located on the top of a tower.

Figure 4.3-Solar tower.

The Heliostats are a two-axis tracking mirrors that follow the sun's path, they can have different form as the canted-glass mirror, that is a single large heliostat that is divided into a number of sub-mirror, or the hexagonal-shape mirrors that reach also a ground coverage of 100%.[10]

Heliostat can have different size from 1 $m^2$to 150 m^2 and can be located at a maximum distance of 100m. They are concentrated in a solar field that causes the major part of the investment costs.

The solar fields location is important in order to optimize the performance so the heliostat field must be placed to the north of the tower in the northern hemisphere while it must be placed to the south of the tower in the southern hemisphere.

Even though the optimization of the field position other losses can occur:

- Optical losses that are due to the azimuth and zenith angle that changing the orientation every second so the effective mirror area is lower than the actual mirror area.
- Blocking losses that are presents when a heliostat cannot reflect part of the radiation on the receiver because is blocked by another heliostat.
- Shadowing losses that are due to a front heliostat that cast a shadow on the behind heliostat or on the sideway.

- Atmospheric attenuation that depends by the turbidity of the sky.
- Mirror reflection losses that depends by the degree of the surface degradation.

The aiming strategies represents the techniques that are used in order to distribute the irradiation on the receiver and obtain a uniform temperature distribution and a good density flux. The main strategies that are used are:

- Single-aim point

  All sun's image is reflected by the heliostats and concentrated in a single point on the receiver.
- One dimensional "smart" aiming

  Smaller and best focused sun's images reflected by the heliostats near the tower are reflected along a vertical line on the receiver surface.
- Two dimensional "smart aiming"

  Smaller and best focused sun's images that are reflected by the heliostats near the tower are aimed along vertical and horizontal line of the receiver.
- Single aim-point lower part of the receiver

  Best images are reflected by the heliostats in a point as close as possible on the bottom part of the receiver.
- One-Dimensional aiming at the lower part of the receiver

  Sun's images are reflected in a horizontal line as close as possible at the bottom of the receiver.

Solar Dish.

Figure 4.4-Solar Dish.

Solar dish is a point focusing system that uses curved solar sun tracking to concentrate direct solar radiation onto a receiver. [11]

This type of technologies is suitable for stand-alone installations, off grids and small grids but are commonly accepted as the most efficient concentrated solar power technologies for the conversion of solar energy into electric or chemical energy.

The perfect concentrator has a parabolic shape but some solar concentrators approximate this shape with multiple, spherically shaped mirrors supported with a truss structure.

The reflective mirrors are mounted on an approximate parabolic-shaped structure using stamped sheet metal. The size of the solar concentrator is determined by the power that is needed in the final applications.

The reflector is also structural component because it must maintain optical accuracy and structural integrity under wind and gravitational loads while in different orientation.

Concentrators use a reflective surface of aluminum or silver, deposited on glass or plastic, an alternative low –cost options could be polymer films. The concave surface is covered by a second-surface glass

mirrors and a partial vacuum is drowning in the space in the space bringing the reflective membrane into an approximately spherical shape.

The dish is mounted on a structure that tracks the sun continuously throughout the day to reflect the highest percentage of sunlight possible onto a thermal receiver.

The most popular tracking system used for the solar dish technologies is the Azimuth-Elevation tracking systems. In this case the primary axis of the reference system is an azimuth dish rotates in a plane parallel to the ground. The secondary axis is an elevation axis which is rotating with the mirror surface around the azimuth axis where the plane is perpendicular to it. This configuration allows at the reflector to rotate up and down and right and left and these rotation changes throughout the day and varies during the year.

An alternative solution used for small solar dish systems is the polar tracking system where the collector rotates around an axis parallel the earth's axis and the other is perpendicular to the polar axis.

Cavity receiver are often used in these kind of technologies because conduction losses are smaller compared to radiation and convective losses.

The elevated solar to chemical efficiency and the reduced costs compare to the other CSP systems makes solar dish the most suitable technologies for our experience.

4.6-Solar Receivers.

Solar receivers absorb the solar radiation and convert it into thermal energy through a heat transfer medium.

There are different types of solar receivers that are classified on the basis of the materials, the heat transfer fluid and the physic process that allow to exchange the heat.

External Receivers.

In an external receiver the concentrated solar radiation directly hit the external surfaces of the structure which are composed by absorbent material that transfers the heat inside the receiver at the heat transfer fluid.

A Tubular shape is the most common solution for this kind of receivers and it guarantees an economic and simple realization.

An external cylindrical tubular receiver is composed by parallel pipes through which the thermal fluid flows.

The Heat Transfer Fluid (HTF) usually is molten salt or water/vapor and its direction is perpendicular at the incident solar radiation. The external surface of the receiver is coated with a material characterized by a high absorptivity.

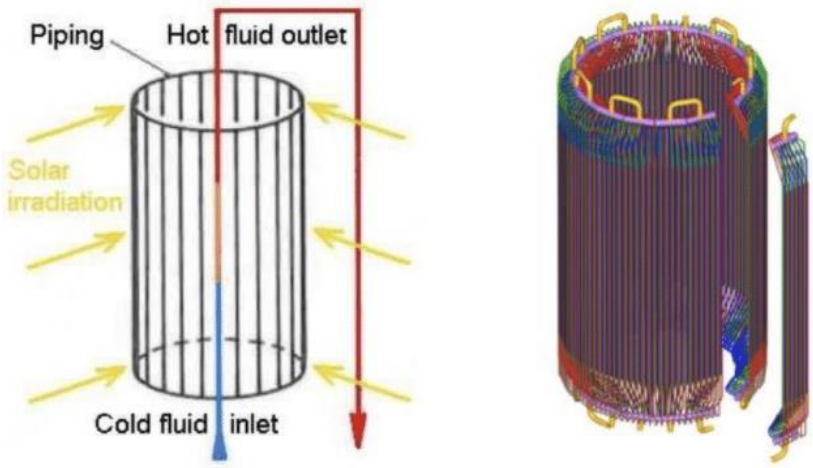

Figure 4.5-External tube receiver.

Cavity Receivers.

In a cavity receiver the concentrated solar radiation is aimed in an aperture which is coated with insulating material.

The internal surfaces of the cavity correspond to the tubular absorber of the external receivers and the heat transfer medium could be molten salt or water but also gaseous substances.

Cavity receivers were designed to reduce the radiative losses because only a little part of the solar radiation that enters in the cavity is reflected back in the atmosphere through the aperture.[12]

However it is necessary to find a right compromise on the size of the aperture because a wide opening guarantees a high quantity of energy but increases the radiative losses.

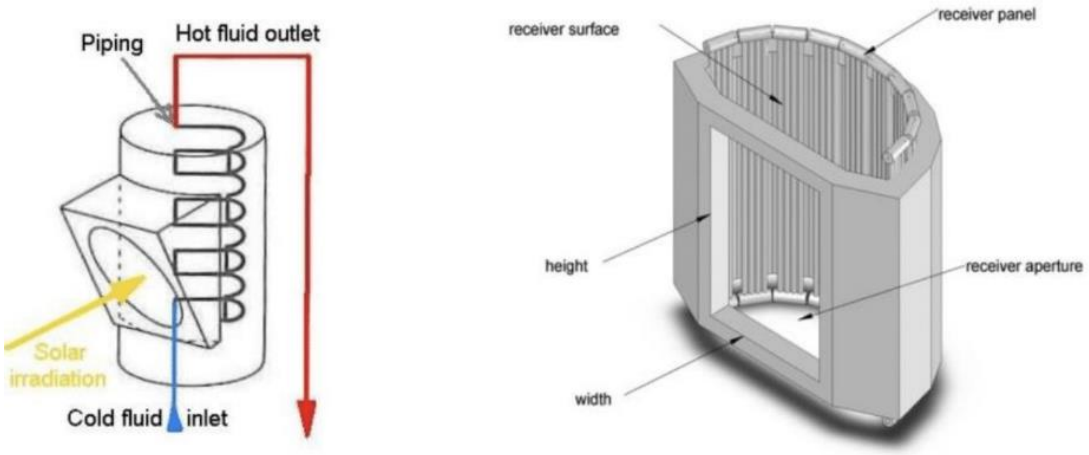

Figure 4.6-Cavity Receiver.

Cavity receiver can be classified in direct receiver in which the heat transfer fluid is the fluid that completes the Stirling cycles in the motors and indirect receiver in which there is a fluid that acts as a mediator between the receiver and the motor.

Molten Salt Liquid Film Receiver.

It is a particular kind of direct-absorber receiver that is applied at the solar tower systems.

It is composed by a cold salt storage tank, a hot salt storage tank, a cone shape receiver that is located at ground level and a steam generator that is directly connected to the receiver.

When the concentrated solar radiation hit the receiver the salt is pumped from the cold salt storage tank through the salt distribution system.

In the receiver's aperture the salt is heated by the solar radiation and becomes molten salt which is pumped to the hot salt storage tank. The molten salt stored is pumped to an indirect steam generator which use the heat that is contained in the salt to create vapor. Finally the salt is pumped back to the cold salt storage.

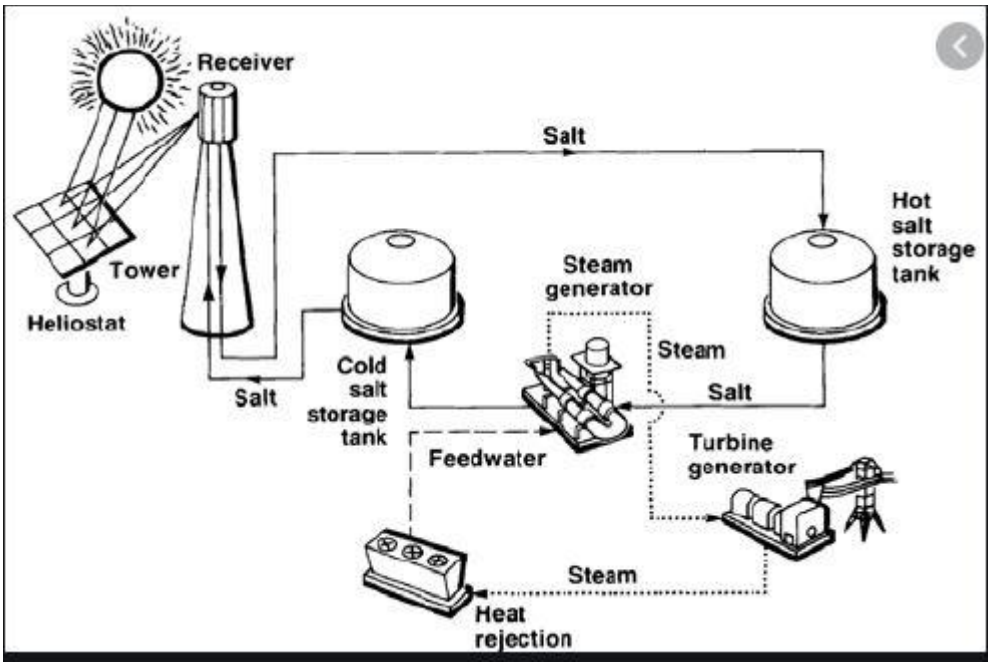

Figure 4.7-Molten salt receiver.

Volumetric Receiver.

Particular kind of receiver in which a fluid or a solid particle is directly exposed at the concentrated solar radiation. It is called “volumetric receiver” because the solar radiation can be absorbed by the entire volume of the absorber.

The absorber can be a stationary matrix (grid, wire mesh, honeycomb structure) or a set of moving solid particles composed by porous materials that absorbs the solar radiation and transfers heat to a gaseous fluid which is forced to pass through the pores of the material.

The main advantage of the volumetric receiver is the use of air as heat transfer fluid despite its low heat transfer coefficient because the heat deposition occurs on the entire three dimensional structure.

In addition through the volumetric effect the outlet air reaches an higher temperature than the receiver’s surface because the direct between the absorber surface and the working fluid allows a very efficient heat transfer.

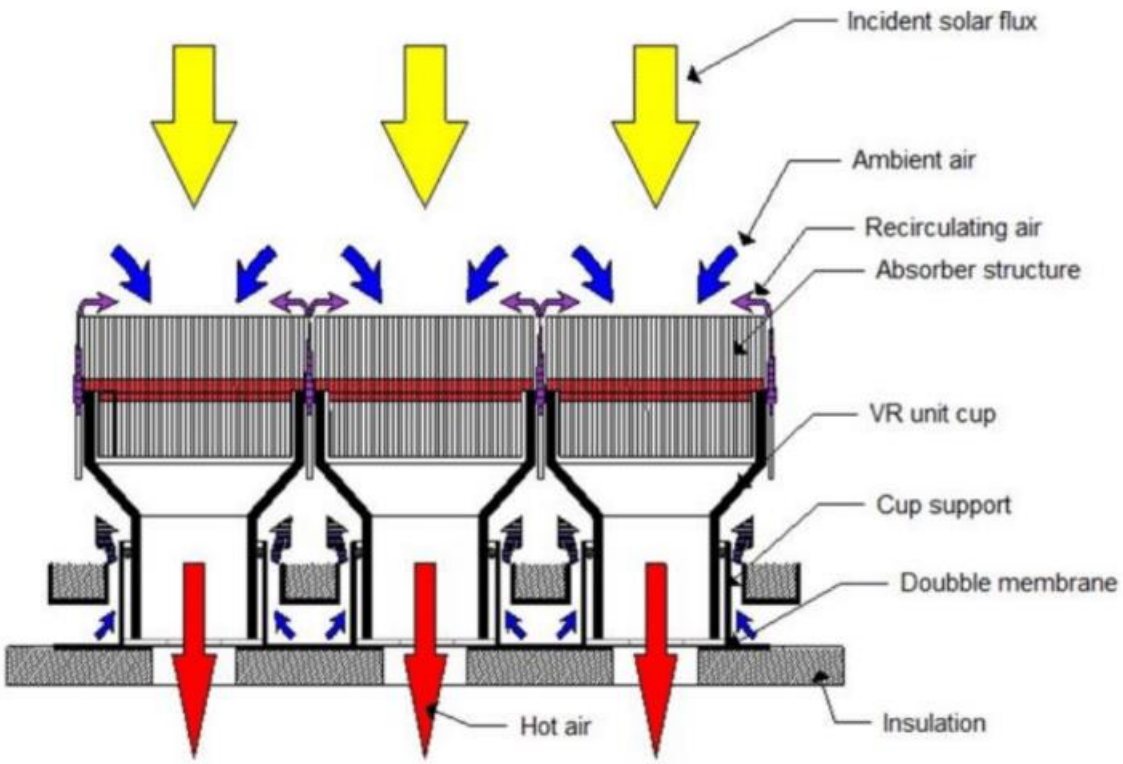

Figure 4.9-Air volumetric receiver.

The average temperature is regulated by varying the air flow rate so as to maintain a constant temperature of 680 C in the ducts downstream of the receiver.

An open volumetric receiver operates directly under ambient pressure and the solar radiation that enters in the absorber is reflected and further absorbed by the structure.

An alternative solution is the pressurized volumetric receiver in which the inlet air used as heat transfer fluid is pressurized at 15 Bar by a compressor.

Fallen particles Receiver.

The fallen particles receivers belong to the category of direct absorber receiver in which the heat transfer fluid is directly exposed at the concentrated solar radiation.

In this case the solid particles

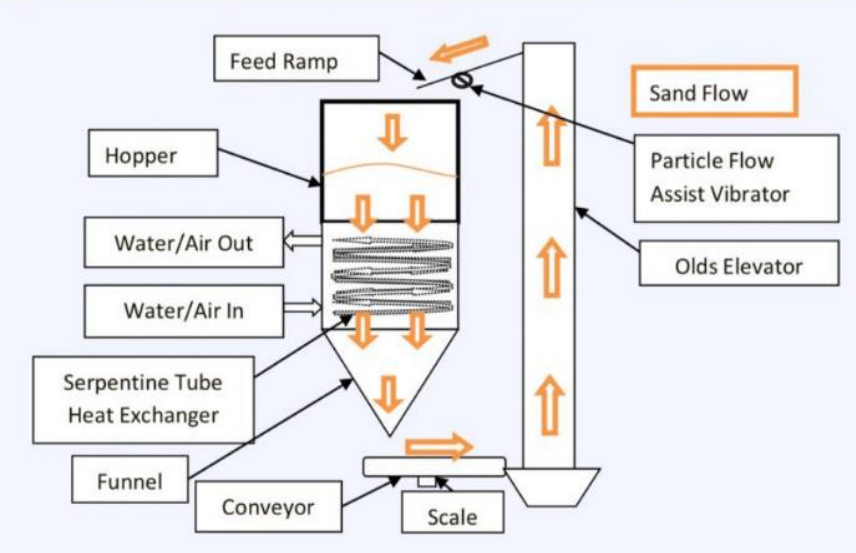

Figure 4.9-Fallen particles receiver.

4.7-Performance and efficiency of solar receiving devices.

In this paragraph we evaluate the main losses related to the receivers that involve thermodynamics cycles for the production of syngas or liquid fuels.

This particular class of receiver is characterized by a high absorption coefficient and low thermal losses furthermore the receiver expansion due to the temperature variation must be reduced as possible.

The tubular receivers are coated with thermal insulators in order to reduce the optical and thermal losses. The following table shows the materials and the operative temperatures for the tubular and volumetric receivers.

Materials for receiver tubes		Operative temperatures [°C]
	Incoloy 800 HT	600
	Inconel 625 LCR	565
Typical steel alloys	Haynes 230	565
	Austenetic stainless steel	> 800
	Silicon-carbide	1500
Ceramic	Alumina-Silica	1200
	Sintered Alumina	>1800
Materials for volumetric receivers absorbers		
	Wire mesh	1000
Porous materials[HEM]	Ceramic Foam	1700

Figure 4.10- Receiver's materials.

The operative temperature of sintered alumina (1800 °C) is higher that the ceria's thermal reduction temperature (1600 °C) so this types of receivers result the most suitable for our experience.

The "Monte-Carlo ray tracing" simulation applied on the collector and the receiver components allows to compare the thermal flows deposited near the receiver in the ideal and real cases.

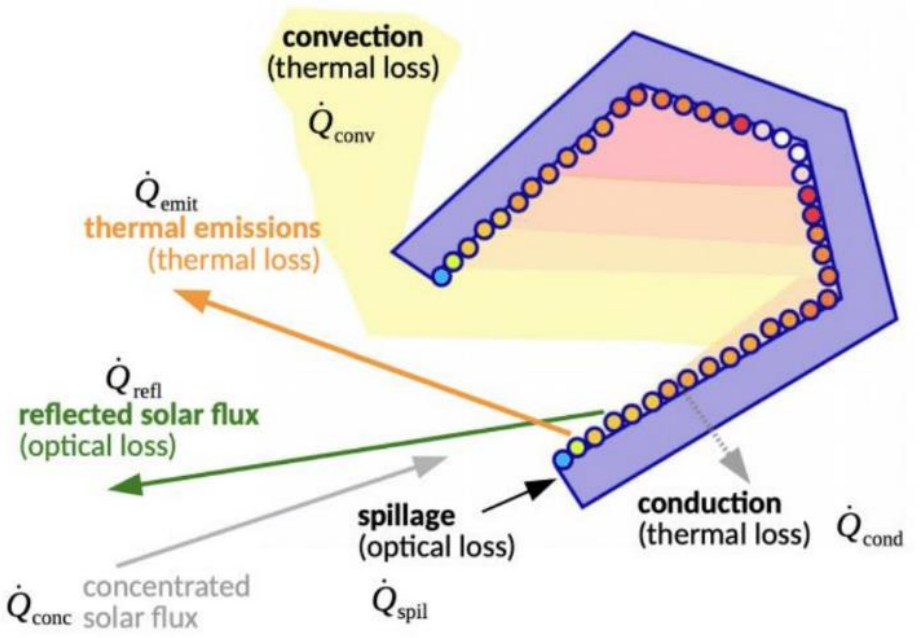

Figure 4.11-Receiver losses.

In this way it is possible to estimate an energy balance on the receiver and to evaluate the device performance that should be designed in order to optimize the efficiency:[13]

$$Q_{usefull} = Q_{conc} - Q_{spill} - Q_{refl} - Q_{emit} - Q_{conv} - Q_{cond} \quad (29)$$

Q_{conc}: Concentrated solar radiation incidents in the direction of the receiver.

Q_{spill}: Solar radiation that does not affect the opening of the receiver.

Q_{refl}: Solar radiation that is reflected off the receiver.

Q_{emit}: Losses due to the emission of thermal radiation.

Q_{conv}: Thermal losses due to natural/forced convection.

Q_{cond}: Conductive losses due to the internal heat exchange.

The solar radiation that is absorbed by the receiver is obtained by the difference between the concentrated solar radiation incidents in the direction of the receiver, the solar radiation that does not affect the opening of the receiver and the solar radiation that is reflected off the receiver:

$$Q_{abs} = Q_{conc} - Q_{spill} - Q_{refl} \quad (30)$$

Moreover we know that the global radiation that is absorbed by the receiver is related to the average ratio of optical concentration, the direct irradiance and the effective absorption coefficient:

$$Q_{abs} = \alpha_{eff} \times C \times G \times A_{apert} \quad (31)$$

α_{eff}: absorption coefficient.

C: average ratio of optical concentration.

G: Direct irradiance.

A_{apert}: Aperture area.

The optical concentration ratio is obtained by the ratio between the intensity of the solar radiation on the receiver and the global intensity of the solar radiation. The average value is obtained integrating the effective value for the receiver area:

$$C_{optical} = \frac{I}{I_{solar}} \quad (32)$$

$$C_{average} = \frac{\int I \, dA_{apert}}{I_{solar} \times A_{apert}} \quad (33)$$

Now it is possible to write a simplified version of the energy balance:

$$Q_{usefull} = Q_{abs} - Q_{emit} - Q_{cond} - Q_{conv} \quad (34)$$

The real receivers have not a plane surface so is possible that the reflected radiation can be absorbed by another part of the surface. This behavior modifies the effective emissivity of the receiver that in the particular case of a cavity receiver can be calculated as:

$$\varepsilon_{eff} = \frac{\varepsilon}{\frac{A_{aperture}}{A_{cavity}} + \varepsilon \times \left(1 - \frac{A_{aperture}}{A_{cavity}}\right)} \quad (35)$$

ε : emissivity.

$A_{aperture}$: Aperture Area.

A_{cavity}: Cavity surface.

The surface that is heated by the solar radiation emits energy according to the Stephan-Boltzman Law:

$$Q_{emit} = \sigma \times \varepsilon_{eff} \times A_{apert} \times (T_{ext}^4 - T_{env}^4) \quad (36)$$

σ: Emission coefficient.

T_{ext}: External temperature.

T_{env}: Environment temperature.

The convective losses depend by the heat transfer coefficient which is a combination between the effects due to the natural and forced convection on the external surface of the receiver.

The natural convection is function of the density variation of the air located near the receiver's surface. The Nusselt number is the adimensional parameter that taking into account the heat transfers from a vertical isothermal plane:

$$Nu_{natural} = \left[0.825 + \frac{0.387 \times Re^{\frac{1}{6}}}{\left[1+\left(\frac{0.492}{Pr}\right)^{\frac{9}{16}}\right]^{\frac{8}{27}}}\right]^2 \quad (37)$$

$$Nu_{forced} = 0.332 \times Re^{\frac{1}{2}} \times Pr^{\frac{1}{3}} \quad (38)$$

Re: Reynolds number.

Pr: Prandtl number.

If the receiver's temperature increases Nu decreases while the heat transfer coefficient raises because the thermal conductivity K of the air is higher:

$$h = \frac{Nu \times k}{L} \quad (39)$$

h: convection coefficient.

The convection coefficient is used to calculate the heat losses due to convection:

$$Q_{conv} = h \times A_{ext} \times (T_{ext} - T_{env}) \quad (40)$$

A_{ext}: External surface of the receiver.

T_{ext}: External temperature.

T_{env}: Environmental temperature.

In a cavity receiver is possible to modify the cavity's shape to reduce the natural and forced convection thermal losses. In a cylindrical receiver the natural convection losses are of the order of 1% while the forced convection losses 2-3%.

The possible minimization of convective losses can be achieved by enclosing the surface of the receiver by a transparent window or, for a cavity receiver, by using an air flow to retain hot air currents inside the receiver. The receiver's windows increase the reflection losses but reduce the thermal radiation that is emitted.

Another method is to insert in the cavity a glass characterized by a low transmissivity for the infrared radiation, in this way is created a useful containment greenhouse effect that reduces the thermal losses.

The last term Q_{cond} in the balance equation () represents the conduction losses:

$$Q_{cond} = A_{ext} \times \frac{T_{ext} - T_{env}}{R_{cond}} \quad (41)$$

R_{cond}: Conductive resistance of the material.

The heat is transfers at the working fluid consequentially for a cylindrical receiver the thermal flux has to flow through the thermal resistance of the main selective coating, the walls and the convective boundary layer inside the tube.

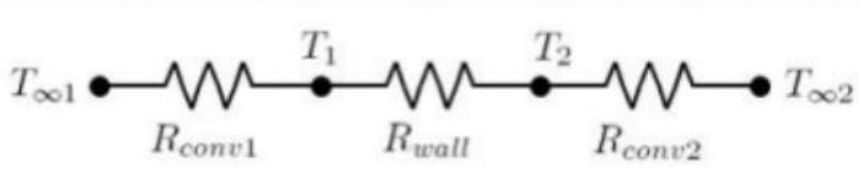

Figure-Conductive thermal resistances.

The thermal resistances in figure () imply a difference of temperature between the heat transfer fluid and the cavity of the receiver that depends by the thermal flux that crosses the walls.

The useful heat is calculated through the use of R_{tot} that is the sum of the different thermal resistances related at the external absorption surface:

$$Q_{useful} = \frac{A_{ext} \times (T_{ext} - T_{fluid})}{R_{wall}} \quad (42)$$

Even though for elevated flux the receivers should reduce the losses as much as possible sometimes arranging smaller surfaces and imposing a greater flow through the receiving wall, the thermal resistance tends to limit the benefit given by the greater availability of heat.

This effect is due to the fact that if the heat transfer fluid temperature is kept constant the temperature of the external walls will increase and as consequences also the thermal losses.

In conclusion the Global energy balance can be written as:

$$\frac{A_{ext} \times (T_{est} - T_{env})}{R_{wall}} = \alpha_{eff} \times C \times G \times A_{apert} - \sigma \times \varepsilon \times A_{apert} \times (T_{ext}^4 - T_{env}^4) - h \times A_{ext} \times (T_{ext} - T_{env}) - A_{ext} \times \frac{(T_{ext} - T_{env})}{R_{cond}} \quad (43)$$

If the internal temperature of the fluid is considered as a constant value equal to the operative temperature is possible to solve the energy balance equation through an iterative method and calculate the average temperature of the external receiver's walls.

Now it is possible to calculate the efficiency of the solar receiver that is equal to the ratio between the useful thermal flux that taking into account the optical and thermal losses and the concentrated incident radiation.

$$\eta_{receiver} = \frac{Q_{useful}}{Q_{incident}} = \frac{\alpha \times C \times G \times A_{aperture} - \sigma \times \varepsilon \times A_{aperture} \times (T_{external}^4 - T_{environment}^4) - h \times A_{external} \times (T_{external} - T_{environment})}{C \times G \times A_{aperture}} \quad (44)$$

In this formula the conductive and geometrical losses are neglected.

In conclusion is possible to create a relation between the receiver's efficiency and the optical concentration factor and the average temperature of the cavity.

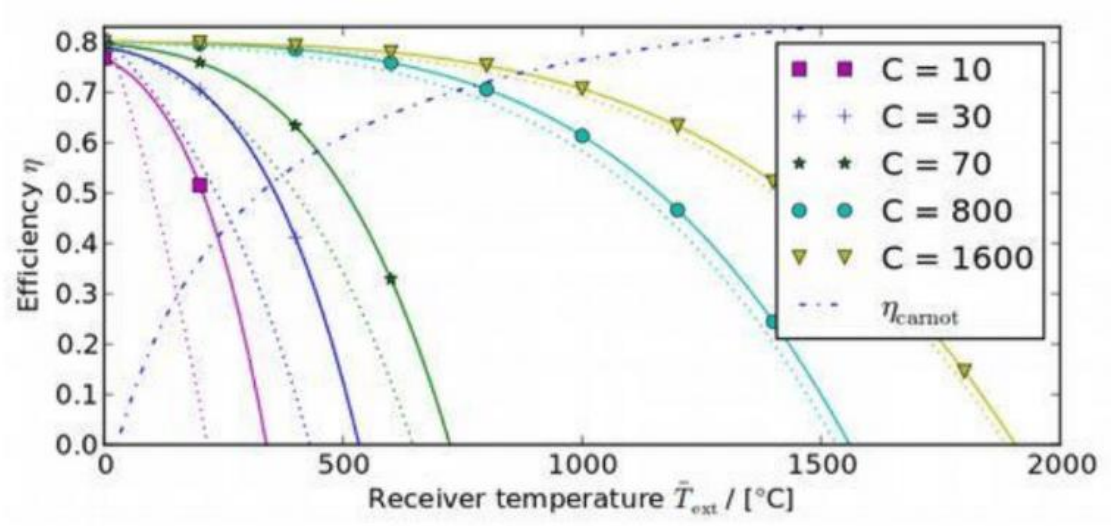

Figure 4.12-Receiver's efficiency.

The thermal losses are proportional to the receiver's dimension so a small aperture area decreases the heat that is dissipated. On the other hand a larger area allows to capture a superior amount of solar radiation, in this way the spillage losses are reduced.

Taking into account these two different effects is possible to find the optimal dimension of the receiver's surface for a certain temperature and heat flux.

4.8-Solar Reactor.

In our experience the technologies used for capturing the solar radiation must be coupled with a traditional reactor.

The reactor is the place where the thermochemical reactions happens and in particular there is an analogy between the redox reactions and the catalytic reactions in which the gaseous species reacts with the surface of a solid catalyst.

The catalytic reactors are classified according to the distribution of the catalyst particles that can be distributed randomly (Fluid bed reactors) or with a criterion in the space (Foam reactors, Membrane reactors). Both the categories of catalytic reactors are suitable to operate as solar reactors in which the fuel is a redox material.

The solid particles of the catalyst can be placed inside tubular receivers that are exposed to the sun (IIR reactors) or can be directly irradiated by the sun (DIR reactors).

The reactors configuration depends by the type of redox materials and cycles.

In case of volatile cycle the system is composed by two separated reactors in which the first one is the place where the reduction process take place and the reactants are composed by a reduced phase mixed with a gaseous oxygen.

The second reactor is dedicated at the oxidation process that happens thanks to the use of a medium fluid usually vapor or CO_2.

On the other hand for the non-volatile cycle the recombination problem is avoided so the reactors are projected in order to perform both reduction and oxidation process.

Roca (Rotating cavity reactors).

It's a particular kind of DIR reactor composed by a rotating cavity with a quartz window that is used for dissociation of zinc oxide and the consequent production of syngas.

This system exploits the centrifugal force to move the ZnO particles towards the external walls;

in this way it's created an external layer of Zinc oxide that is directly exposed to the solar radiation and it has a function of radiative absorber, thermal insulator and chemical reagent.[6]

The process is constantly fed with a gaseous flow that has the function to clean up the quartz window and cool down the system.

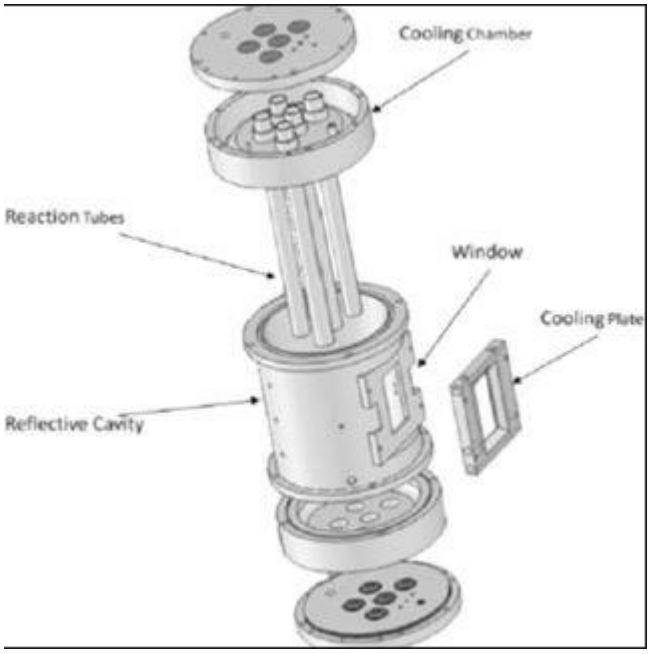

Figure 4.13-Roca reactor.

Porous Ceramic Foam Reactors.

Reactors that are directly irradiated by the solar radiation and use a ceramic foam composed by redox materials.

In the cavity of the system there is a monolithic cylinder composed by cerium oxide whose internal walls are irradiated by the concentrated solar radiation that enters through an opening window.

The reagent gases pass through the porous structure until they reach the internal cavity while the exhaust gases leave the system through an aperture that is located on the bottom of the reactor.

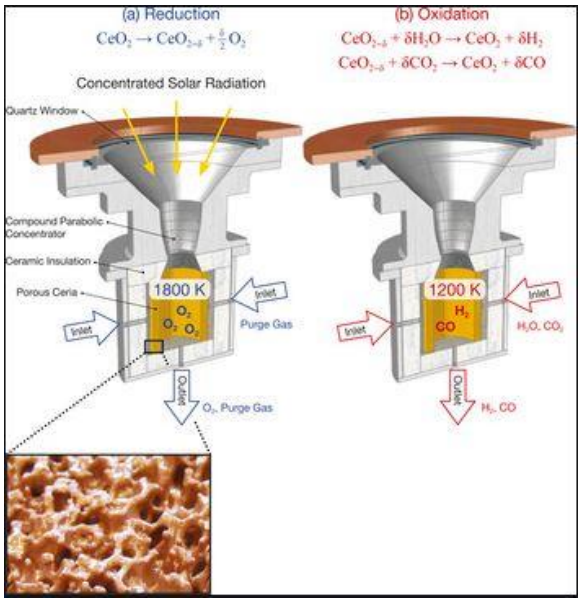

Figure 4.14-Ceramic foam reactor.

Aerosol Reactor.

Aerosol reactors represent the best performing solution for the Ceria's chemical looping.

The system consists of a receiving cavity crossed by a vertical aluminum tube in which solid particles of ceria fall down under the gravity's effect while an inert gas used to separate the oxygen from the reduced Ceria flows in the opposite direction.

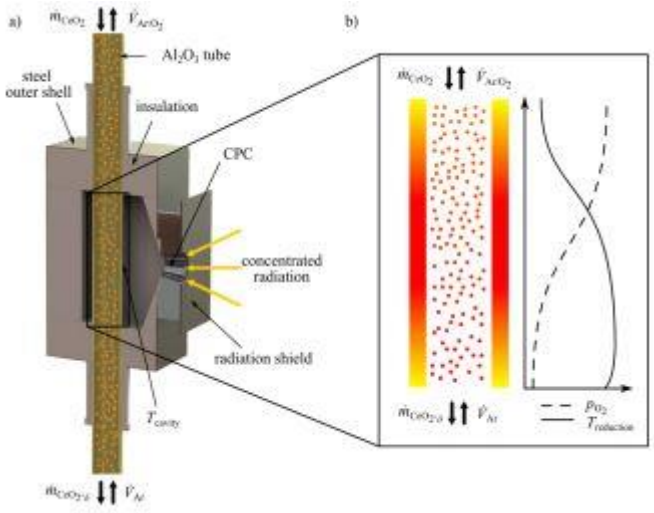

Figure 4.15-Aereosol reactor.

The main advantage related to the Aerosol's technologies is the opportunity to modulate and scale the whole system implementing the number of pipes. Furthermore the reactors that operate with particle

streams allow to decouple the oxidation and reduction phases in order to avoid the sintering of the powders thanks to the dynamics of the moving particles.

4.9-Measurements.

Radiation measurements is important in order to know the maximum irradiance that is possible to obtain by concentrated solar power technologies.

Ground measurements.

Ground measurements of the solar radiation is obtained through pyranometers which are solarimeters that operate through a thermopile. These particular tools measure the difference of temperature between a surface and a body having a suitable thermal mass not exposed to the sun.

The peculiarity of the pyranometers is to measure a very wide spectrum band of solar radiation furthermore their hemispherical windshield allows to neglect the cosine losses.

Figure 4.16-Pyranometer.

Pyranometers are classified by the component of the solar radiation that is measured:

- Pirheliometers which measure the direct component of the solar radiation.
- Pyranometers which measure the solar global radiation.
- Shaded band pyranometers which measure the diffuse components of the solar radiation.

Satellite measurements.

The weather measuring satellites allow to complete and integrate the information from ground measurements because provide data relating to areas without weather stations. The satellites allow to photograph the earth's surface and measure the global irradiance, in this way is possible to determine the temperature and humidity of the atmosphere.

Figure 4.17-Satellite.

The data obtains by the satellites are processed in order to obtain a cloud index related to a certain location in an accurate time period.

Reflection measurements.

The final performance of the power plant is strongly influenced by the optical quality of the solar collectors. In order to qualify and reduce the optical losses, several reflection measurements are used.

- Photogrammetry can be used to measure the local shape deviation of solar concentrators; During the last decade digital photogrammetry has progressed to an exact and efficient short distance measurement systems for analyzing the quality of optical components of a solar concentrator.

- Deflectometry is an alternative solution that uses projections of tests cords to characterize reflecting surfaces. The range of application covers analysis of basic elements of optical instruments.

- Laser analysis uses a scan with a laser beam to scan the local slopes of a mirror , finding the point of incidence of the reflected beam and calculating the resulting surface normal.
  Infrared light can be used to measure the absorbers temperatures. There are limitations due to the fact that the glass tube is not transparent to radiation with wavelength greater than 4 um. On the other hand, the infrared signal should not be affected by the reflected solar radiation in order to detect a signal that corresponds well to the absorber surface temperatures, filters have to be used that transmit only a thin band of radiation.

- Para – scan measurement consists of two separate detectors that are installed on the absorber tube and which scan the reflected incoming sunlight radiation by moving across the length of the tube though a moving aim.

Figure 4.18-Para-Scan measurement.

Weather station.

The “Politecnico di Torino” is equipped with a weather station which measures the main metereological properties (temperature, relative humidity, wind velocity and direction and solar irradiance) and detects the air quality.

The instrumentations installed on the roof of the building, produced by the EKO company, is composed by a solar tracker on which are mounted a pyranometer, a pyrheliometer and a radiometer spectrum.

Figure 4.19- Weather station.

The tracking system is composed by solar sensor and a control system that allows to calculate the sun's position.

A photodiode detector allows to identify the sun's position and to balance a hypothetical misalignment of the locator caused by an incorrect installation. In general, the tracking modality will be automatically commutated according to the solar radiation condition in order to maintain an elevated accuracy.

5-Redox Couples.

Different redox couples are used in the thermochemical cycles in order to check which one allows to obtain the best performance that in our case corresponds to a higher O_2 and H_2/CO yield production.

Another relevant parameter is the thermal reduction temperature that should be lower as possible.

5.1-Volatile cycles.

In all the systems that use this kind of cycle a quenching device is used in order to reduce the partial pressure of Oxygen and avoid the recombination between the volatile substances and the O_2.

Zn/ZnO.

This cycle was long considered the most promising candidate for thermochemical fuel production. It is characterized by a combination of favorable thermodynamic properties:

Zn is sufficiently non-precious to react with water, it has low atomic weight and therefore comparatively high energy content per mass being attractive as a transportable energy vector. The specific fuel capacity of ZnO is very high compared to non-volatile metal oxides because the entire mass participates in the redox cycle.

The endothermic thermal reduction of ZnO into Zn happens at near 2300 K and it is followed by the exothermic hydrolysis which is performed in a separate step at lower temperature above 1300 K.[14]

Thermal reduction:

$$ZnO \rightarrow Zn + O_2 \tag{45}$$

Oxidation:

$$Zn + H_2O \rightarrow ZnO + H_2 \quad \text{or} \quad Zn + CO_2 \rightarrow ZnO + CO \tag{46}$$

This type of cycle allows to obtain a maximum solar to chemical energy conversion of 39% but in order to increase the efficiency is possible to use Zr_4+ doping ions that have a greater reducibility but require a larger difference of temperature between the oxidation and the reduction.

However experience has shown issues related to the separation of Zn and O_2 produced and kinetic limitations that make it challenging to reach the full potential of this redox cycle. The general strategy is to use large amount of inert gas for product separation but the energetic costs of this process reduce the efficiency, this is the main reason because research has shifted away from volatile metal oxides and towards the partial reduction of non –volatile materials.

CdO/Cd cycle.

Cadmium's cycle was one of the first cycle considered for the solar reduction experiments.

The thermal reduction temperatures are between 1423 and 1723 K and happens in a fluidized bed reactor.

Thermal reduction:

$$CdO \rightarrow Cd + \frac{1}{2}O_2 \quad (47)$$

Oxidation:

$$Cd + H_2O \rightarrow CdO + H_2 \quad \text{or} \quad Cd + CO_2 \rightarrow CdO + CO \quad (48)$$

The main issues connected with this cycle are due to the fact the Cd is toxic so it can be dangerous.

SnO_2/SnO.

The dissociation rate of SnO_2 is high and it is less dependent on the quenching rate respect Zn. On the other hand Zn has a higher reactivity with O_2 when the reactions happen at high temperatures.[15]

Thermal reduction:

$$SnO_2 \rightarrow Sn + \frac{1}{2}O_2 \quad (49)$$

Oxidation:

$$SnO + H_2O \rightarrow SnO_2 + H_2 \quad \text{or} \quad SnO + CO_2 \rightarrow SnO_2 + CO \quad (50)$$

The thermal reduction occurs under atmospheric condition at about 1600 C while hydrolysis is efficient at 800-900 K.[16]

The hydrolysis of Zn nanoparticles reached only up to 55% of H_2 yield whereas SnO hydrolysis was almost complete. In contrast Zn hydrolysis is much faster than SnO hydrolysis but Zn deactivation occur suddenly.

GeO_2/GeO.

Thermal reduction:

$$GeO_2 \rightarrow GeO + \frac{1}{2}O_2 \quad (51)$$

Oxidation:

$$GeO + H_2O \rightarrow GeO_2 + H_2 \quad \text{or} \quad GeO + CO_2 \rightarrow GeO_2 + CO \tag{52}$$

This type of cycle is attractive for the high solar-to-chemical efficiency (34,6%) that is possible to obtain despite of the low reduction temperature that is between 1400-1800 K.[17]

5.2-Non-volatyle cycles.

Ceria Cycle CeO_2/CeO.

Ceria redox pairs has been used in automotive emissions control as an oxygen storage system due to its high rates of oxygen chemical diffusivity that contributes to a faster redox kinetics reaction.

Thermal reduction:

$$CeO_2 \rightarrow CeO + \frac{1}{2}O_2 \tag{53}$$

Oxidation:

$$CeO + H_2O \rightarrow CeO_2 + H_2 \quad \text{or} \quad CeO + CO_2 \rightarrow CeO_2 + CO \tag{54}$$

In normal conditions the reduction of the Ceria happens at 2200 K but in order to reduce the temperature of reduction usually is used Ceria's partial reduction cycle in which the maximum temperature that is reached during the process is 1800 K that is below its melting point and so it is a non-volatile cycle.[18]

Thermal reduction:

$$CeO_{(2-\delta ox)} \rightarrow CeO + \frac{(\delta red - \delta ox)}{2} O_2 \tag{55}$$

Oxidation:

$$CeO_{(2-\delta red)} + (\delta_{red} - \delta_{ox})H_2O \rightarrow CeO_{(2-\delta ox)} + (\delta_{red} - \delta_{ox})H_2 \tag{56}$$

δ in general is proportional at the temperature of reduction and increases with decreasing oxygen partial pressure.

At last Ceria can be used also for a combined Ceria reduction and methane reforming that allows to produce directly produce syngas:

$$CeO_2 + CH_4 \rightarrow CeO_{(2-\delta)} + \delta(CO + H_2) \tag{57}$$

Tungsten cycle.

This cycle offers a higher gravimetric fuel productivity that can operate at lower temperature.

It requires two different chamber one for the H_2 production and the other for the O_2 production.

The Tungsten melting point is 1643 K.[19]

Thermal reduction:

$$\mathrm{W} + 3\mathrm{H_2O} \rightarrow \mathrm{WO_3} + 3\mathrm{H_2} \tag{58}$$

Oxidation:

$$\mathrm{W} + 3\mathrm{CO_2} \rightarrow \mathrm{WO_3} + 3\mathrm{CO} \tag{59}$$

The cycle will utilize a porous powder of the material and the stability of the oxides depends on a critical oxygen partial pressure above which the oxide will advance to the next higher oxide.

The system will utilize a powder bed in which gas-solid reaction will occur. In a fixed and isothermal powder bed, the reactions take place as a moving front.

The volatility of Tungsten metal and oxides must be controlled to ensure that there is no loss of powder bed by vapor phase removal so the sublimation of Tungsten during the thermal reduction must be avoided.

Hercynite Cycle.

The idea is to exploit the redox effect of iron oxides in conjunction with the thermal stability of aluminum oxides.

The Hercynite occurred due to the reaction between $CaFe_2O_4$ and Al_2O_3 at the elevated temperatures.

Thermal reduction:

$$CaFe_2O_4 + 3Al_2O_3 \rightarrow CaAl_2O_4 + 2FeAl_2O_4 + \frac{1}{2}O_2 \tag{60}$$

Oxidation:

$$CaAl_2O_4 + 2FeAl_2O_4 + H_2O \rightarrow CaFe_2O_4 + 3Al_2O_3 + H_2 \tag{61}$$

This cycle is characterized by a low thermal reduction temperature 1000 C.

Production of Lime.

The thermal decomposition of limestone is the main endothermic step in the production of lime and cement.

$$CaCO_3 + CH_4 \rightarrow CaO + 2CO + 2H_2 \quad (62)$$

The thermal reduction happens in a temperature range of 1200-1600 K for lime up to 1750 K for clinker. About 1,8 t of limestone are required in order to produce 1 t of quich-lime. [20]

Replacing fossil fuels with CSP is a clear and sustainable means to reduce CO_2 emissions connected with the Cement production.

Perovskites cycle.

Perovskites of the form ABO_3 has recently been proposed as an alternative to CeO_2 for two-step fuel production to address the low reduction extents and high operating temperatures associated with its use.

Thermal reduction:

$$ABO_{(3-\delta ox)} \rightarrow ABO_{(3-\delta|red)} + \frac{(\delta|red|-\delta ox)}{2} O_2 \quad (63)$$

Oxidation:

$$ABO_{(3-\delta|red)} + (\delta|red|-\delta ox)H_2O \rightarrow ABO_{(3-\delta ox)} + \frac{(\delta|red|-\delta ox)}{2} O_2 \quad (64)$$

Compared to CeO_2, Perovskites show increased O_2 evolution during thermal reduction and a notable decrease in operating temperatures.

The larger deviation from stoichiometry provides as higher upper limit for fuel production but the oxidation reaction must be favorable such that the reduced perovskites can fully replenish the oxygen lost during the reduction.[18]

The most used pervoskites is the Lanthanium-strontium-manganates LSM/$LA_{(1-x)}$ $Sr_{(x)}MnO_{(3-x)}$

(FORMULA)

The thermal reduction occurs at 1273 K and allow to obtain an higher O_2 yield compared to the Ceria cycle. However this cycle is characterized by an incomplete re-oxidation.

Thermodynamically speaking the partial molar enthalpy of reduction for LSM perovskites decreases monotonically with the increasing of Sr_2+ content while O_2 evolutions during reduction of LSM perovskites increase with increasing of LA_2+ dopant concentration. Such a change in properties leads to a greater difference of temperature between redox steps.

Iron-Based Oxide Cycle.

We studied Fe_3O_4/FeO processes and more in general ferrite process that are metal oxide processes via solutions between Fe_3O_4/FeO and Me_3O_4/Mo.

Thermal reduction:

$$Fe_3O_4 \rightarrow 3FeO + \frac{1}{2}O_2 \quad (65)$$

Oxidation:

$$3FeO + H_2O \rightarrow Fe_3O_4 + H_2 \quad (66)$$

The thermal reduction temperature varies with the partial pressure of the oxygen PO_2= 10^{-6}/10^{-8} bar.

The melting point of FeO is around 1400 C but with the right pressure is possible to obtain the thermal reduction at 1300/1400 C.

Fe_3O_4 as a reactive material is prepared through a spin-coating method that is a process that requires a liquid-vapor interface and allows to obtain a uniform film onto a solid surface by using centrifugal force.[21]

This redox couples causes coagulation and sintering of the iron-oxide particles during the cycle reaction for this reason the iron-oxides are supported with monoclinic zirconia that has a good coagulation and sintering resistance at 1400 C and this is due to m-ZrO_2 that has an higher melting point than Ferrite.[22]

An alternative solution can be the Yttria-Stabilized zirconia in which Fe-YSZ is successful in H_2 productions especially as foam instead of powders.

The most reactive foam is resulted $NiFe_2O_4$/$m\text{-}_{ZrO2}$.

Finally is possible to use a mixed solutions between Fe_3O_4/FeO and Me_3O_4/Mo in order to obtain (Fe(1-x)M(x))$_3O_4$/ (Fe(1-x)M(x))O in this way is possible to decrease the temperature that is needed for the thermal reduction.

6-Simulation.

The experimental demonstrations are supported with analytical calculations implemented in the software COMSOL MULTIPHYSICS.

In detail we have considered two different models: the first one describes the whole system composed by the parabolic and the receiver while the second focus on the receiver and allows to obtain the temperatures distribution on it.

The aim of the simulation is to determine the temperature reached by the receiver during the process and to evaluate which are the most suitable redox couples and the materials for use in system assembly. Moreover the model shows relevant data about the syngas production and the feasibility of the thermo-chemical process during the different seasons.

6.1-Software.

COMSOL is a program used for the simulation of project, devices and technological processes from industry to research. It includes all the steps of the modeling workflow: the definition of geometries, material properties and physics to the description of specific phenomena, up to resolution and post processing to produce accurate and reliable results.

The key to successful simulations is to develop experimentally validated models that can replace the exclusive use of physical tests and prototypes, to provide a deeper understanding of the project or process under analysis. Compared to performing physical tests or testing prototypes modeling allows faster and more efficient and accurate optimization of processes and devices. Moreover, COMSOL allows to move in a single software environment between simulations of electromagnetism structural phenomena, acoustics, fluid dynamic, heat transfer and chemical reaction phenomena, or any other physics phenomena modeled by a PDE system. It is possible to combine the physical phenomena of all these nears into one model.

After selecting a particular physical interface, the software suggests the types of study available such as stationary or time dependent solvers. The software also automatically recommends the numerical discretization of the most appropriate mathematical model, the solver sequence and the specific displays and past-processing settings for physical phenomena.

6.2-Modeling of the solar concentrator.

Introduction.

The aim of this part of the project is to use Comsol to create an as real as possible model of the system composed by the solar dish and the receiver that are located on the roof of the energy center.

The model should taking into account the radiation, convective and conducting losses and calculates the temperatures distribution on the receiver, the power flux focused on the focal point and the optical parameters as the ray trajectories after the reflection. In detail the results show the concentration ratio useful to evaluate the reflection's performance of the paraboloid and the uniformity of the flux on the receiver's surface that has a significant influence on the efficiency of the thermo-chemical reaction.

Space.

The study is effectuated in a 3-dimensional space so the reference system is composed by the X,Y and Z Cartesian axis.

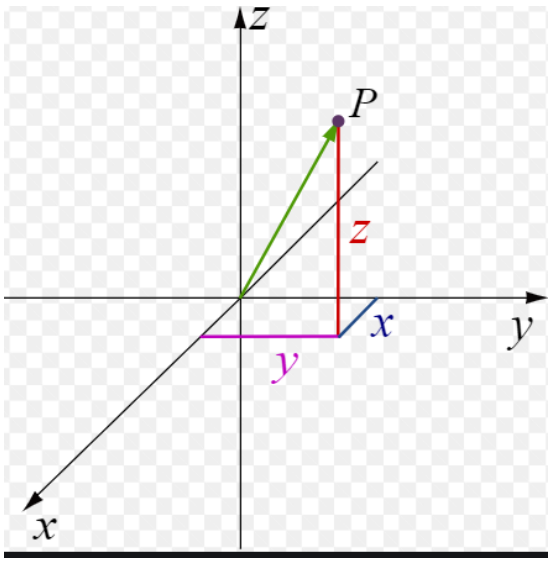

Figure 6.1-cartesian axis.

Physics.

The physics that underlies our study is the geometrical optics according to the solar radiation can be subjected to two different phenomena:

- Refraction phenomena that is described by the Law of Snell:

  $n_1 * \sin(\theta_1) = n_2 * \sin(\theta_2)$

  n_1: refractive index in the medium 1.

  n_2: refractive index in the medium 2.

θ_1: angle between the incident beam and the normal to surface.

θ_2: angle of refraction between the refracted beam and the normal to surface

- Reflection phenomena that happens when the radiation is reflected by a smooth surface according to the reflection law incident and reflected rays form identical angles respectively normal to surfaces.

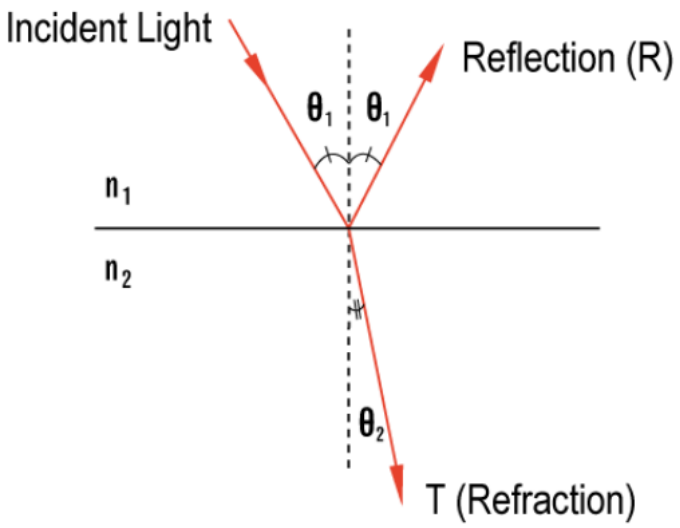

Figure 6.2- Refraction and reflection phenomena.

The direction of refracted or reflected radiation is obtained through several steps:

1- Determination of the point of incidence of the radiation.
2- Determination of the direction of the radiation and of the shape of the surface.
3- Determination of the surface normal.
4- Determination of the direction of the reflected/ refracted ray.

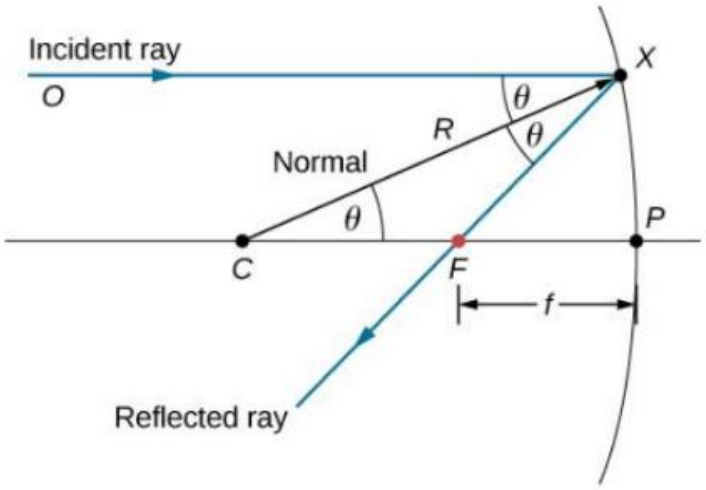

Figure 6.3-Reflected ray trajectories.

Every ray that is emitted has a power that depends from the total power of the source but this parameter will be assigned in a future step.

Definition of the study.

The study that is selected is the Ray optics module that allows to analyze the system from an optical point of view. It utilizes the ray tracing that is a particular techniques of geometrical optics that allows to modeling the propagation of electromagnetic waves, the different interaction between the surfaces and to calculate the sunlight pathway.

The beams generation depends by a random function and the probabilistic approach that is adopted for the simulation is based on the Montecarlo method.

The sunlight pathway is calculated through the interaction between the sun rays and the surface and the propagated waves are considered as rays that can be reflected, refracted or absorbed by the model surfaces.

The Ray optics module is equipped with a particular library that allows to import on Comsol different optical tools as paraboloidal reflector, Newtonian telescope, Hubble space telescope and double glass lens system.

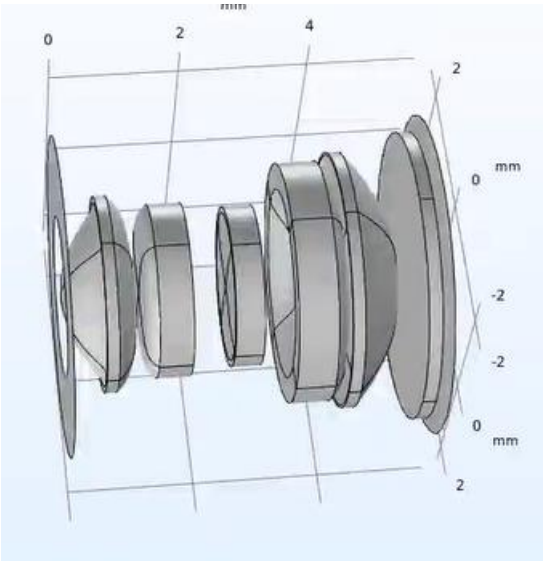

Figure 6.4-Double glass lens system.

Parameters.

The initialization of the parameters is the first step after the set-up of the environment study. The parameters that are used in the project are:

f	1.4448 m	1,4448 m
Ψ	45 deg	0.7854 rad
d	4*f*(csc(Phi)-cot(Phi))	2.3938 m
ϕ_{sim}	4.65 mrad	0.00465 rad
A	$P*d^2/4$	4.5006 m^2
sig	1,75 mrad	0.00175 rad
Io	0.8 Kw/m^2	800 W/m^2

Figure 7.3-Parameters

- f: focal length of the receiver.
- Ψ: Rim angle of the receiver.
- d: Dish diameter.
- A: Dish projected surface area.
- ϕ_{sim}: Maximum solar disc angle.
- Sig: Surface slope error.
- Io: solar Irradiance.

Geometry.

Once that is defined the environment of our study and the main parameters is necessary to insert the dimensions of the concentrator and the receiver in order to create a 3D geometry similar as possible to the real ones.

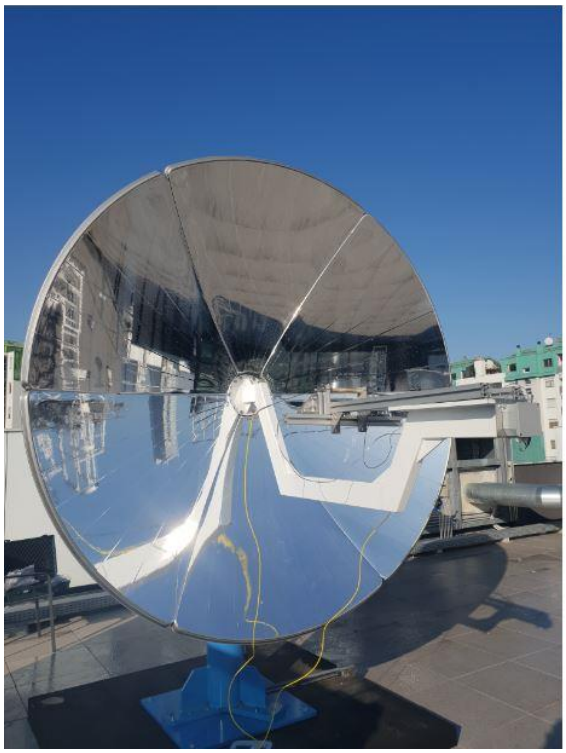

Figure 6.4-Solar Dish on the roof of the energy center.

- Concentrator.

The solar dish concentrator is obtained through the COMSOL library related to the ray optics module.

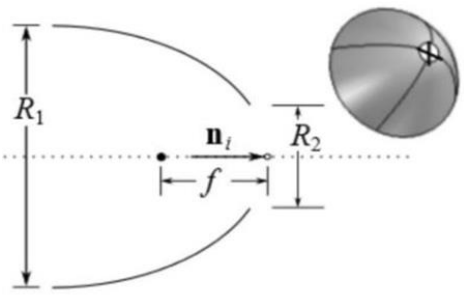

Figure 6.5-Parabolic reflector.

The parameters that are required to define the paraboloidal reflector shell are the rim angle, the focal length and the diameter.

- Receiver

The receiver is represented as a hollow cylinder with a diameter of 10 mm and a height of 997 mm. It is divided in three different section, the central one represents the focal plane while the other two at the extremes represents the thermocouples.

The receiver's structure is composed by two different types of thermocouples:

- B type thermocouples that measures the difference of temperature between the environment and the receiver.
- K type thermocouples that measures the difference of temperature between the reactor and the receiver.

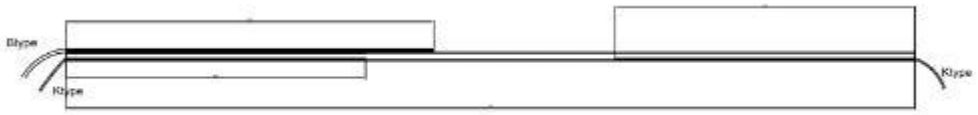

Figure 6.6-Receiver.

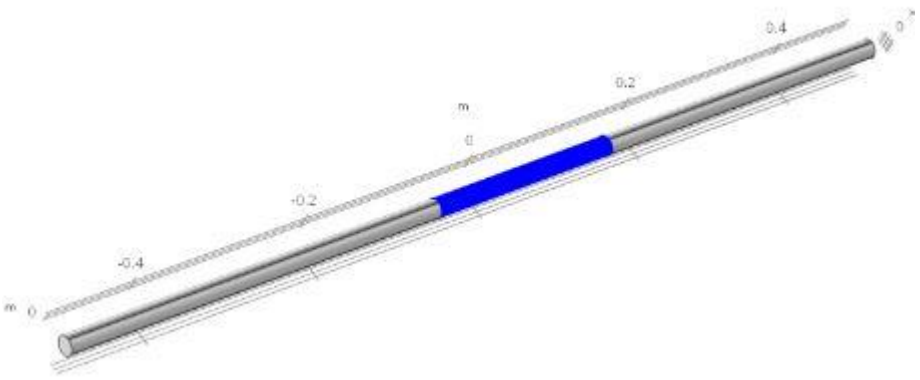

Figure 6.7- Thermal receiver in Comsol.

In the end through the command "FORM UNION" is possible to obtain the final geometry:

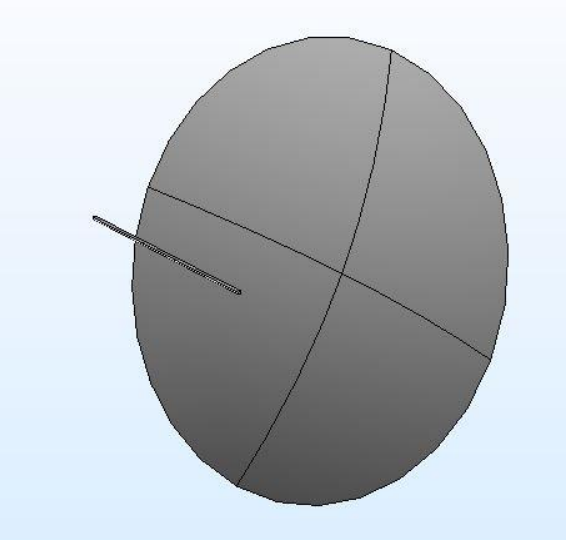

Figure 6.8-Model of the horizontal receiver and the paraboloidal reflector shell.

Material.

The receiver is composed of 94% Al_2O_3 that is a particular oxide that has an elevated thermal insulation that allows to decrease the thermal losses. Moreover Alumina guarantees a good resistance against the corrosion in acidic and alkaline environments and a good wear resistance.

Mesh.

The numerical modeling is based on the hybrid technologies BEM-TEM (boundary element method-finite element method) which allows to operate through the finite element method, discretizing the continuum with a set of repeats of finite dimension, interconnected to each other at point defined as nodes.

The connection between the different nodes creates a Mesh that can be more or less dense.

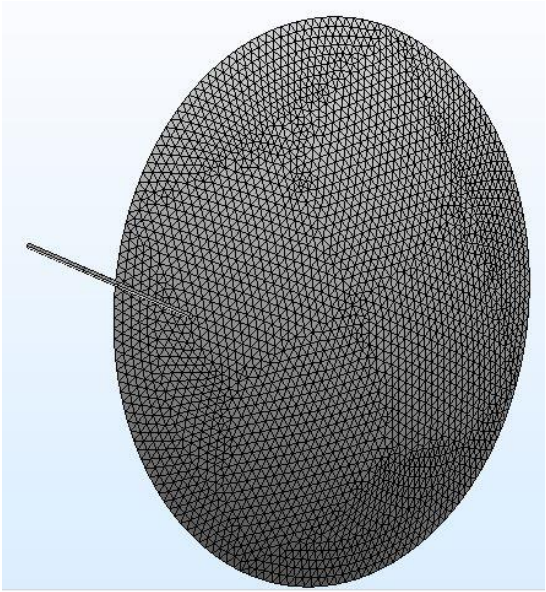

Figure 6.9- Mesh of the receiver's surface and the paraboloidal reflector.

Geometrical optics.

The function "illuminated surface" allows to evaluate the solar radiation that is reflected or directly realized by the parabolic shell.

The simulated rays are emitted from 100 000 separate points, their direction is a function of the incoming radius vector and the normal to surface while their intensity depends by the source power which is calculated as:

$$P = I_0 \times A \tag{67}$$

Io: solar irradiance.

A: Parabolic reflector's surface.

The sun rays are arrested when reach the focal plane through the "WALL" function that models the absorbent surface of the receiver while the intensity of the reflected radiation and its trajectory depends by the curvature of the paraboloid.

Ideal case.

The first simulation is an ideal case in which the only phenomena that is considered is the sunshape so, from a theoretical point of view, the parabolic reflector should concentrate the incident radiation on one point.

The sunshape's term is referred at the effects due to the finite dimensions of the solar disk. Although the Sun is located at 150 milions kilometers from the earth it is enough big to create significant angles

between solar radiations that comes from different parts of the solar disk that, in a hypothetical case in which the sun's dimension could be neglected, would have been parallel.

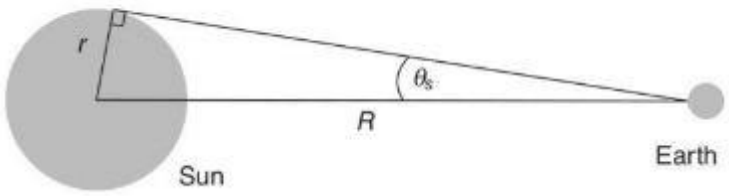

Figure 6.10- sun shape.

In Comsol the incident rays on earth are sampled to form a very narrow cone with a half angle of

θ_s=4.65 mrad. In addition in the reality some radiations are emitted by the circumsolar region that is the bright site that surround the Sun, this phenomenon is expressed through the circumsolar relationship (CRS) that in our case is neglected.

The rays are sampled according to the conical distribution with a maximum opening angle equal to ϕ_{sim}=4.65 rad while the incident ray's power is fixed equal to 800 W/m^2 that is the maximum rate of irradiance available declared by the manufacter. The intensity threshold of the reflected rays is set equal to: I_{th}= 10^{-3} W/m^2.

In conclusion the external surface is considered perfectly smooth and reflective so the absorption coefficient is zero.

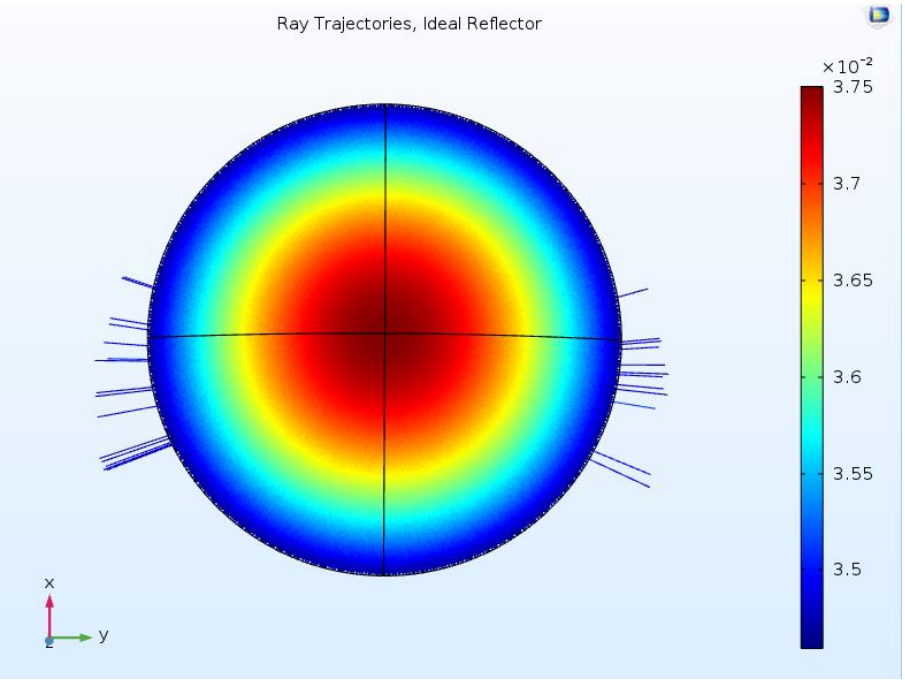

Figure 6.11-Ray trajectories ideal reflector.

The majority of the solar radiation is incident in the internal surface of the receiver where is deposited a higher power. Moreover, as the radial distance increases, the radiation density decreases so the solar radiation deposited on the focal plane by the peripheral areas of the paraboloid has a lower incidence.

The ideal model is characterized by an elevated accuracy in fact almost the totality of the rays is absorbed by the receiver and only a little part of the radiation is rejected. The solar rays that are not incidence in the center of the receiver creates two specular beams.

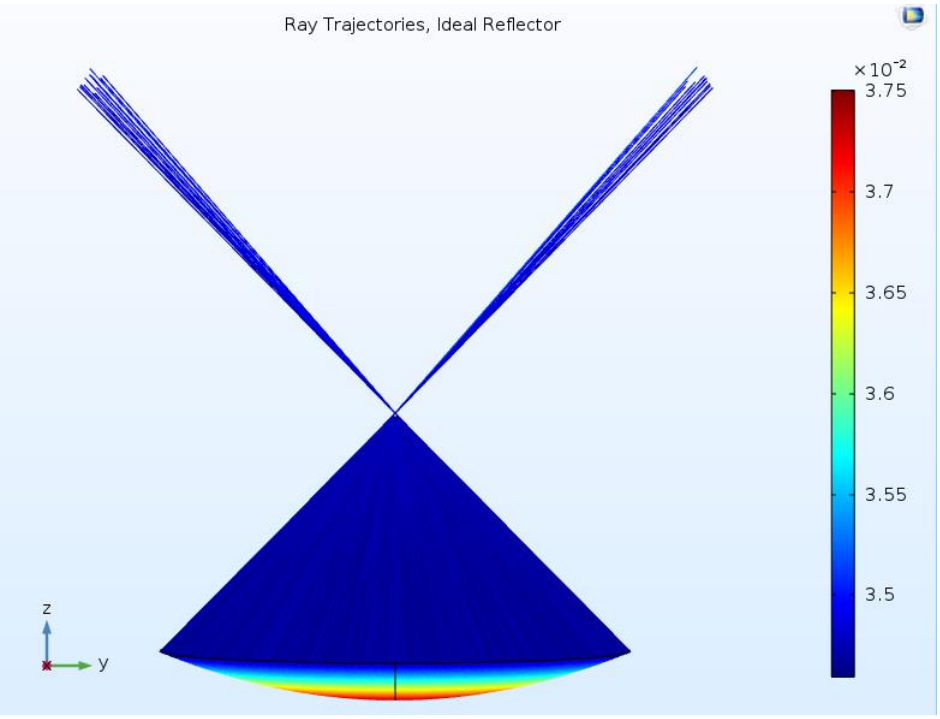

Figure 6.12-Specular beams.

The aim of the project is to accumulate a heat flux in the center of the receiver that allows to reach the thermal reduction's temperature and activate the thermochemical reactions.

The Comsol's function "Deposited ray Power" allows to evaluate the heat flux deposited on the focal plane and the temperature distribution:

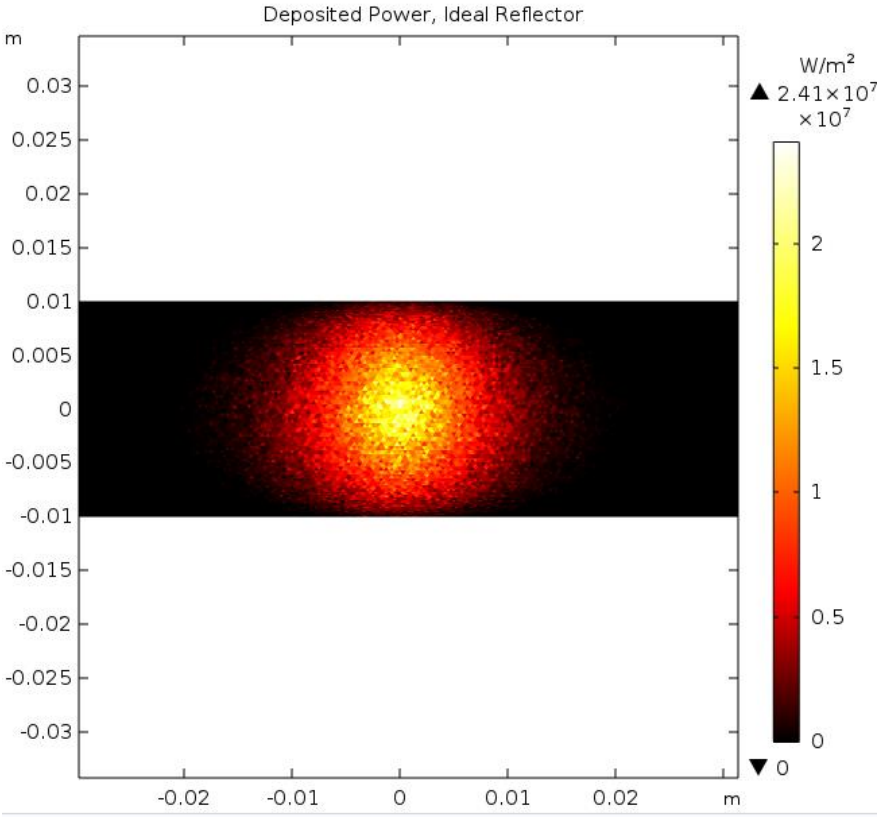

Figure 6.13-Ideal deposited power.

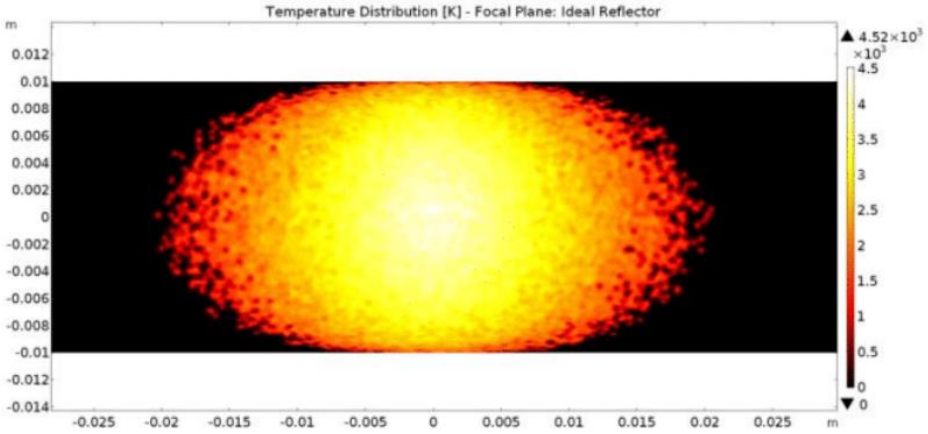

Figure 6.14-Ideal temperature distribution.

The thermal power deposited is extremely elevated and reaches a peaks of $2.41*10^7$ W/m^2 in the focal plane. The distribution is homogeneous and has a circular shape while the temperature reaches a peak of 4520 K.

Real Case.

The second study consider the real case and taking into account all the phenomena that reduce the efficiency of the process:

- Absorption

  Part of the incidence solar radiation is absorbed and not reflected by the parabolic shell. The absorption coefficient is set equal to 0,2, as declared by the manufacter, this means that eighty percent of the solar radiations is reflected while the remaining part is absorbed.

- Superficial roughness

  In this experiments the parabolic dish's surface is characterized by a surface roughness that causes a random deviation from the theoretical direction of the reflected radiation. In this way the solar radiation will be concentrated imperfectly and the heat flux will spread over a larger surface than the focal plane.

- Limb Darkening

  The Sun's density and temperature decrease as the distance from the center of the star increases. In this way the radiation that comes from the center of the solar disk are brighter than those emitted from the external part.[23]

  The function "illuminated surface" allows to taking into account this phenomena and describe it as a function of an empirical law whose has an exponential trend and depends by the solar radiation's wavelength.

In the end the rays sample, the intensity of the incident radiation and the total power of the source remains unaltered.

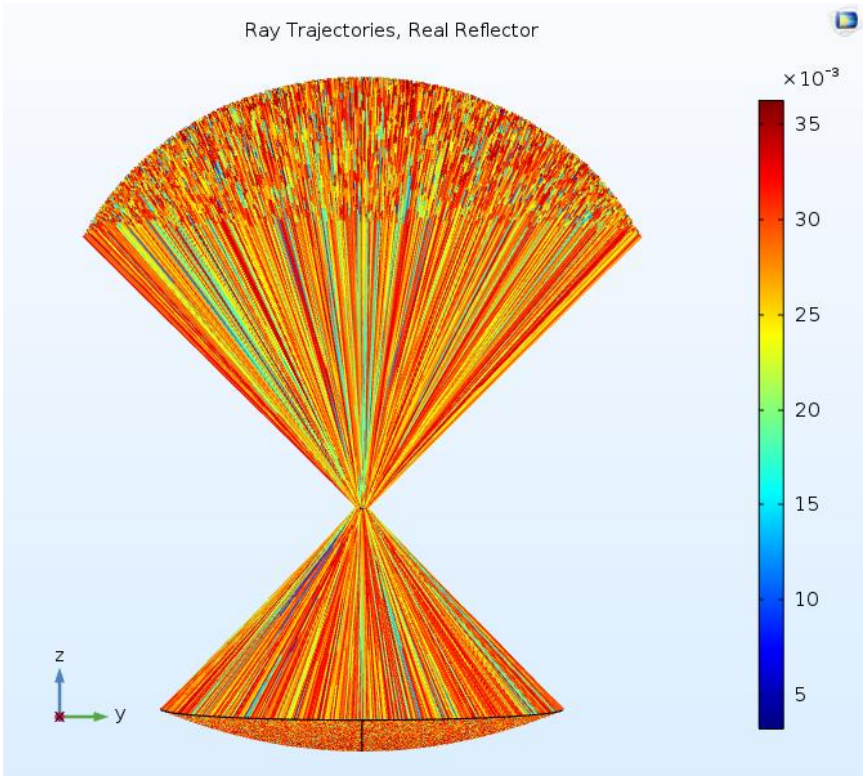

Figure 6.15-Ray trajectories real reflector.

As a consequences of the limb darkening the spatial distribution of the rays captured by the surfaces in terms of deposited power is more heterogeneous, the rays randomly affect the paraboloid surface without defining an area characterized by a greater power density. In addition the reflection is not ideal so the power flux obtained in the real cases is lower that the ideal one.

At this point it is possible to study the heat flux deposited and the temperature distribution on the focal plane as in the previous case:

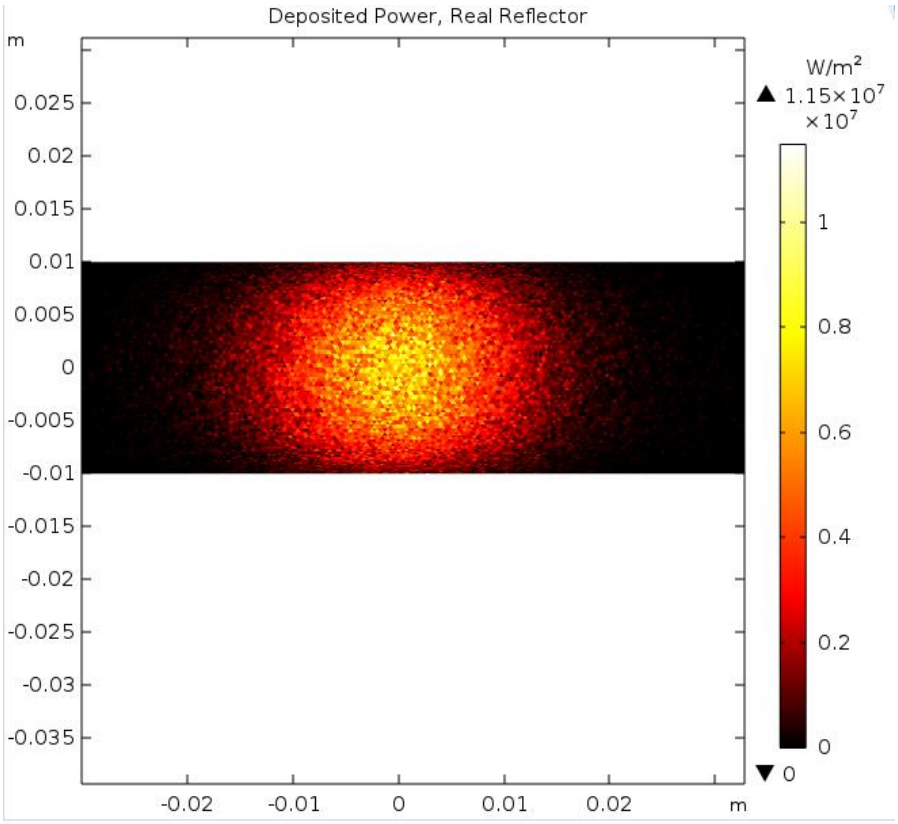

Figure 6.16-Real deposited power.

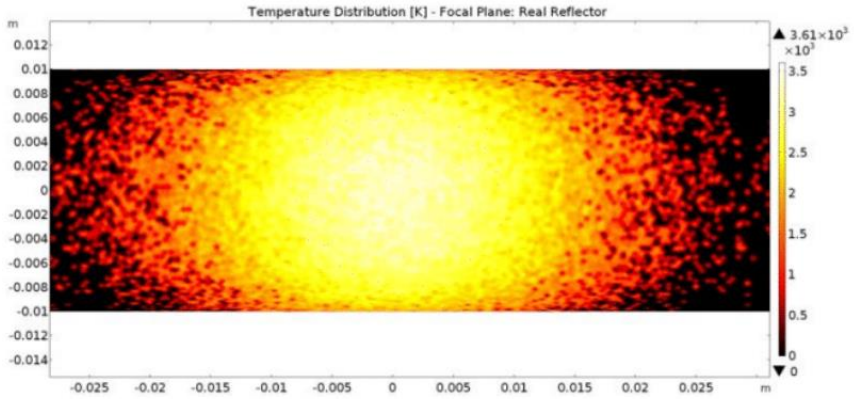

Figure 6.17-Real temperature distribution.

A considerable number of beams do not strike the focal plane in this way the deposited thermal flux is halved and reaches a maximum value of 1.15 *10^7 W/m^2. The shape is similar to an ellipse and the flux is more heterogeneous.

The heat losses increase and the temperature reaches a peak of 3600 K in the center of the focal plane.

6.3-2D modeling of the solar receiver.

In the previous simulation is possible to determine the temperature that is reached by the receiver assuming that it's not exposed at the external environment; the aim of this part of the project is to evaluate the temperature distribution on the whole surface while the receiver is exposed to the external atmosphere.

Before starting the 2D-modeling of the receiver, the data concerning the temperature distribution and the deposited ray power on the receiver obtained from the Ray Optics Simulation are exported from Comsol and imported on Matlab in order to calculate the average temperature and heat fluxes on the focal plane. The script that is used on Matlab is the following:

```
close all
clear all
clc
meas= load('Realdepositedpower');

x = meas(:,1);
y = meas(:,2);
flux = meas(:,3);

j = 0;
sig = 5.67e-8; % W/m2K

for i = 1:length(flux)
    if flux(i) > 0
        j = j+1;
        FLUX(j) = flux(i);
        TT(j) = (flux(i)/sig).^(1/4);
    end
end


Flux_Mean = mean(FLUX)
Temp_Mean = mean(TT)
```

Figure 6.18-Matlab script.

Realdepositedpower is a script imported from Comsol in which the first column represents the coordinates on the x-axis, the second column the coordinates on the y-axis and the third column the different value of the flux/temperature at the corresponding point.

Taking into account a focal area with a diameter of 2 cm we obtain:

$$\Phi_{average} = 2563 \times 10^6 \frac{W}{m^2} \quad (68)$$

$T_{average}$=2242 K

Space.

The simulation is set in a bi-dimensional space that allows to obtain a wide and realistic vision of the temperature distribution on the whole surface of the receiver.

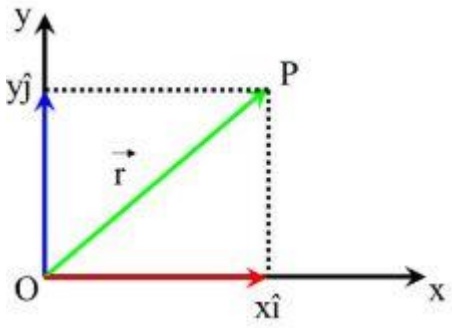

Figure 6.19-Bidimensional space.

Physics and definition of the study.

The physics that underlies the 2D-modeling of the receiver is the "heat transfer in solid" that can be studied in a stationary or transient regime. In our case we evaluate the thermal losses due to natural convection between the ends of the receiver and the external air that are calculated as:

$$\Phi_{conv} = h_{conv} \times (T_{average} - T_0) \quad (69)$$

T_0: environment temperature.

$T_{average}$: average temperature of the receiver.

h_{conv}: Air natural convection coefficient

Parameters.

The main parameters that are initialized are:

T_0	293,15 K	293,15 K
$\Phi_{average}$	2563*10^6 W/m^2	2563*10^6 W/m^2
$d_{focal\ point}$	0,01 m	0,01 m

$A_{focal\ plane}$	Pi* $(d_{focal\ point})^2/4$	$7.854*10^{-5}$ m^2
$P_{average}$	$\Phi_{average} \times A_{focal\ plane}$	151.7958288 W
$d_{cylinder}$	0,0179 m	0,0179 m

The initial temperature of the receiver is assumed equal to the environment temperature and in steady state the constant heat source $P_{average}$ is located in the focal plane.

Geometry and materials.

The bi-dimensional geometry of the receiver is approximated as a rectangle with a circular shape in the center that represents the focal plane.

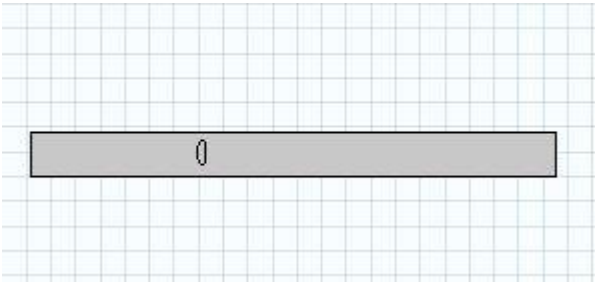

Figure 6.20- Receiver geometry.

The height and width of the rectangle are obtained from the real dimension of the receiver while the diameter of the focal plane is calculated as:

$$d = \frac{fx*\theta}{\cos(\theta)*(1+\cos(\theta))} \quad (70)$$

In conclusion the Material used for the receiver is Alumina (Al_2O_3) the same used in the Ray optics simulation.

Results.

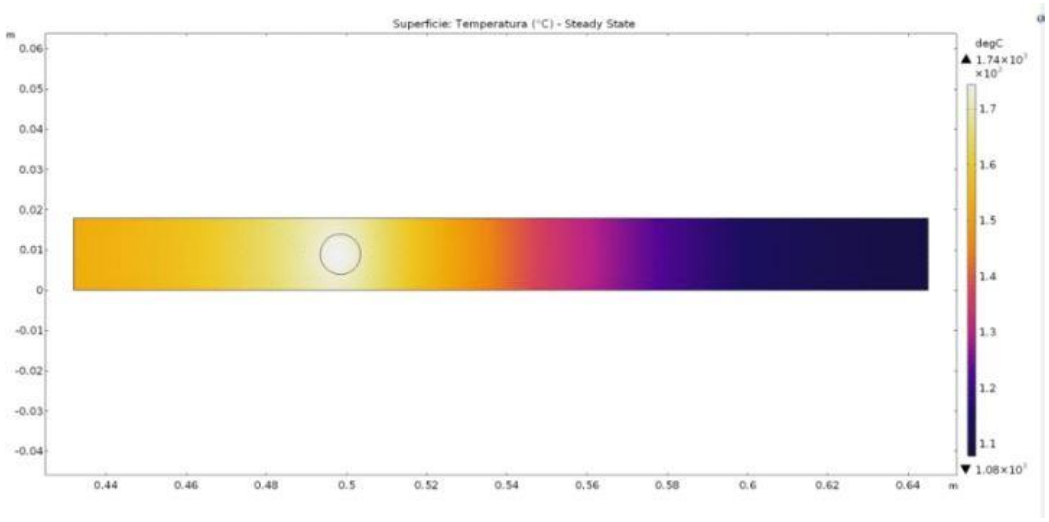

Figure 6.21-Temperature distribution.

As expected, in the 2D-simulation the losses due to the exchanges by convection between the receiver and the air causes a drop of temperature respect the ideal case. For an ideal solar radiation of 800 W/m^2 the temperature reaches a peak of 1800 C in the focal plane that is the same value declared by the manufacter for a concentrator that operating in conditions of maximum available irradiations.

6.3-FEM simulation.

In this paragraph we focus on the plant behavior when it is forced to operate at real conditions of variable irradiation both during the day and during the seasons.

This simulation should represent a useful forecast model that allows to estimate the productivity of the plant during the different period of the year. The temperature and global radiation data are supplied by the weather stations positioned on the roof of the energy center. During the year the two physical quantities have a cyclic trend that depending by the location that is considered, on the other hand every monthly measurements is subjected at random rate of variations in climatic conditions.

The best procedure to evaluate the global radiation trends for the four different seasons of the year is to consider the average between the values corresponding to the instants of time relating to the central day of each month in the case of clear and sunny day. Once the reference days have been identified is possible to calculate the seasonal distribution of global irradiance:

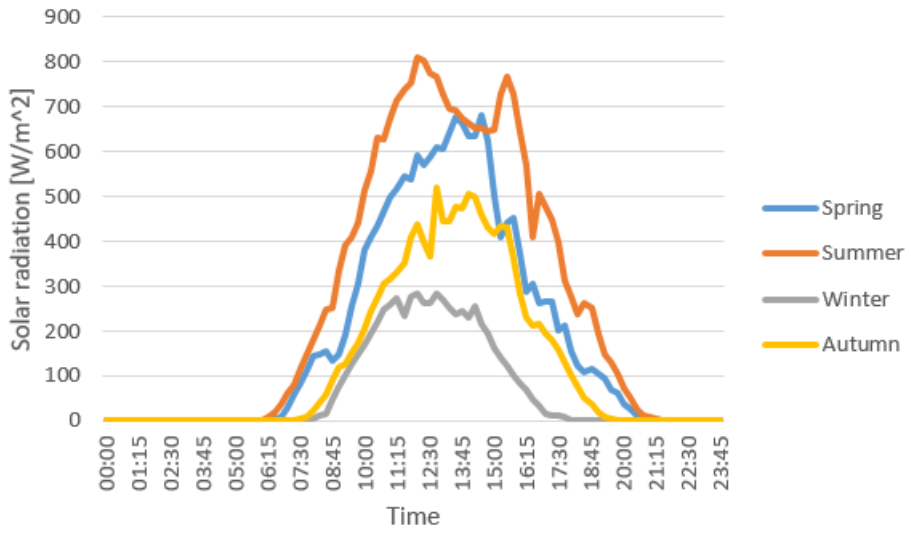

Figure 6.22- Seasonal global radiation.

It's evident that the external curves offer an elevated global radiation for a longer period than the inner trends. In detail the summer global radiation curve reaches a peaks of 808 W/m^2.

The elevated radiative intensity of the warmer months increases the energy absorbed by the receiver and so the solar to chemical efficiency of the global process.

Summer.

The solar technologies have the best performances during the summer months (June, July, September) when the global radiation reaches the highest values.

The global radiation values during the summer months (June, July, September) are the most elevated so for solar technologies the best results in terms of efficiency are obtained during this period.

As seen in the previous paragraph the data supplied by the weather station allow to calculate the seasonal distribution of global radiation but in order to implement an accurate analysis it's important to taking into account the seasonal average wind velocity and the seasonal average precipitation.

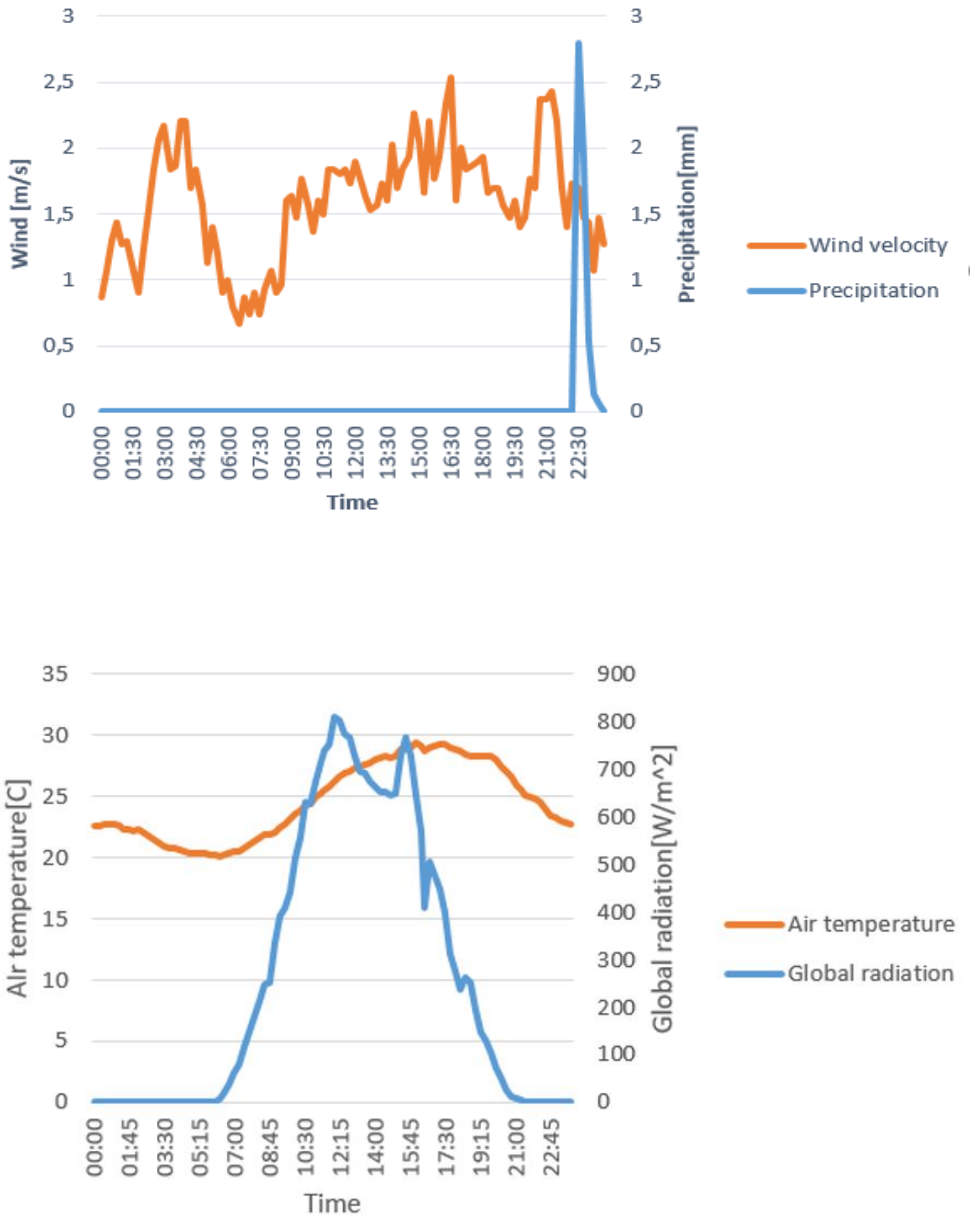

Figure 6.23-Meteorological data concerning summer period.

The graph shows a peak of the average precipitation between the 22 and the 23.30 pm caused by a passing storm while the wind velocity oscillates between 0,5 and 2,5 m/s with highest values in the late afternoon.

The air temperature reaches a peak of 30 C between the 15.45 and the 17.30 pm while the maximum solar radiation value of 808 W/m^2 is reached at noon.

After analyzing the data it's possible to import the global radiation's trend on the "Ray optics Model" in Comsol in order to process the data in Matlab and obtain the trend of the average heat flux and the average temperature distribution on the focal plane:

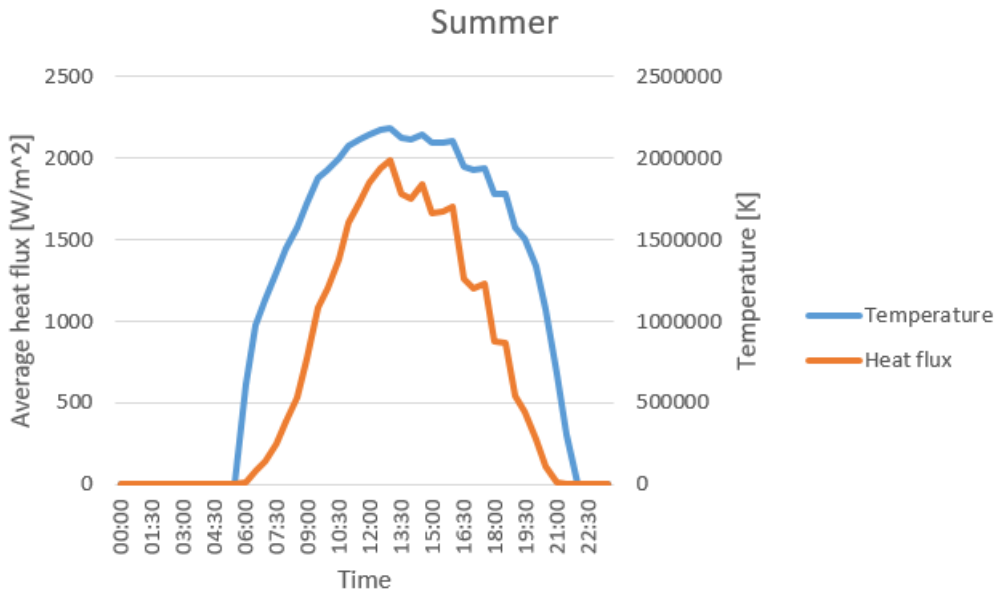

Figure 6.24- Average summer heat flux and temperature distribution on the receiver's focal plane.

At last the average heat flux is imported in the "2D-modelling of the solar receiver" to obtain the temperature's trend when the receiver is exposed at the external atmosphere in steady-state conditions:

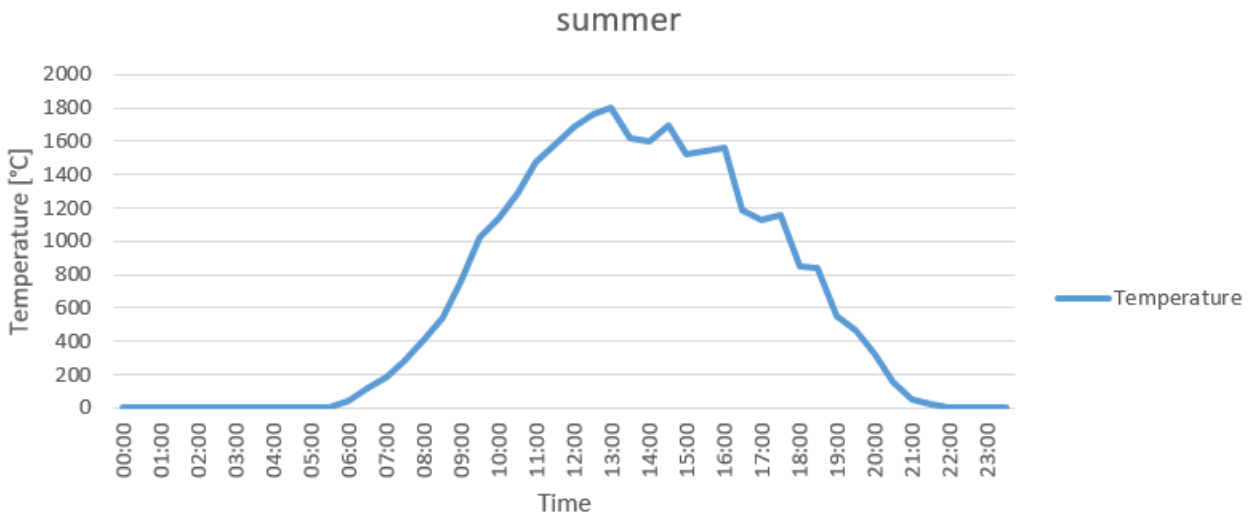

Figure 6.25-Summer temperature distribution when the receiver is exposed at the external atmosphere.

The graph shows that during the summer months the Ceria's thermal reduction temperature of 1600 C is reached between the 11.45 and the 15.15.

Spring.

The spring season (March, April, May) is a transition period from the winter to the summer; for this reasons the global radiation assumes intermediate values.

As for the summer period is possible to plot the main parameters:

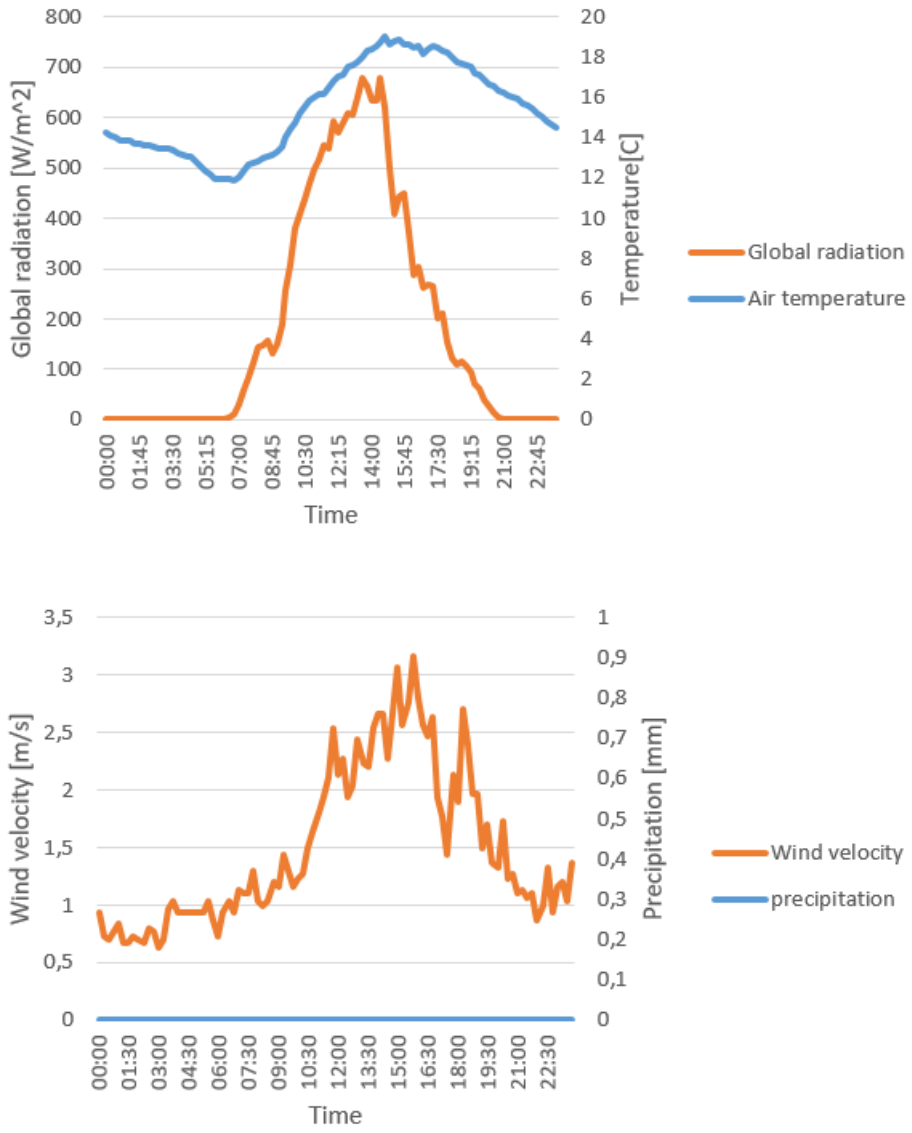

Figure 6.26- Meteorological data concerning spring period.

The global radiation reaches a maximum of 678 W/m^2 at the 13.30 so compare to the summer period the peak is shifted of half an hour. The wind velocity is elevated while the precipitation in the sample period that we consider are null.

Spring is characterized by a mitigate climate and this is reflected in the air temperature values which are included between 11 C and 19 C.

As in the previous case is possible to import the meteorological data in the Comsol “Ray optics model” and “2D-modelling of the solar receiver” in order to plot the average heat flux and temperature on the focal plane and the temperature’s trend on the focal plane when the receiver is exposed at the external atmosphere.

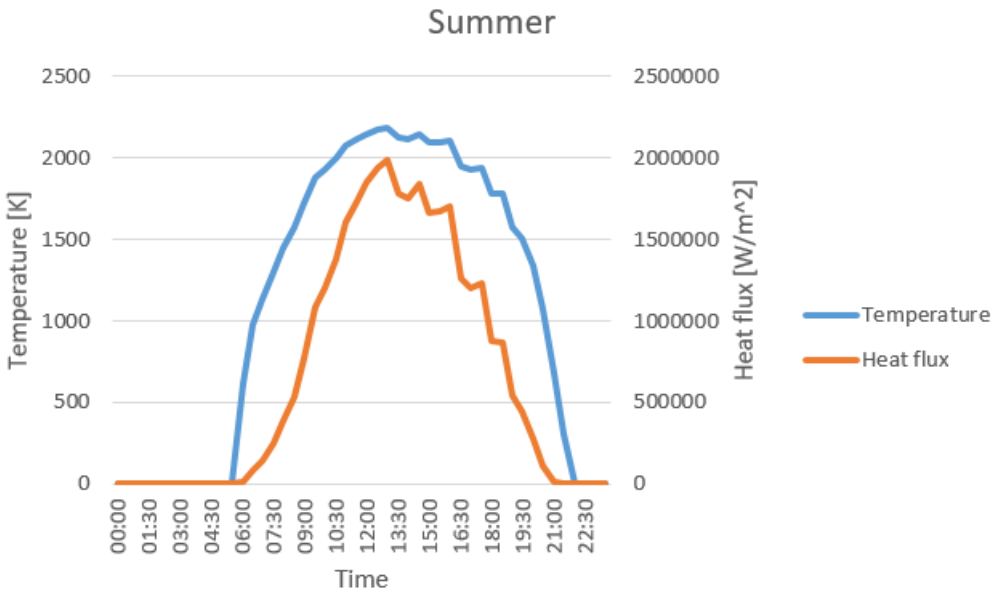

Figure 6.27- Average spring heat flux and temperature distribution on the receiver’s focal plane.

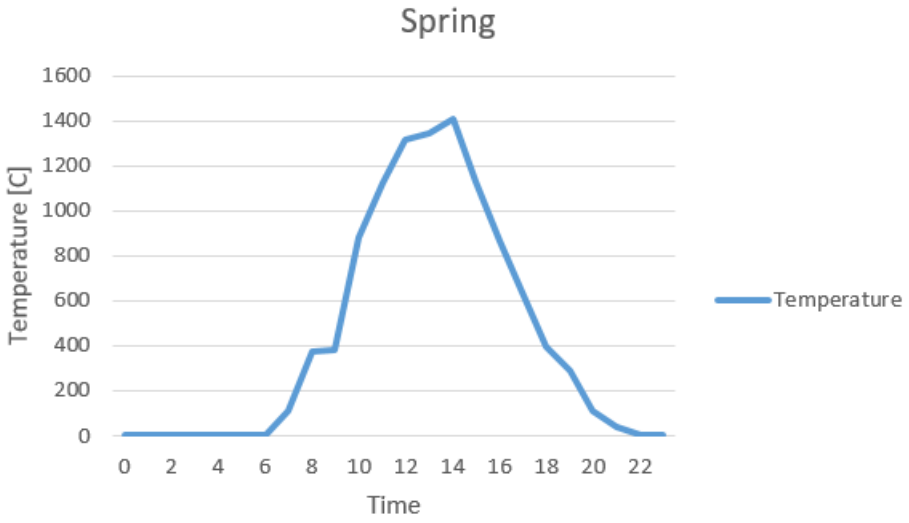

Figure 6.28-Spring temperature distribution when the receiver is exposed at the external atmosphere.

The temperature reached a maximum value of 1408 C that is not sufficient to activate the Ceria's thermo-chemical cycle. However thermos couples with a lower thermal reduction temperature could be more suitable, in detail

Winter and Autumn.

Winter (December, January, February) and Autumn (September, October, November) are seasons characterized by a cold climate with an elevated rate of precipitation. The global radiation corresponding to this period of the year has low values compared to the other seasons especially for the winter period.

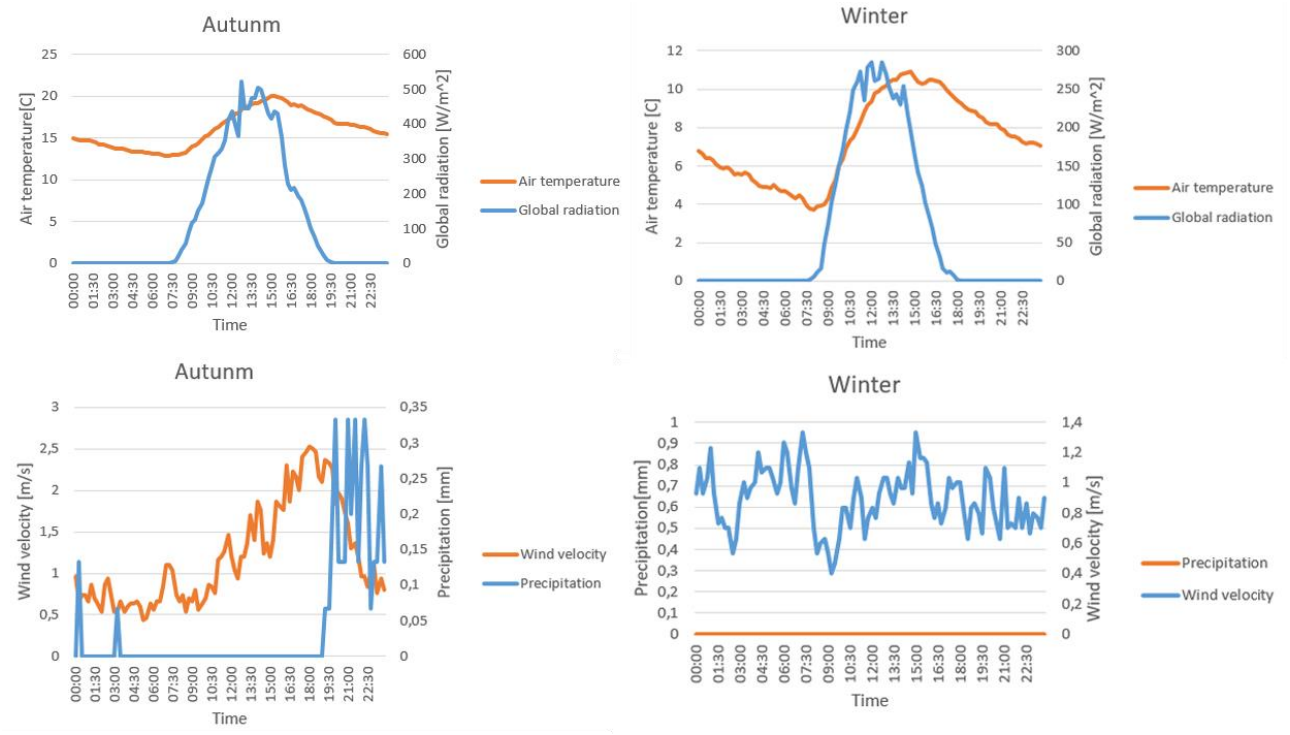

Figure 6.29-Meteorological data concerning winter and autumn period.

The graph shows that although the Autumn's air temperature has medium values included between 12 and 20 degrees Celsius the precipitation rate is the most elevated of the year.

On the other hand the winter period is characterized by low air temperature which reaches a maximum value of 11 C but the precipitation rate for the considered sample period is null. (The last condition is due to pure chance).

As for the other seasons through the Comsol models is possible to calculate the average flux on the focal plane and the temperature distribution on the focal plane when the receivers is exposed at the external atmosphere:

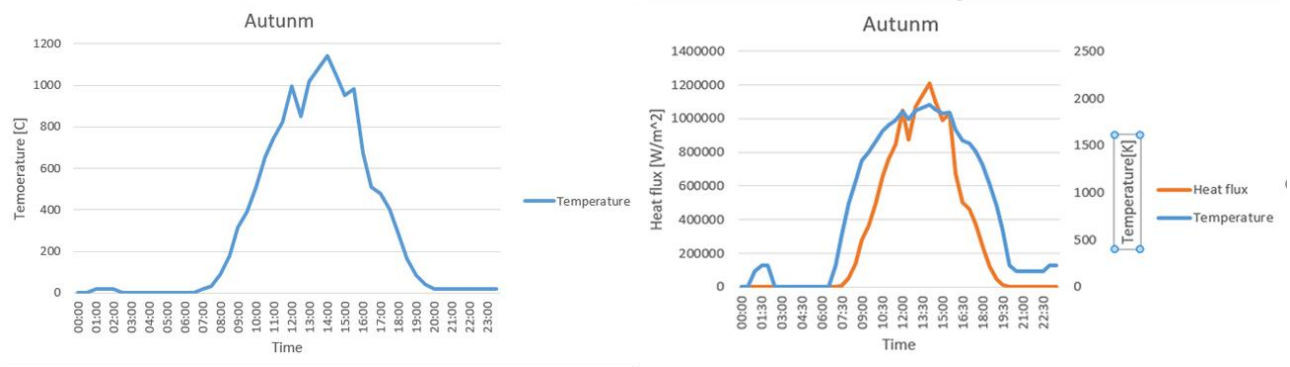

Figure- Autumn temperature distribution when the receiver is exposed at the external atmosphere and

Autumn average heat flux on the receiver's focal plane.

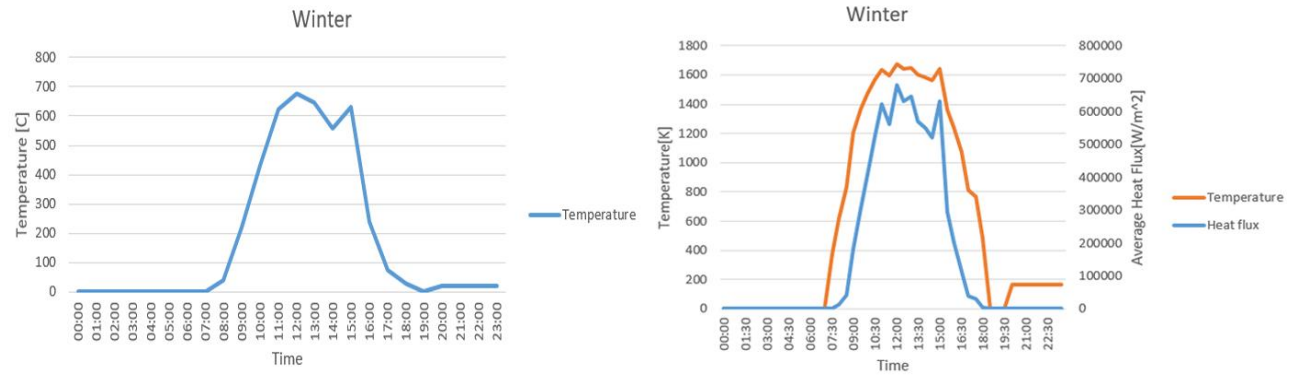

Figure 6.30- Winter temperature distribution when the receiver is exposed at the external atmosphere and

winter average heat flux on the receiver's focal plane.

As expected the temperatures reached by the receiver during the winter period are not high enough to activate any thermochemical cycle.

On the other hand the Autumn's temperature trend between the 13 and the 14.30 pm is higher than 1000 °C a high enough value to activate others thermochemical cycle.

7-Experiments.

7.1-Experimental test: Thermogravimetric analysis related to a Ceria redox cycle for the splitting of CO_2.

The thermogravimetric analysis (TGA) is a thermal analysis that describes the mass variation of a material as a function of time or temperature of a process that happens in conditions of controlled and inert atmosphere.[24]

The results obtained by the analysis are showed on a thermogram that is a graph in which the y-axis represents the mass variation in absolute values or percentage of time and the x-axis represents the time or the temperature.

At the energy department of the "Politecnico di Torino" we did the thermogravimetric analysis related to a Ceria redox cycle for the splitting of CO_2. The aim of the project is to evaluate the O_2 and CO production and calculate the efficiency of the process that will be repeated for five different cycles.[25]

Thermogravimeter.

In our experience we have used a thermogravimeter that is a particular tool that detect the mass variations of a sample due to an increase of temperature or as a consequences of the release of gaseous products.[26]

The precision tool that is used in laboratory is STA 2500 REGULUS a particular thermogravimeter model composed by:

- Thermal scale: balance in which the sample is heated from the environment temperature to the thermal reduction temperature through thermal ascent/discent ramps.
- Furnace: made of refractory material is the chamber that is heated in order to reach the desired temperature.
- Crucibles: particular receptacles, composed of Aluminum or steel, used to contain the sample that we want to test and a reference counterweight.
- Spurge gas system: safety system that guarantees a controlled atmosphere inside the furnace. The gaseous recycle allows to eject the volatile substances that are released as a consequences of the sample's decomposition.
- Temperature monitoring system: necessary to maintain the right temperature inside the furnace. The continuous measurement is realized through particular thermocouples which are inserted on the wall of the furnace.

- Digital interface: System used for instrument control, data acquisition and visualization.

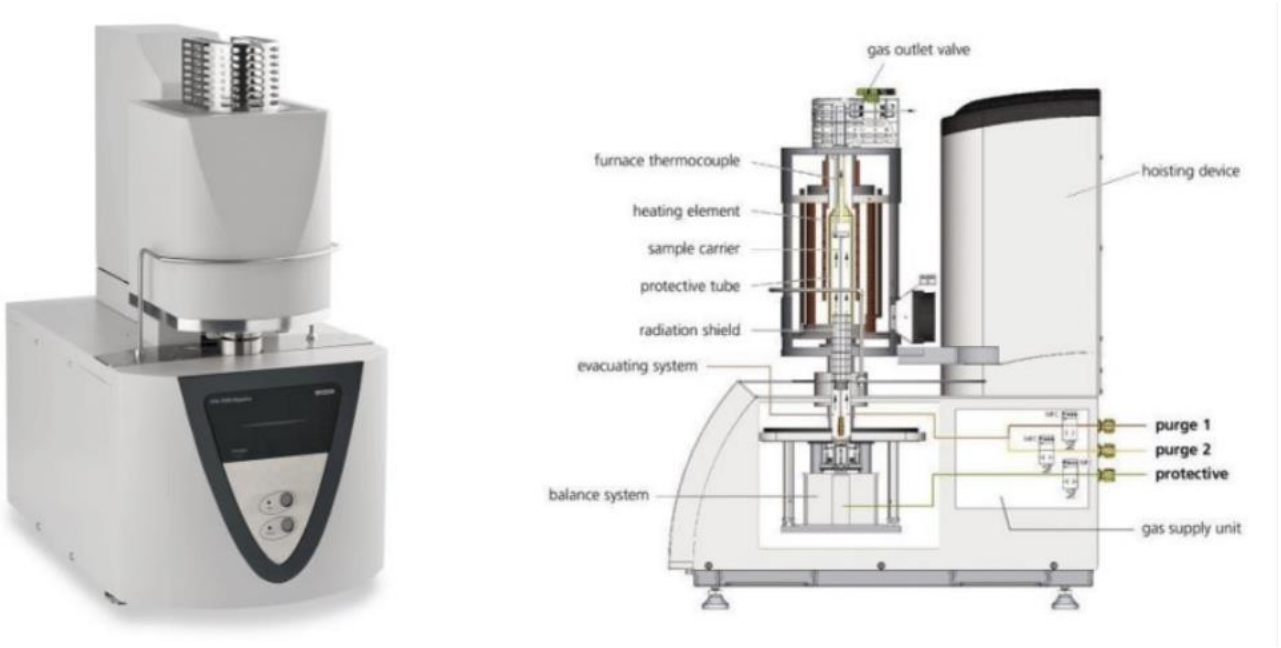

Figure 7.1 – STA 2500 REGULUS.

The thermogravimeter is also equipped with a differential balancing system with top load that operates through two thin symmetrical arms connected with the rod that supports the reference crucible and the rod related to the sample to analyze.

The differential balancing system is usefull also to compensate the possible buoyancy effects caused by the variations of the gaseous flux.

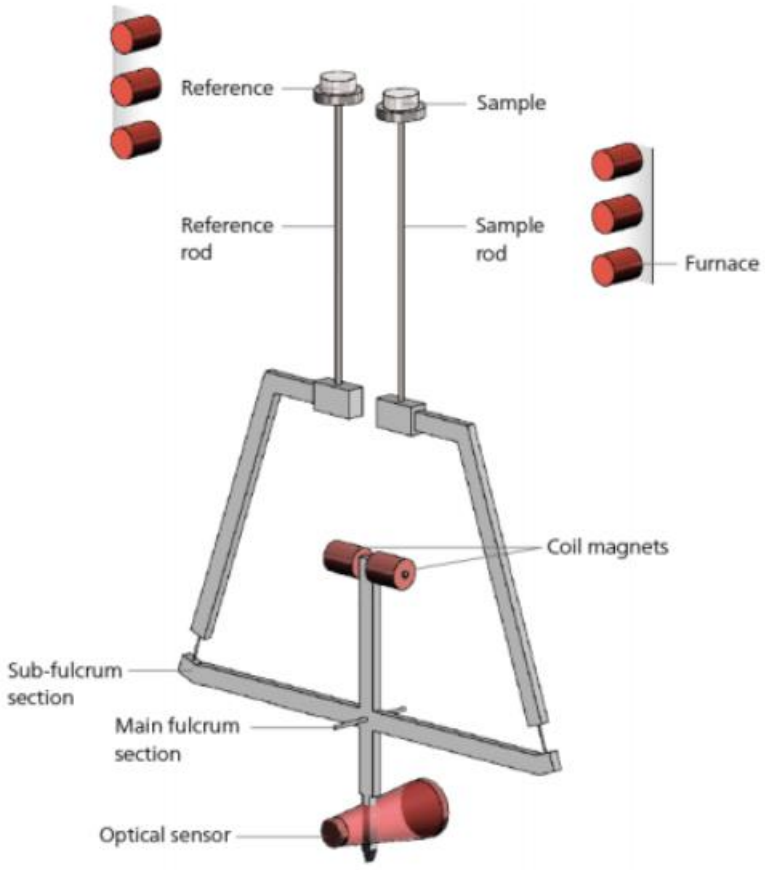

Figure 7.2- Differential balancing system.

The use of the STA 2500 REGULUS simulator instead of a real reactor has different advantages:

- The energetics transformation and mass change are obtained on one sample in one run.

- The time necessary for the tests is cut in half.

- Comparability of characteristics temperatures of the mass changes and caloric effects is ensured.

- Problems resulting from differences in the sample composition for the two simultaneous measurements are removed for inhomogeneous materials.

- It's possible to perform different measurements in inert and oxidizing atmospheres but also under vacuum.

TGA.

First of all the initial protocol that is used to initialize the thermogravimetric analysis is:

1- Open the values for both nitrogen and air cylinders;
2- Turn on the TGA;

3- Start the software, click “open” an existing file or click “new” to set up the conditions;
4- Up the furnace, keep the reference crucible always on the left hand side;
5- Place the empty sample crucible on the right hand side, then “down” the furnace;
6- Go to the software, click “tare”. Make sure the reading is stable then “up” the furnace and place the sample in the right hand side crucible;
7- “Down” the furnace, then click “weight” the sample. Wait 30 seconds until see a stable reading;
8- Go to next step of the software to set the conditions, gas flow and temperature programs;
9- Wait until the temperature bellow 300 C to clean the crucible.

The experimental demonstration is set in order to repeat the Ceria’s cycle five times and the environment temperature is set equal to 20 C.

The sample has been heated up through a thermal ramp that increase/decrease the temperature of 50 C every minutes.

A crucible of Aluminum (Al_2O_3) with mass of 100 mg is filled with Ceria powder (9.58 mg) that is positioned in order to expose the surface of the sample at the external heated environment.

At the beginning of the experiment the temperature is stabilized at 20 C for five minutes in order to remove the residual moisture.

When the moisture content of the Ceria is null the sample is heated up through the thermal ramps and the thermal reduction’s temperature of 1600 C is reached in 31 minutes.

At this point of the reaction the temperature is maintained for 30 min in order to obtain the total reduction of the ceria and the consequent released of O_2.

In conclusion there is a cool down process in which the sample reaches the oxidation’s temperature of 800 C in 15 minutes and remains stabilized at this temperature for 25 minutes in order to produce CO.

[C]	[K/min]	[t]	[pts/min]	[pts/K]
20		0.05	60	
1600	50	0.31	60	1.20
1600		0.30	60	
800	50	0.16	60	1.20
800		0.05	60	
800		0.15	60	
800		0.05	60	

Figure 7.3- Initial data Tga.

- The K/min measurements represent the increase of temperature that happens every minute in the heated chamber.
- pts/min and pts/K indicates the number of measurements that happens in one minutes/ Kelvin.
- C measurements represent the temperatures that are reached by the furnace.
- t represents the minutes that are required in order to reach the temperatures that is required.

The Ceria is reduced through an Argon's flux of 40 ml/min while the oxidation happens thanks to a mixture composed by 40 ml/min of CO_2 and 40 ml/min of Argon.

The exhaust gases are composed by carbon monoxide (CO), carbon dioxide (CO_2) and oxygen (O_2) and part of them are sucked by a vacuum pump and sent to a spectrometer that analyzes their composition.

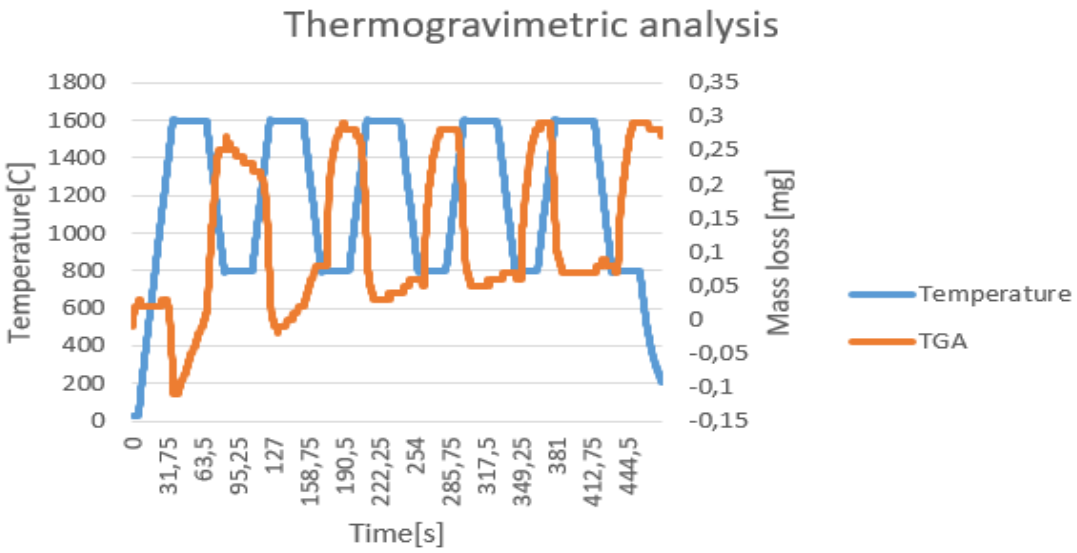

Figure 7.4-Thermogravimetric analysis.

The graph shows the ramps of temperature programmed for the different cycles and the trend of the TGA related to the mass variation.

In the first cycle the mass of the ceria is constant until the sample reaches the thermal reduction's temperature when the curve falls down and reaches the minimum value of -0.1 mg. After a few minutes the mass variation increases and reaches a peak of +0.275 mg during the oxidation's stabilization phase at temperature of 800 C.

In the second cycle the mass of the sample starts to decrease during the previous oxidation's phase and reaches a relative minimum few moments later the thermal reduction's phase.

After that the trend of the curve increases and reaches a maximum of 0.3 mg during the stabilization at 800 C.

The TGA's trend during the third cycle is similar to the previous one while in the fourth cycle the mass of the sample falls down few moments before the thermal reduction phase and started to increase few moments before the oxidation phase, in this way the maximum value of the curve is reached almost in correspondence with the subsequent reduction phase.

During the last cycle the TGA decreases when reaches the thermal reduction's temperature and started to grow up during the oxidation phase.

The TGA analysis allows to plot the gas flow's trend at the different inlets:

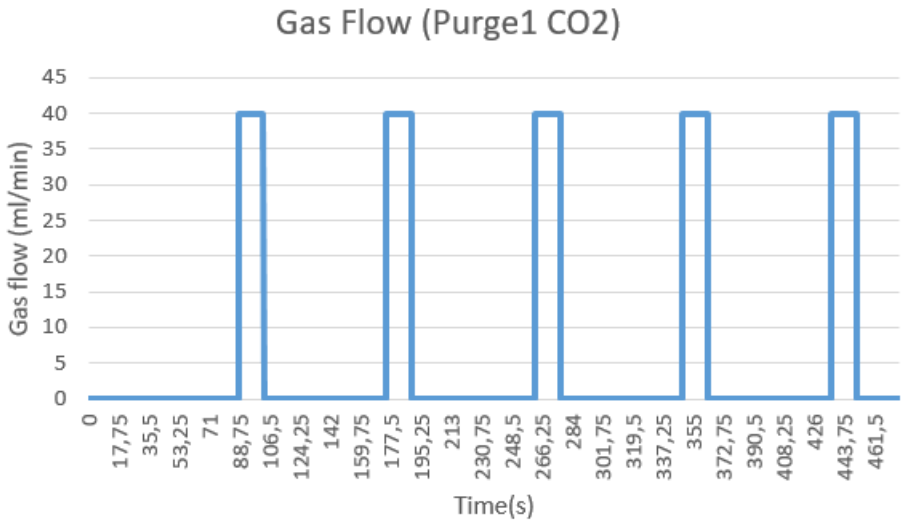

Figure 7.5-Gas flow purge.

The gas flow in the "Purge1" shows the trend of the CO_2 flux.

The graph confirms that the CO_2 is emitted during the oxidation phase with a flow rate of 40 ml/min.

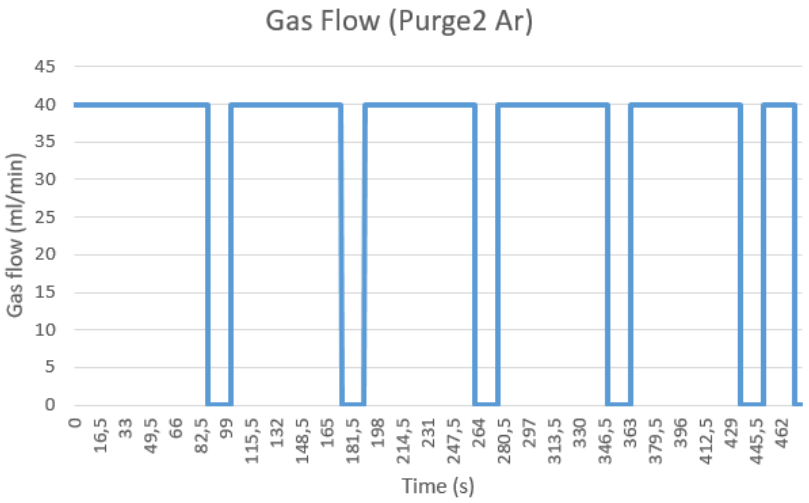

Figure 7.6-Argon gas flow.

An Argon's flow rate of 40 ml/min is used as medium fluid and is emitted during the reduction phases.

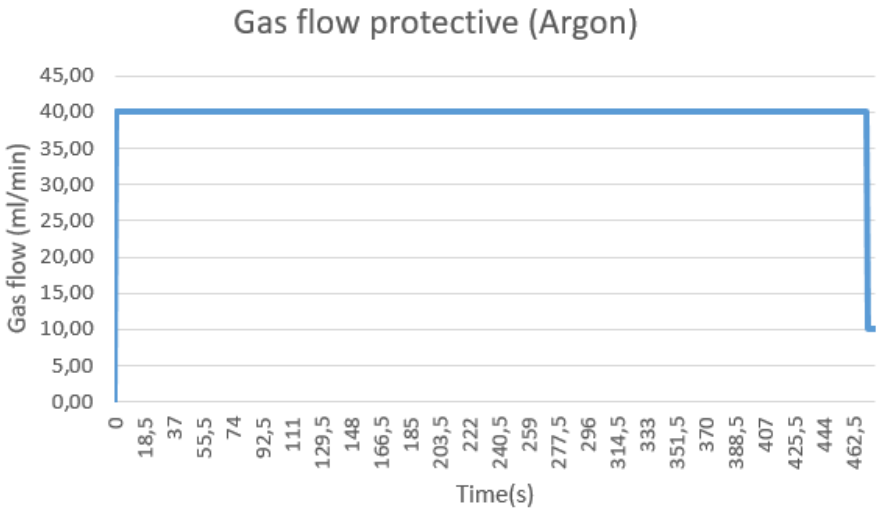

Figure 7.7-Protective Gas Flow.

An Argon's flow rate of 40 ml/min is emitted during the entire process, its function is to eject the volatile substances that are emitted during the reduction phase and to protects the structure from possible overheating.

The last step is to carry out the shutdown procedure:

1- Clean the sample crucible properly with acetone, may purchase some cotton bud; may heat the furnace to 900 C with air if there is coke deposited.
2- "Down" the furnace, press the button on the back of the equipment to shut down;

3- Close the valves for nitrogen and air;

4- Close the software.

OEC.

In the partial reduction of the Ceria the difference between the non-stoichiometric of the thermochemically stable oxygen of the redox material in the oxidation and in the reduction conditions is defined as the Oxygen Exchange Capacity (OEC):

Reduction: $$CeO_{(2-\delta_{ox})} \leftrightarrow CeO_{(2-\delta_{red})} + \frac{\Delta\delta}{2} O_2 \quad (71)$$

Oxidation: $$CeO_{(2-\delta_{red})+}\Delta\delta CO_2 \leftrightarrow CeO_{(2-\delta_{ox})} + \Delta\delta CO \quad (72)$$

$$CeO_{(2-\delta_{red})} + \Delta\delta H_2O \leftrightarrow CeO_{(2-\delta_{ox})} + \Delta\delta H_2 \quad (73)$$

$$\text{OEC}=\Delta\delta = \left(\delta_{red} - \delta_{ox)}\right) \quad (74)$$

OEC defines the amount of fuel capable of being produced per mole of CeO_2 and it is a key parameter for the optimization of the cycle because is directly connected with the final production of syngas.

There is a correlation between the Thermogravimetric analysis and the OEC parameter that can be calculated as the relative difference between the sample weight after the reduction and the sample weight perfectly oxidized.

Spectrometer.

The flow rate from the thermogravimeter is sent to a spectrometer with the aim to analyze the final composition of the exhaust gases.

The spectrometric analysis is an analytical technique in which the gaseous molecules are bombed with electrons than the ions are separated on the basis of the different ration between their mass and charge.[27]

Figure 7.8 –Spectrometer.

In order to compare the different data from the thermogravimetric analysis and the spectrometric analysis it's important to taking into account the delay due to the travel time of the gas in the duct that connect the spectrometer and thermogravimeter.

The delay of time can be calculated as:

$$t_{delay} = \frac{V_{tube}\, m^3}{V_{argon}\, \frac{m^3}{s}} = \frac{A_{section} * L_{tube}}{V_{argon}} = \frac{1.25 * 10^5 * 2.23}{667 * 10^{-9}} = 43\ s \quad (75)$$

The results that are obtained for the spectrometer are:

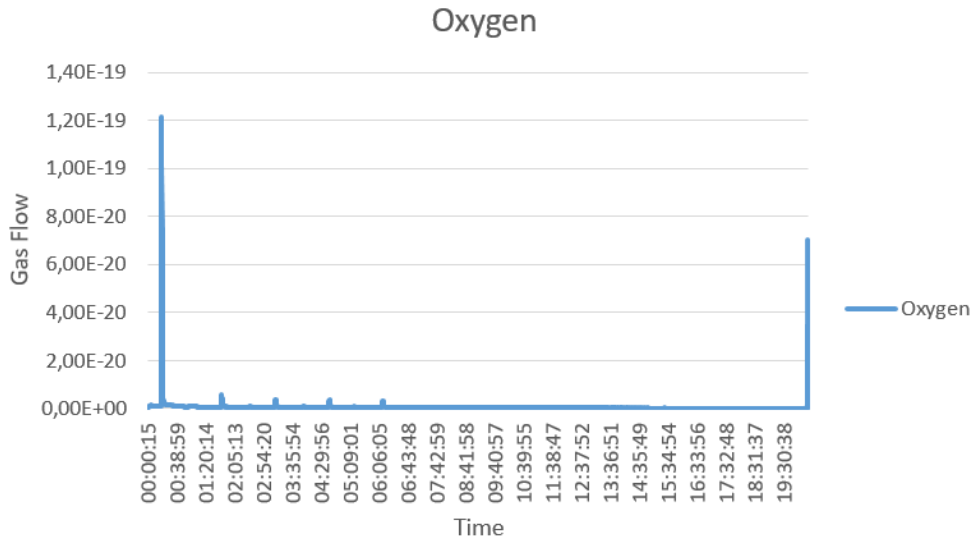

Figure 7.9- Oxygen Flow in the spectrometer.

This first graph shows the oxygen's trend that reached relative minimum values during the oxidation phase because the powder of ceria gets back the oxygen that was gained during the thermal reduction. Furthermore the mass of the sample increases of the same value that was lost during the reduction.

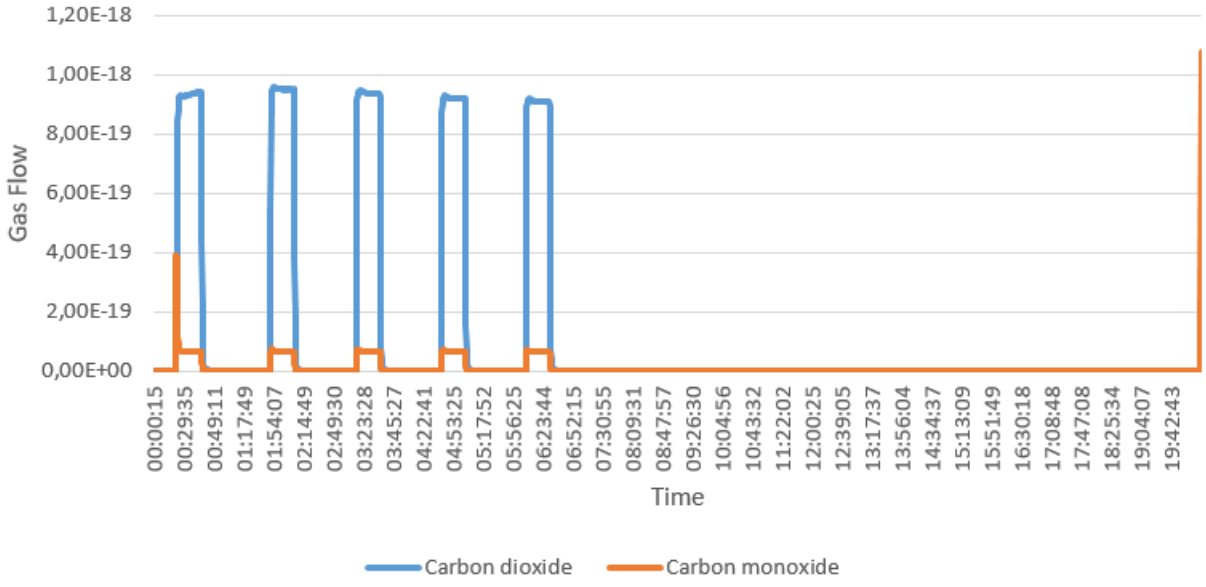

Figure 7.10- Carbon dioxide and Carbon monoxide flow in the spectrometer.

This second graph underline that during the oxidation process the direct exposition of the sample at the flux of CO_2 causes CO peak which then stabilizes at a constant value.

Efficiency.

In this paragraph is analyzed the efficiency obtained by the different cycle during the thermogravimetric analysis.

In detail is calculated the solar to chemical efficiency that is defined as the portion of solar energy input that is converted into possible work and can be extracted from the products when transformed back to the reactant in a reversible ideal fuel cell. It represents the ration between the useful power that can be obtained from the gaseous flow rate of the products and the power expended for the process realization. It is calculated as:

$$\eta_{solar-to-chemical} = \frac{2\times \mathrm{HHV_{CO}} \times \int \delta \times \mathrm{n_{CeO_2}}\,\mathrm{dt}}{\mathrm{P_{th}} + \mathrm{Einert} \times \int \mathrm{n_{inert}}\,\mathrm{dt}} = \frac{HHV_{H_2}\times V_{H_2} + HHV_{CO}\times V_{CO}}{P_{th} + E_{inert}\times n_{inert}} \quad (76)$$

$\mathrm{HHV_{H_2}}$= Higher heating value of H_2.

$\mathrm{HHV_{CO}}$= Higher heating value of CO.

$\mathrm{E_{inert}}$ = Energy required to separate the inert gas.

$\mathrm{n_{CeO_2}}$ = Molar flow rate of Ceria.

$\mathrm{V_{H2}}$= Hydrogen's volumetric flow rate.

$\mathrm{V_{CO}}$= Carbon monoxide's volumetric flow rate

$\mathrm{n_{inert}}$= Molar flow rate of the inert gas.

$\mathrm{P_{th}}$= Thermal power supplied by the CSP.

In detail for the specific case of the of the CO_2 splitting through the Ceria's thermochemical the formula is simplified:

$$\eta_{\,solar-to-chemical} = \frac{2\times HHV_{CO}\times V_{co}}{P_{th} + (E_{inert}\times n_{inert})} \quad (77)$$

The High heating value is considered equal to the enthalpy of combustion of CO at the environment conditions ($14\frac{Mj}{mol}$) while the energy required to seprate the inert gas is equal to 20000 $\frac{J}{mol}$.

The thermal power supplied at the sample is estimated taking into account that the heated chamber is a cylinder with a diameter of 2 cm and height of 2 cm. The mass of the Ceria's sample is equal to 9.58

mg while the crucible is composed by Aluminum and weighs 2 g. At this point, considering the densities and the specific heats as known, it is possible to estimate the thermal power:

$$V_{tot} = \pi \times \frac{d^2}{4} \times h = 3.14 \times \frac{0.02^2}{4} \times 0.2 = 0.00000628\ m^3 \quad (78)$$

$$V_{ceria} = \frac{m_{ceria}}{\rho_{ceria}} = \frac{0.00958}{7.22 \times 10^6} = 1.33 \times 10^{-9}\ m^3 \quad (79)$$

$$V_{aluminum} = \frac{m_{aluminum}}{\rho_{aluminum}} = \frac{2}{3.95 \times 10^6} = 5.06 \times 10^{-7}\ m^3 \quad (80)$$

$$V_{argon} = V_{tot} - V_{aluminum} - V_{ceria} = 5.27 \times 10^{-6}\ m^3 \quad (81)$$

$$m_{argon} = V_{argon} \times \rho_{argon} = 5.27 \times 10^{-6} \times 1784 = 9.39 \times 10^{-3}\ g \quad (82)$$

$$Q_{th} = m_{aluminum} \times cp_{aluminum} \times (1600 - 20) + m_{ceria} \times cp_{ceria}(1600 - 20) + m_{argon} \times cp_{argon}(1600 - 20) = 5385.63\ W \quad (83)$$

$$P_{th} = \frac{Q_{th}}{t} = 2.8\ W \quad (84)$$

V_{tot}= Total volume of the cylinder.

V_{ceria}= Volume of the Ceria's sample.

$V_{aluminum}$= Volume of the aluminum crucible.

V_{argon}= Volume of the inert gas.

Cp= specific heat.

t= thermal ramp = 31 min= 1896 s

According to the mass balance of the thermal reduction reaction of the Ceria's Oxide the molar ratio between the CO and the O_2 should be equal to 2 with a complete use of the non-stoichiometric oxide.

In reality a little deviation from the ideal value occurs and this is due to sensitivity errors in the measurement system and small losses in the connection system between the spectrometer and the thermogravimeter.

In order to obtain the Carbon monoxide production it is necessary to calculate the mass variation of the CeO_2 (Δm_{CeO2}) for each cycle during the reduction phase from the Thermogravimetric analysis:

Cycle	$CeO_{2inital}$ [mg]	CeO_{2final} [mg]	Δm_{CeO2} [mg]
1	-0,1	0,1	0,11
2	0,05	0,02	0,03
3	0,1	0,04	0,06
4	0,13	0,06	0,07
5	0,15	0,07	0,08

The Oxygen ($\mathrm{n_{O2}}$) and Ceria oxide ($\mathrm{n_{CeO2}}$) molar flow rates can be calculated from the Ceria mass variation through the respective molar weights:

$$\mathrm{n_{CeO2}} = \frac{\Delta \mathrm{m_{CeO2}}}{Mw_{CeO_2}} \quad (85)$$

$$\mathrm{n_{O2}} = \frac{\Delta \mathrm{m_{CeO2}}}{Mw_{O_2}} \quad (86)$$

Mw_{CeO_2}: Ceria oxide's molar weight= 172 g/mol

Mw_{O_2}: Oxygen's molar weight = 32 g/mol

The difference between the weight of perfectly oxidized sample and the weight of the same sample once oxidized corresponds at the oxygen's quantity that is released during the thermal reduction:

$$\text{OEC}=\Delta\delta = \left(\delta_{red} - \delta_{ox)}\right) = \mathrm{n_{O2}} \quad (87)$$

In the next step through the oxidation's reaction is possible to calculate the carbon monoxide's molar flow rate:

$$CeO_2 \rightarrow CeO + \frac{1}{2}O_2 \quad (88)$$

$$CeO + CO_2 \rightarrow CeO_2 + CO \quad (89)$$

$$n_{co} = 2 \times \mathrm{n_{O2}} \quad (90)$$

We assume that the thermal reduction's reaction happens in a period of time lower than a second so is possible to approximate the moles of carbon monoxide that are producted as a flow rate. In addition we hypothesize that carbon monoxide is a perfect gas so its molar volume is equal to 22,4 l/mol:

$$m_{co}^3 = n_{co} \times 22{,}4\frac{l}{mol} \times 10^{-3}\frac{m^3}{l} \tag{91}$$

$$V_{co\frac{m^3}{s}} = m_{co}^3\, m^3 \tag{92}$$

The molar flow rate of the inert gases (Argon) is equal to 40 ml/min while the energy that is required to separate it from the products is equal to 20 Kj/mol.

It's possible to calculate the Argon molar flow rate as:

$$V_{argon} = 40\frac{ml}{min} = 0.666\frac{ml}{s} = 0{,}666 \times 10^{-3}\frac{l}{s} = 0{,}666 \times 10^{-6}\frac{m^3}{s} \tag{93}$$

$$M_{argon} = V_{argon} \times \rho_{argon} = 0.666 \times 10^{-6}\frac{m^3}{s} \times 1784\frac{g}{s} = 1.888 \times 10^{3}\frac{g}{s} \tag{94}$$

$$n_{argon} = \frac{M_{argon}}{MW_{argon}} = \frac{1.888\times10^{3}\frac{g}{s}}{39.9\frac{g}{mol}} = 2.976 \times 10^{-8}\frac{mol}{s} \tag{95}$$

At this point is possible to estimate the thermo-chemical efficiency of the process which quantifies the conversion rate of thermal energy into chemical energy of the compounds obtained.

The main parameters for the different thermo-chemical cycles are showed in the following table

Cycle	Δm_{CeO2} [mg]	n_{CeO2} $[mol]$	$\Delta\delta$ [mol]	n_{co} [mol]
1	0.11	$6{,}39*10^{-7}$	$3{,}44*10^{-6}$	$6{,}88*10^{-6}$
2	0.03	$1{,}74*10^{-7}$	$9{,}38*10^{-7}$	$1{,}88*10^{-6}$
3	0.06	$3{,}49*10^{-7}$	$1{,}88*10^{-6}$	$3{,}75*10^{-6}$
4	0.07	$4{,}07*10^{-7}$	$2{,}19*10^{-6}$	$4{,}38*10^{-6}$
5	0.08	$4{,}65*10^{-7}$	$2{,}50*10^{-6}$	$5*10^{-6}$

Cycle	$m_{co}^{3}[m^{3}]$	$V_{co}[m^{3}/s]$	$\eta_{solar\text{-}to\text{-}chemical}$	$n_{inert}[mol/s]$
1	$1{,}54*10^{-7}$	$1{,}54*10^{-7}$	0.77	$2{,}976*10^{-8}$
2	$4{,}2*10^{-8}$	$4{,}2*10^{-8}$	0.21	$2{,}976*10^{-8}$
3	$8{,}41*10^{-8}$	$8{,}41*10^{-8}$	0.42	$2{,}976*10^{-8}$
4	$9.81*10^{-8}$	$9.81*10^{-8}$	0.49	$2{,}976*10^{-8}$
5	$1{,}12*10^{-7}$	$1{,}12*10^{-7}$	0.56	$2{,}976*10^{-8}$

The table underlines the close relationship between the Ceria oxide's mass variation Δm_{CeO2} and the Oxygen Exchange Capacity $\Delta\delta$, the quantity of oxygen released is directly proportional to the mass variation of the sample during the thermal reduction.

The efficiency data confirms the spectrometer analysis in fact the first cycle characterized by a very high release of carbon monoxide and oxygen has the higher efficiency rate while the second one that is the last cycle in terms of production has the lowest efficiency.

7.2-Thermal reduction of Ceria within an Aerosol reactor for H_2O and CO_2 splitting.

In this paragraph is reported an experimental demonstration debated by a group of Zurich's researchers whose have studied an Aerosol reactor used for the splitting of H_2O and CO_2 through the Ceria's thermochemical cycle.

This experience is interesting because it is very similar to the thermogravimetric analysis that we have done at the Politecnico so the final results can be compared.

The aerosol reactor has a standard counter flow configuration composed by a flux of ceria and a counter current flow of Argon that is the inert gas of the system. The vertical tube is composed by Alumina and the Ceria is heated instantly so it is reduced in less than a second.[28]

The aim of the simulation is to guarantee an efficient separation of reduced Ceria from the gaseous oxygen exploiting the ability to decouple the reduction and oxidation phases of the aerosol reactor.

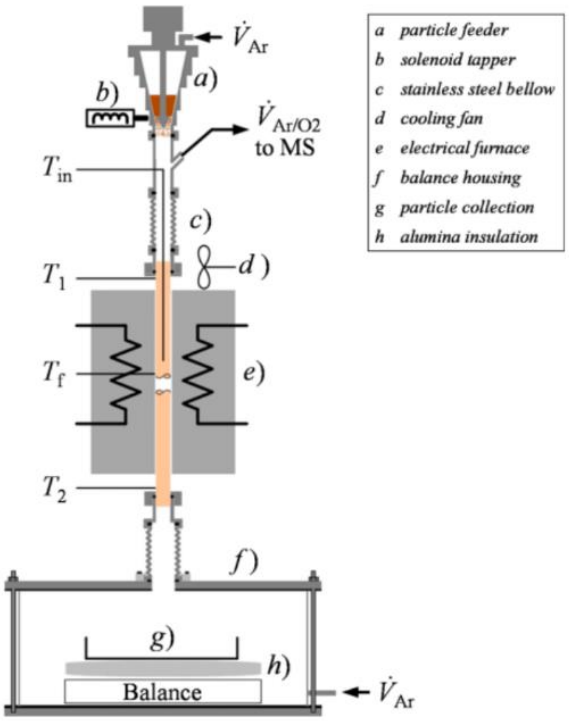

Figure 7.11- Prototype of the particle flow reactor.

The figure shows a scheme relating the experimental demonstration. The reactor is fed through an adjustable orifice that is located at the top of the prototype.

The vertical tube is located inside an electrically heated oven while the ceria's falling particles are collected in a container placed on a scale that measures the mass flow of ceria and the total reduced mass released.

During the experimental phase the system has been heated through thermal gradient of 20 K/min to an isothermal temperature included between 1723 and 1873 K.

The thermal response given by the thermogravimetric analysis shows that with the introduction of 105 mg of ceria into the reactor at 1873 K the mass of Ceria increases after 5 seconds while after 10 seconds the whole sample of ceria is reduced.

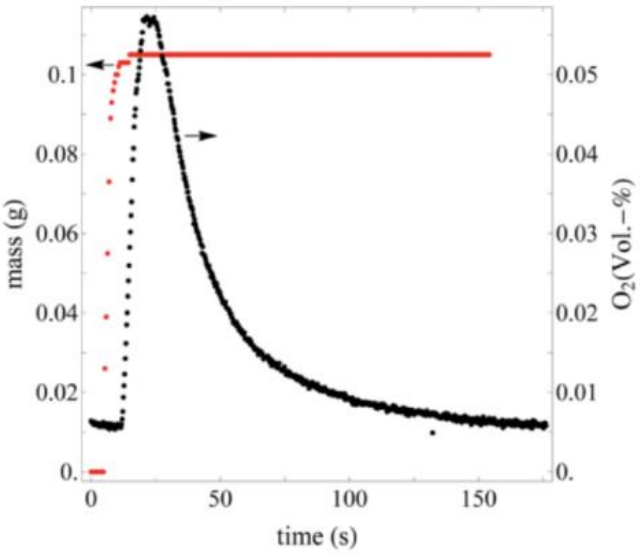

Figure 7.12- Ceria's thermal response and mass variation.

The average molar difference of the reduced Ceria is equal to 0.0035.

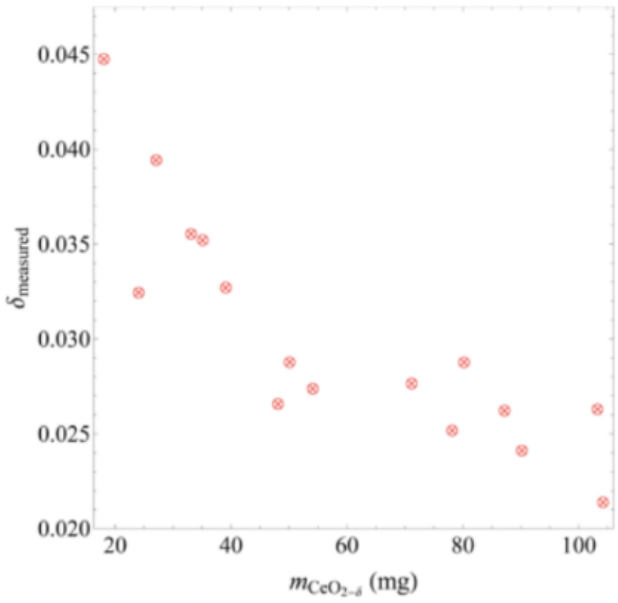

Figure 7.13-Molar difference as a function of the mass of Ceria as a function of the thermal reduction at 1772 K.

The graph underlines that an increases of the Ceria's mass from 18 to 50 mg correspond a decreases of the OEC parameter from an initial value of 0.045 to 0.028.

This phenomenon can be explained through the thermodynamic, the reduction of an elevated quantity of ceria causes a higher O_2 production that increases the oxygen partial pressure P_{O2}. The increases of

the partial pressure at constant temperature causes a reduction of the reduction extensions and so of the OEC parameter.

In conclusion the researchers have calculated the solar to chemical efficiency of the process related to different mass of the sample:

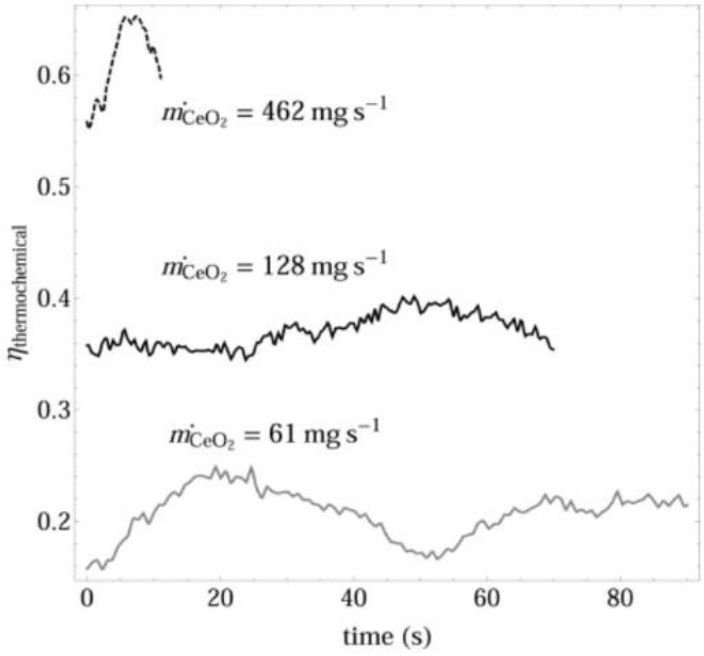

Figure 7.14- Solar to chemical efficiency for three different sample mass values.

The two curves at the top show the efficiency trend while the sample is heated at 1873 K and the inert gas flow rate is equal to 800 $\frac{ml}{min}$. The bottom curve is calculated at the same temperature but with an Argon flow rate of 500 $\frac{ml}{min}$.

It is evident that the solar to chemical efficiency is proportional at the mass flow rate of the ceria.

8-Conclusions.

This thesis analyses the syngas production through the technologies currently available on the market. Two main aspects were discussed of the exploitations of this resource: the temperature distribution focus on a horizontal cylinder through a concentrated solar receiver technology and the solar to chemical efficiency of a Ceria redox cycle simulated through a thermogravimetric analysis.[29]

The results obtained from the Comsol simulations underline that the operation of the solar concentrator during the winter period is not efficient. The temperatures reached by the receiver are not high enough to activate the thermal reduction of any thermochemical cycle.

On the other hand the models show that during the summer period the solar technology has an elevated efficiency and reaches temperatures that ensure the Ceria's thermal reduction for at least three hours per day.

Regarding the mid-seasons, temperatures high enough to activate the Ceria's thermochemical cycle are not reached, however redox couples with a lower thermal reduction temperature could be suitable. In detail the Hercynite cycle characterized by a thermal reduction temperature of 1000 °C results efficient in Autumn for at least two hours per day.

At last, the spring period is characterized by temperature higher than 1200 °C for three hours per day so Iron-based oxide cycle or Cadmio's cycle result more suitable for this period of the year.

The CeO_2 exhibits rapid reaction kinetics and oxygen diffusion rates and shows exceptional resistance to sintering due to its high melting point. Furthermore, CeO_2 [1]is able to maintain its cubic fluorite structure during cycling over a wide range of operating conditions and reduction extent. These properties and the abundant presence of Ceria in nature make the non-stoichiometric CeO_2 cycle the current state of art in terms of redox performance.

An alternative solution to reduce the thermal reduction temperature and activate the Ceria's thermochemical cycle during the mid-seasons could be the use of a carbo-thermal reduction in which the reaction of an oxide with carbon or natural gas to produce the elementary metal can replace the first step of thermal reduction. The most used carbon-thermal reduction is the methane reduction in which CeO_2 is totally reduced into Ce_2O_3 at 900 °C:[30]

$$2CeO_2 + CH_4 \rightarrow Ce_2O_3 + CO + 2H_2 \quad (96)$$

The efficiency data obtained from trial performed at Politecnico provide proof of the feasibility of the process although the experience involved limited sample masses. The efficiency values are included between 0.77 and 0.21.

Our results are in line with the ones obtained from the Zurich's researchers. In their experiment the efficiency oscillated between 0.2 and 0.6 in proportion to the mass of the sample considered. The efficiency value corresponding to the sample's mass of 61 mg is equal to 0.2 so, taking into account that the efficiency is proportional to the mass of the Ceria, and that the results that we obtained are referred to a mass of 9.81 mg of Ceria, our experiment's results are very promising. Moreover it is important to consider that the Aerosol reactor, thanks to its capacity to decoupling the reduction and oxidation phases, is the most efficient technology for the Ceria's thermochemical cycle, while we use a simple thermogravimeter.

In conclusion, although still under development, the analyzed system represents an alternative solution to the fossil fuel technologies even though the prototypes powered by hydrogen/syngas are currently too small to replace commercial power plants.

The syngas is already used as energetic vector and primary fuel, however the fossil fuel technologies used to produce it are more competitive from an economic point of view than the solar concentrator because of the low taxation on CO and fossil resources.

The current cost of a solar dish, similar to the one located on the roof of the energy center, made of concentrator, motors with electronic tracking gearboxes and mechanics, is around 18000 €. To which it has to be added the solar reactor's indicative price of 100000 €.

The high costs associated with this technology makes it impractical in this historical moment, however the energetic transition to a carbon neutral economy will incentivize the future development of the chemicals production through thermo-chemical cycle.

Thanks to the continuous progress made by the researchers, investors and big companies are taking interest to this kind of technology. Nevertheless the study of the process and the reduction of the costs must be optimized in order to make the system designable on large scale.

A possible future development could be the study of the best materials to use in the system in order to reduce the costs and increase the efficiency. Moreover a monthly instead of seasonal FEM simulation guarantees even more precise results.

Bibliography

[1] E. Montà, “Realizzazione di processi di chemical looping e produzione di gas sintetico mediante solare termico a concentrazione,” 2020.

[2] L. R. e M.Santarelli, “Polygeneration and advanced energy systems.”

[3] H. I. Villafán-Vidales, C. A. Arancibia-Bulnes, D. Riveros-Rosas, H. Romero-Paredes, and C. A. Estrada, “An overview of the solar thermochemical processes for hydrogen and syngas production: Reactors, and facilities,” *Renew. Sustain. Energy Rev.*, vol. 75, no. October 2015, pp. 894–908, 2017, doi: 10.1016/j.rser.2016.11.070.

[4] S. Chuayboon, S. Abanades, and S. Rodat, “Solar chemical looping gasification of biomass with the ZnO/Zn redox system for syngas and zinc production in a continuously-fed solar reactor,” *Fuel*, vol. 215, no. November 2017, pp. 66–79, 2018, doi: 10.1016/j.fuel.2017.11.021.

[5] M. Welte, K. Warren, J. R. Scheffe, and A. Steinfeld, “Combined Ceria Reduction and Methane Reforming in a Solar-Driven Particle-Transport Reactor,” *Ind. Eng. Chem. Res.*, vol. 56, no. 37, pp. 10300–10308, 2017, doi: 10.1021/acs.iecr.7b02738.

[6] T. Kodama, S. Bellan, N. Gokon, and H. S. Cho, “Particle reactors for solar thermochemical processes,” *Sol. Energy*, vol. 156, pp. 113–132, 2017, doi: 10.1016/j.solener.2017.05.084.

[7] C.Zamparelli, “Collettori a concentrazione per l’impiego dell’energia termica solare,” 2013. www.solarconcentrators.eu/thermodynamic/it/introduzione%0A-%0Aai%0A-%0Aconcentratori%0A-%0Asolari/35%0A-%0Adescrizione%0A-%0Asistemi%0A-%0Asolar%0Ai%0A-%0Aa%0A-%0Aconcentrazione/46%0A-%0Acollettori%0A-%0Asolari%0A-%0Aa%0A-%0Aconcentrazione.html.

[8] M.Simonetti e G.Fracastoro, “Technology for renewable energy sources,” *Dispens. del corso*.

[9] A. Z. Hafez, A. Soliman, K. A. El-Metwally, and I. M. Ismail, “Design analysis factors and specifications of solar dish technologies for different systems and applications,” *Renew. Sustain. Energy Rev.*, vol. 67, pp. 1019–1036, 2017, doi: 10.1016/j.rser.2016.09.077.

[10] B. Hoffschmidt, S. Alexopoulos, J. Göttsche, M. Sauerborn, and O. Kaufhold, *High concentration solar collectors*, vol. 3. Elsevier Ltd., 2012.

[11] J. Coventry and C. Andraka, “Dish systems for CSP,” *Sol. Energy*, vol. 152, pp. 140–170, 2017, doi: 10.1016/j.solener.2017.02.056.

[12] F. Varsano *et al.*, “Hydrogen production by water splitting on manganese ferrite-sodium carbonate mixture: Feasibility tests in a packed bed solar reactor-receiver,” *Int. J. Hydrogen Energy*, vol. 39, no. 36, pp. 20920–20929, 2014, doi: 10.1016/j.ijhydene.2014.10.105.

[13] M. Lanchi *et al.*, “Thermal characterization of a cavity receiver for hydrogen production by thermochemical cycles operating at moderate temperatures,” *Sol. Energy*, vol. 92, pp. 256–268, 2013, doi: 10.1016/j.solener.2013.03.008.

[14] P. G. Loutzenhiser, A. Meier, and A. Steinfeld, “Review of the Two-Step H2O/CO2-Splitting solar thermochemical cycle based on Zn/ZnO redox reactions,” *Materials (Basel).*, vol. 3, no. 11, pp. 4922–4938, 2010, doi: 10.3390/ma3114922.

[15] F. Ingegneria, I. Meccanica, C. Solari, A. D. Alta, P. Ing, and G. Cerri, “Dipartimento di Ingegneria Meccanica e Industriale PER IL CICLO TERMOCHIMICO ZOLFO IODIO Docente Guida Prof . Ing . Edoardo Bemporad.”

[16] C. Agrafiotis, M. Roeb, and C. Sattler, “A review on solar thermal syngas production via redox pair-based water/carbon dioxide splitting thermochemical cycles,” *Renew. Sustain. Energy Rev.*, vol. 42, pp. 254–285, 2015, doi: 10.1016/j.rser.2014.09.039.

[17] L. Xiao, S. Y. Wu, and Y. R. Li, “Advances in solar hydrogen production via two-step water-splitting thermochemical cycles based on metal redox reactions,” *Renew. Energy*, vol. 41, pp. 1–12, 2012, doi: 10.1016/j.renene.2011.11.023.

[18] R. J. Carrillo and J. R. Scheffe, “Advances and trends in redox materials for solar thermochemical fuel production,” *Sol. Energy*, vol. 156, pp. 3–20, 2017, doi: 10.1016/j.solener.2017.05.032.

[19] J. D. Milshtein, E. Gratz, S. N. Basu, S. Gopalan, and U. B. Pal, “Study of the two-step W/WO3 solar to fuel conversion cycle for syngas production,” *J. Power Sources*, vol. 236, pp. 95–102, 2013, doi: 10.1016/j.jpowsour.2013.02.038.

[20] E. Koepf, I. Alxneit, C. Wieckert, and A. Meier, “A review of high temperature solar driven reactor technology: 25 years of experience in research and development at the Paul

Scherrer Institute," *Appl. Energy*, vol. 188, pp. 620–651, 2017, doi: 10.1016/j.apenergy.2016.11.088.

[21] N. Gokon, S. Takahashi, H. Yamamoto, and T. Kodama, "New solar water-splitting reactor with ferrite particles in an internally circulating fluidized bed," *J. Sol. Energy Eng. Trans. ASME*, vol. 131, no. 1, pp. 0110071–0110079, 2009, doi: 10.1115/1.3027511.

[22] N. Gokon, H. Murayama, A. Nagasaki, and T. Kodama, "Thermochemical two-step water splitting cycles by monoclinic ZrO2-supported NiFe2O4 and Fe3O4 powders and ceramic foam devices," *Sol. Energy*, vol. 83, no. 4, pp. 527–537, 2009, doi: 10.1016/j.solener.2008.10.003.

[23] Enciclopedia britannica, "Oscuramento al bordo," 2019. https://it.wikipedia.org/wiki/Oscuramento_al_bordo.

[24] Online, "Analisi termogravimetrica." https://it.wikipedia.org/wiki/Termogravimetria.

[25] "Analisi termica differenziale," 2014, [Online]. Available: https://www.chimicamo.org/chimica%0A-%0Aanalitica/a%0Analisi%0A-%0Atermica%0A-%0Adifferenziale.html.

[26] "Analisi termogravimetrica," 2016. ttps://www.chimicamo.org/chimica%0A-%0Aanalitica/analisi%0A-%0Atermogravimetrica.html.

[27] "spettrometria di massa," 2012. https://www.chimicamo.org/chimica%0A-%0Aanalitica/spettrometria%0A-%0Adi%0A-%0Amassa.html.

[28] J. R. Scheffe, M. Welte, and A. Steinfeld, "Thermal reduction of ceria within an aerosol reactor for H2O and CO2 splitting," *Ind. Eng. Chem. Res.*, vol. 53, no. 6, pp. 2175–2182, 2014, doi: 10.1021/ie402620k.

[29] P. D. Papurello and D. Romaniello, "Realizzazione di processi di chemical looping e produzione di gas sintetico mediante solare termico a concentrazione," 2020.

[30] A. Farooqui, F. Di Tomaso, A. Bose, D. Ferrero, J. Llorca, and M. Santarelli, "Techno-economic and exergy analysis of polygeneration plant for power and DME production with the integration of chemical looping CO2/H2O splitting," *Energy Convers. Manag.*, vol. 186,

no. December 2018, pp. 200–219, 2019, doi: 10.1016/j.enconman.2019.02.043.